AN ABSTRACT OF THE THESIS OF

David A. Spackman for the degree of Master of Science in Radiation Health Physics
presented on June 11, 2013.
Title: Design and Analysis of Radiation Shielding Eyewear

Abstract approved: _____
David M. Hamby

The recent reductions to the international dose limit recommendations for the lens of the eye have renewed interest in radiation protection strategies in interventional fluoroscopy, where eye-lens radiation exposure occurs frequently. Radiation-shielding eyewear can significantly reduce lens dose in these scenarios, but accurate protection factors are elusive because they depend on a variety of factors. This work aims to investigate variables that affect eye shield performance in fluoroscopy rooms, test several shield designs, and rate the shield designs based on shielding performance. Eight separate shields were modeled in MCNP5 using detailed head and eye geometry, and the shields were evaluated at eight individual source positions. Results showed that shields of different thicknesses and shapes can provide similar protection to the operator. A total protection factor of about 5 is the most protection a 0.10 mm lead equivalent material can reasonably provide, and small shields constructed of this material can provide protection factors of about 3. Shield performance can vary greatly depending on the irradiation angle, and this could cause an overestimation of the dose reduction provided by the shield if vulnerable angles are exploited. With increasing evidence of cataract risk at low lens doses, fluoroscopy operators need radiation protection equipment that can provide well characterized protection, and radiation-shielding eyewear can provide excellent dose reduction if they are designed well and used correctly.

# Design and Analysis of Radiation Shielding Eyewear

by
David A. Spackman

A THESIS

submitted to

Oregon State University

in partial fulfillment of
the requirements for the
degree of

Master of Science

Presented June 11, 2013
Commencement June 2013

Master of Science thesis of David A. Spackman presented on June 11, 2013.

APPROVED:

_____

Major Professor, representing Radiation Health Physics

_____

Head of the Department of Nuclear Engineering and Radiation Health Physics

_____

Dean of the Graduate School

I understand that my thesis will become part of the permanent collection of Oregon State University libraries. My signature below authorizes release of my thesis to any reader upon request.

_____

David A. Spackman, Author

ACKNOWLEDGEMENTS

There were many people who helped me to complete this research in one way or another. I would like to express my gratitude to my advisor Dr. Hamby for his valuable and constructive suggestions, and also for giving me ample freedom to pursue ideas of my own. I would also like to thank everyone in room C-128 of the Radiation Center. Your collective input, perspective, and subtle spirit of competition kept me working hard and always on my toes.

TABLE OF CONTENTS

TABLE OF CONTENTS (Continued)

Page

TABLE OF CONTENTS (Continued)

LIST OF FIGURES

LIST OF TABLES

LIST OF APPENDIX FIGURES

LIST OF APPENDIX FIGURES (Continued)

LIST OF APPENDIX FIGURES (Continued)

# DEDICATION

This work is dedicated to my wife Jessica.

# DESIGN AND ANALYSIS OF RADIATION SHIELDING EYEWEAR

## CHAPTER 1 – INTRODUCTION

### 1.1 Overview

Less than ten years after Roentgen's discovery of x-rays in 1895, radiation-induced cataracts had been reported in a worker exposed to ionizing radiation, making it one of the longest known effects of exposure to ionizing radiation [1]. Until recently, radiation induced cataracts have been regarded as a deterministic effect of radiation exposure with a threshold for detectable opacities of 5 Sv for chronic and 0.5-2.0 Sv for acute exposure [1-2]. It has been thought that at dose levels below these thresholds, no response will be observed. However, several recent epidemiological studies of cataract formation in Chernobyl cleanup workers, atomic bomb survivors, and radiologic technicians suggest that there may not in fact be a response threshold for radiation induced cataracts [3-5]. In April of 2011, in response to this growing body of evidence, the ICRP revised their dose recommendations for the lens of the eye. Now, the absorbed dose threshold is considered to be 0.5 Sv, and the recommended occupational equivalent dose limits are 20 mSv per year averaged over a period of 5 years with no single year exceeding 50 mSv [6]. This represents a dramatic reduction in the recommended occupational dose limits compared to the currently observed occupational dose limits in the United States of 150 mSv per year. The lens of the human eye is now known to be more radiosensitive than previously thought, and this suggests that certain occupational groups that are consistently exposed to ionizing radiation may need to take additional measures to limit their eye-lens dose.

One of these groups is the medical staff involved with performing fluoroscopy procedures. Fluoroscopy is a type of medical imaging that uses x-rays to create moving pictures of body parts, instruments, or contrast agents inside of the patient's body [7]. Fluoroscopy can be used for a wide array of procedures, and as technology progresses, this imaging technique is being utilized more and more [8]. For most procedures, the operator stands over the patient as the x-ray images are taken and displayed on in-room monitors; this makes operator exposure to scattered photons almost certain. To limit the operator's radiation exposure, it is common for them to wear a 0.75 mm lead equivalent apron and thyroid collar [8]. Additional shielding around the x-ray machine and room, like ceiling suspended shields and table mounted leg shields, are also common, but they rely heavily on correct placement to be effective[9]. The use of radiation-shielding eye wear is less common than the use of protective aprons, and the a recent study found that only 30-35% of operators wear protective eye wear while many them incurred annual eye lens doses greater than 20 mSv [8]. It is clear that the use of radiation-shielding eye wear is a simple strategy to significantly and selectively reduce the absorbed dose to the lens of the operator's eye in interventional fluoroscopy suites [8, 10-11].

Typical radiation eye shields are constructed with 0.75 mm lead equivalent glass lenses, and some designs have optional side shields if increased coverage is desired. Full coverage face shields made of 0.1 mm lead equivalent acrylic are also available. However, fluoroscopy operators need to perform detailed tasks during their procedures, and uncomfortable eye wear is not conducive to these tasks. Although the most common eye shields are constructed with 0.75 mm lead equivalent material, they are not rated with any specifically implied amount of protection, and this means that an operator wearing a poorly fitting or otherwise inappropriate 0.75mm lead equivalent eye shield may not be getting the protection that they expect [10]. Fluoroscopy rooms and procedures are rarely ever the same [8], and

good radiation-shielding eye wear should perform well in the different shielding scenarios in which they are used. Therefore, it is important to quantify the amount of protection that certain eye shields can be expected to provide so that assurance can be made that eye lens dose is being minimized.

## 1.2 Research Objectives

The objectives of this research are: 1) to investigate how shielding scenario variables like irradiation angle, shield design, and shield thickness affect the performance of radiation shielding eye wear; 2) to test the feasibility and performance of eye shields constructed of 0.1 mm lead equivalent material; and 3) to develop a method to quantify the overall protection provided by different eye shields. These objectives will be addressed with computer simulations of several eye shields and shielding scenarios using the program MCNP5.

# CHAPTER 2 – BACKGROUND

## 2.1 Eye Anatomy

The eyes are compact, durable, and sophisticated visual instruments; they also contain some of the most radiosensitive tissues in the human body [19, 14]. On average the eyes are 24 mm in diameter and weigh 8 grams (Figure 2.1) [19]. The wall of the eye is made of several layers which contain fibrous connective tissue, blood vessels, and nerves [19]. The interior of the eye consists mainly of the posterior chamber containing vitreous humour, the anterior chamber containing aqueous humour, and the lens.

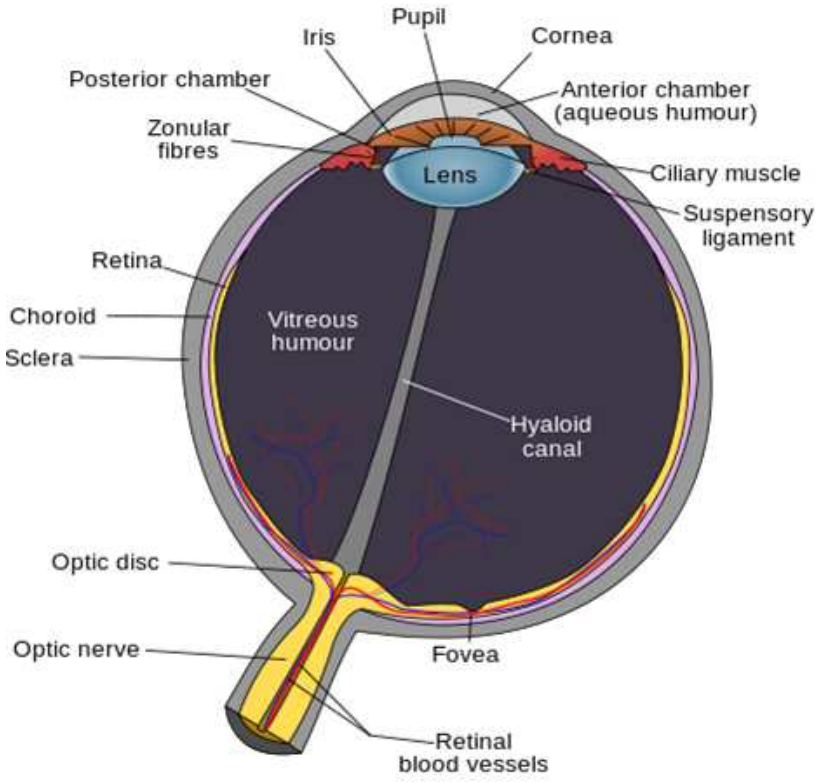


Figure 2.1: Anatomy of the eye

The lens of the eye acts to focus the visual image onto the photoreceptors at the back of the eye [19]. To perform this task, the lens must be transparent to light and malleable in order to allow the deformation necessary for focusing. The outer surface of the lens is made up of densely packed and neatly organized concentric cells and these cells allow the lens to deform and spring back to shape [19]. The interior cells, called lens fibers, are specialized cells that have elongated and lost all of their organelles [19]. The lens fibers contain stable transparent proteins that are responsible for lens clarity, and they remain functional for the entire life of the lens [19]. When the precise conditions for lens health are disrupted in some way, the lenses can lose their transparency resulting in lens opacities called cataracts. One such disruption to the lens of the eye is exposure to ionizing radiation.

## 2.2 Photon Dosimetry and Shielding

In order to protect the radiosensitive tissues of the eye from ionizing radiation, it is important to understand how radiation dose is delivered to the lens by photons, and how to effectively shield photons. For the photon energies addressed in this study (20-80 keV), two photon interactions dominate the physics for dosimetry and shielding concerns, photoelectric absorption and Compton scatter [17]. These two reactions will account for most of the reactions that lead to lens dose. Absorbed dose is defined as the amount of energy deposited per unit mass in a material. For photons, absorbed dose can be calculated by

$$D = \emptyset \cdot E \cdot \frac{\mu_{ab}}{\rho} \qquad (1)$$

where $\emptyset$ is photon flux, E is photon energy, $\mu_{ab}$ is the photon energy absorption coefficient for the material, and $\rho$ is the density of the material [16]. The energy absorption coefficient dictates how much of the incident photon energy will be absorbed in the material, and it depends on proton number (Z) and photon energy.

In principle, Equation 1 can be used to calculate eye lens dose due to a spectrum of photon energies if all of the variable are known.

The shielding of 20-80 keV photons is also governed by photoelectric absorption and Compton scatter. Photoelectric absorption cross-sections increase strongly with increasing proton number (Z) and decreasing photon energy [17]. For this study, the photon energies are relatively low, and this means that a high Z shielding material can provide excellent shielding properties even if it is relatively thin. To calculate the photon intensity (I) after the photons have been shielding with a thickness (x) of shield material Equation 2 can be used,

$$I = I_0 \cdot e^{(-\mu \cdot x)} \qquad (2)$$

where $I_0$ is the initial photon intensity, and μ is the linear photon attenuation coefficient. μ describes how effective the material is at removing photons from the initial beam per unit length through all photon interactions combined. Equation 2 can be used in determining the photon shielding abilities for many materials including lead. In many photon shielding scenarios lead (Z=82), or a material that contains lead, is an ideal choice for photon shielding because of its high Z.

## 2.3 Leaded Acrylic and Glass

Much of the shielding in interventional fluoroscopy rooms is made of either leaded glass or leaded acrylic. Both materials can be impregnated with lead to increase their x-ray shielding capabilities while remaining optically clear. However they have different material properties that make them suitable for different uses. Most notably, leaded glass can provide the same amount of shielding protection as leaded acrylic while being about five times thinner [18]. This is why 0.75 mm lead

equivalent radiation-shielding eyewear is most commonly made of leaded glass. If the same 0.75 mm lead equivalent eye shields were made of leaded acrylic, the shield would have to be about 220 mm thick. However, it becomes reasonable to manufacture and wear leaded acrylic eye shields when the shielding requirements call for 0.10 mm lead equivalent material or less. At this thickness of lead equivalence, a leaded acrylic shield would need to be less than 3 mm thick [18]. Additionally, leaded acrylic can be shaped and formed using the same techniques used for regular acrylic [18]. This means that the manufacture of custom shaped 0.10 mm lead equivalent eye shields for fluoroscopy operators is not unreasonable especially if this type of shield can be shown to provide adequate radiation shielding capabilities.

## 2.4 Radiation Cataractogenesis

Cataract is an opacification of the lens of the eye, and it is one of the largest causes of blindness and vision impairment worldwide [1]. The development of cataracts can be attributed to a goodly number of causes which can occur in combination or individually including age, diabetes, genetics, alcohol and nicotine use, and exposure to ionizing radiation [12]. It can be difficult to determine the source of causation; however, studies with large numbers of participants can use cataract formation statistics to narrow in on likely causes. Most cataracts can be grouped into three main groups, nuclear, cortical, and posterior subcapsular (PSC) [1]. PSC is the least common form of age related cataract, but it is most common type of cataract linked with ionizing radiation exposure[1, 12]. The exact mechanism(s) for radiation induced cataracts are still under investigation, but it is generally accepted that radiation damage to the front of the lens, where the cells are differentiating and dividing, leads to complex biochemical changes in the lens that eventually migrate to the interior of the lens (lens fibers) and aggregate to form opacities [1, 12-13].

Importantly, the timing and severity of radiation induced cataracts are correlated with the amount of radiation dose to the lens. As absorbed dose to the lens increases, the latency period decreases, and the severity of the cataracts increases [1, 12]. This means that exposure to low doses of radiation will tend to increase the latency time and decrease the severity of cataract formation. This makes the detection of cataract formation due to low doses of radiation more difficult to identify than due to large eye lens doses. Early studies of radiation cataractogenesis that were used as the basis for ICRP dose limit recommendations often had relatively short follow up times and few study subjects with lens doses below a few Gy [1, 13]. This information supported the belief that radiation induced cataract formation was a deterministic effect of radiation exposure with a threshold below which no effects were observed of 5 Sv for chronic, and 0.5-2.0 Sv for acute exposure [1]. However, within the last ten years, several long-term radiation cataractogenesis studies consisting of large cohorts exposed to relatively low doses of radiation have presented data that challenge the preconception of a dose threshold for radiation induced cataract formation [3-5].

In 2004, Minamoto et al [5] published a study of cataractogenesis in 913 atomic bomb survivors 55 years after their exposure. The subjects of this study were examined with digital photography, slit-lamps exams, and a cataract grading system for the nuclear, cortical, and posterior subcapsular regions of the lens. The majority of the study participants had received less than 0.5 Sv of lens dose and were under the age of 13 at the time of exposure [5]. The results of this study showed an increased likelihood of lens opacities for subjects exposed to less than 2 Sv even after correcting for explanatory variables like subject age, sex, and city of residence [5]. The study also showed a strong correlation between higher radiation doses and an increasing frequency and severity of cortical and posterior subcapsular lens opacities [5].

In 2007, Worgul et al [3] published study of cataract formation in over 8,600 Chernobyl clean-up workers at 12 and 14 years after exposure. The large majority of the study subject (95%) had lens doses less than 0.5 Gy with a mean of 123 mGy [3, 13]. The occurrence of lens opacities was established with two blinded lens exams spaced two years apart from one another [3]. Results showed that posterior subcapsular and cortical cataracts due to radiation exposure were present in 25% of the subjects [3]. Additionally, analysis of the dose threshold for cataract formation pointed to a dose-effect threshold of less than 1 Gy [3]. The authors recommended that their results should be considered in a revision of the ICRP's eye risk guidelines. However, some concern remains in regard to the dose estimates assigned to the individual clean-up workers, and dose uncertainty could contribute to errors in the overall recommendations of this study [13].

In 2008, Chodick et al [4] published one of the largest cataract risk studies to date. It is of particular interest here, because of the occupations of the study participants. The study followed more than 35,000 radiologic technologists for nearly 20 years to determine their risk of cataract formation [4]. The study used questionnaires regarding work history and film badge dosimetry data to assign lens dose to the study subjects [4]. The risk factors for cataract formation other than radiation exposure were accounted for and investigated alongside radiation exposure [4]. The mean estimated lens dose across the study was 28 mGy with the highest dose group centered around 60 mGy [4, 13]. This highest-dose group accounted for a cataract formation hazard ratio of 1.18 (95% confidence: 0.99, 1.40) suggesting that exposure to relatively low doses of radiation can harm the lens of the eye and increase the lifetime risk of cataract formation [4].

Citing the aforementioned studies, as well as several others, the ICRP issued a "Statement on Tissue Reactions" in April of 2011 in which they reduced the recommended dose limit to the eye by a factor of almost eight [6]. The ICRP also suggested that the drastically lower dose recommendations for the eye have implications in occupations where radiation exposure of the eye is common and frequent [14]. Some of these occupations include interventional cardiologists and radiologists, radiographers, some nurses, and fluoroscopists. These occupations often require exposure to high scatter radiation fields for several hours a day, and without proper radiation protection equipment and techniques, exposure to the eyes in these professions can be high [14].

## 2.5 The ORAMED Project

Due to the ICRP eye-lens dose limit recommendations and the fact that some medical personnel are regularly exposed to substantial amounts of ionizing radiation, it is important to quantify and understand the nature of the occupational doses that they can be expected to receive. Additionally, the use of radiation protection techniques and equipment needs to be characterized so that the protection they provide is well understood. The Optimization of Radiation Protection of Medical Staff (ORAMED) project was initiated in 2008 with goals to assess and reduce the radiation exposure to medical staff, and the results of Work Package 1 (the first of 5 research tasks) were published collectively in late 2011 [15]. Work Package 1 consisted of a coordinated measurement campaign in several different hospitals across Europe, as well as a simultaneous computer simulation campaign in order to determine the main parameters that influence eye and extremity dose in interventional fluoroscopy [8]. The results of the ORAMED study highlight the radiation exposure risks in interventional fluoroscopy, and detail how

radiation protection equipment in these facilities is being used and in what areas it can improve.

### *2.5.1 Measurement Campaign*

The measurement campaign was conducted in six European countries and followed medical staff performing a variety of eight different medical procedures [8]. The operators were monitored for dose with eight individual TLDs which were placed on the arms, legs, trunk, and head (to monitor lens dose) [8]. In addition to the dosimetry data, information was recorded about each procedure including procedure type, the operator's experience and position in the room, the presence of shielding equipment in the room, the use of personal protective equipment, and the x-ray tube specifications [8].

For the 1,300 procedures observed, dose to the operator's eye lenses was typically 40-60 μSv per procedure [8]. However, several operators received more than 1000 μSv per procedure in certain cases, and some procedures systematically produced higher lens doses than others [8]. These dose values are reported as if the operator was not wearing protective eyewear because the dosimeters used to measure dose to the eye were placed outside of any protective eye wear (worn about 30% of the time). The presence of a ceiling suspended shield in the fluoroscopy room provides a reduction to eye lens dose by a factor of 1.3-1.6 with the higher protection coming from procedures that require the x-ray tube to be position over, instead of under, the patient [8]. The dose to the eyes is also systematically lower when the x-ray tube is located under the patient rather than above the patient [8]. The authors used the dosimetry data to extrapolate annual doses to the operator's eyes, and they concluded that 45% of the operators would exceed 9 mSv/year lens dose and 24%

would exceed the new ICRP limit of 20 mSv/year if they continued operating with their current equipment and radiation protection techniques in place [8].

In addition to the numerical dosimetry data, the measurement campaign gathered valuable information about the nature and use of shielding and PPE in interventional fluoroscopy rooms. The majority of procedures (90%) are performed with an under-couch tube configuration, and this is favorable to reducing eye lens dose [8]. Of the rooms studied for each type of procedure, 24%-46% did not have any room protective equipment whatsoever, including ceiling suspended shields that could aid in the reduction of eye lens dose [8]. Further compounding increased dose to the eyes due to the lack of ceiling suspended shield use, is the finding that 65-70% of operators do not wear leaded protective eye wear [8].

### *2.5.2 Simulation Campaign*

The ORAMED simulation campaign was initiated to investigate the individual variables associated in the dose to medical staff [8]. Some dose-contributing variables that are difficult to control in real world scenarios can be manipulated separately from one another using Monte Carlo simulations to understand their individual contribution. The simulations for the ORAMED project were made using MCNPX v2.5, and the x-ray spectrum they chose corresponds to a tube voltage of 80 kVp and 3 mm of aluminum shielding [8]. Procedural variables that were modeled and manipulated within the simulation campaign include the x-ray tube voltage and filtration, the x-ray beam projection angle and size, the position of the operator, the presence of room shielding, and the presence and specifications of leaded eyewear [8]. The two ceiling-suspended shields were modeled (rectangular and arc type) using “good” and “bad” shield positioning, and the dose reduction effect of leaded

eyewear was also measured when no ceiling suspended shield was modeled [8]. The effect of each shielding component was compared to the corresponding unshielded scenario in order to assign a protection ratio to quantify the dose reduction [8].

Results from the ORAMED simulation campaign describe the performance of selected shielding solutions in controlled simulations. For ceiling suspended shields, eye lens dose for both eyes is reported to be reduced by 22-93% depending on beam projection and shield placement [8]. Leaded glasses are reported to reduce left lens (the eye closest to the scatter radiation) dose by 83-90%, however, no mention is made of the right lens dose performance in this case [8]. An additional separate simulation analysis of leaded eyewear designed with different thicknesses and sizes was also conducted for two different beam projections. Results show that protective eye shields that are thicker than 0.5 mm (ORAMED tested 0.5 mm and 1.0 mm lead shields) of lead do not improve the protection of the eye lenses significantly, but shields that are larger and provide more coverage accounted for better protection of the eyes [8].

This simulation campaign shows that both ceiling suspended shields and leaded eyewear can significantly reduce eye lens dose to operators in fluoroscopy suites. The performance of ceiling suspended shields appears to be related to how well they are positioned in the room, and how the operator addresses the shield. The performance of leaded eyewear suggests that increasing the coverage area of a shield design could account for better shielding than making the eye shield thicker.

## 2.6 Additional Recent Eye Shield Studies

As the results of the ORAMED project were beginning to be released, several other groups began to publish research about radiation-shielding eyewear. In 2011, Geber et al [10] published an investigation of eye-lens dosimetry in interventional procedures that included an analysis of the shielding performance of eight separate and commercially available eye shields (all had the same thickness). This study was conducted with realistic phantoms in an interventional fluoroscopy room, and TLDs were used to measure the shielded and unshielded dose for two operator positions. Additionally, the operator phantom was loaded with dosimetric film in order to visualize how and where the dose is deposited within the head and around the eyes of the operator.

Results for the eight shields tested by Geber et al showed relatively equal shielding performance can be expected for all shields when they are irradiated from the front [10]. However, when the radiation source is moved underneath and oblique to the operator, shield performance drops substantially and is inconsistent between the left and right eye and across the eight shields tested [10]. The authors conclude that protective eye wear may be being used with a false sense of adequate protection, especially when the shields are not irradiated from the front [10]. Additionally, the design and fit of protective eyewear that minimizes gaps and provides good coverage is very important to the overall performance of protective eyewear [10]. These conclusions were also confirmed the following eye shield study.

In early 2013 Sturchio et al [11] published an analysis of the protective performance of three commercially available leaded eye wear models. The shields were evaluated in an interventional fluoroscopy suite with realistic phantoms representing the

operator and the patient. To measure the dose to the eye, an optically stimulated luminescent dosimeter was placed on the eye (closest to the beam) underneath the eye shield. The x-ray voltage used was 91 kVp with 3.5mm of aluminum shielding. The eye shields were evaluated according to three different irradiation angles related to different operator positions during the procedure. Two of the shields consisted of 0.75 mm lead equivalent glass lenses of different sizes, and the third shield was constructed from large 0.07 mm lead equivalent acrylic. The shields were evaluated against unshielded scenarios and assigned protection factors depending on their performance at each irradiation angle.

When the shields were irradiated from the front, shield thickness was the dominant factor in shield performance, and the thicker shields performed best [11]. The thick lenses provided protection factors of 8-9 while the thin shield provided a protection factor of about 2.5 [11]. As the operator phantom was positioned at increasing angles to the x-ray machine, the shield coverage began to dominate the shield protection performance. At irradiation angles of 45 and 90 degrees, the thick shields had protection factors of 1.5-5 and the thin shield provided protection of 2-3 [11]. This study highlights the importance of shield coverage when irradiation angles are high, as is commonly encountered in fluoroscopy rooms. The authors concluded that a shield's lead equivalence is not an appropriate way to determine its shielding capabilities, and they recommended that additional research is needed in understanding the demands of eye protection and investigating the feasibility of alternate shielding strategies for fluoroscopy operators [11].

The current state of research regarding radiation protection in interventional fluoroscopy suggests that 1) the risk of radiation-induced cataract formation is increased by low level radiation exposure [1, 3-6, 14]; 2) operators can and do incur

lens doses in excess of the ICRP's recommendations which may put them at increased risk for cataracts [8] ; and 3) radiation-shielding eyewear can significantly reduce lens dose, but certain eye shields provide better shielding than others and more research is necessary to develop effective shielding strategies [8, 10, 11].

# CHAPTER 3 – MATERIALS AND METHODS

## 3.1 Software and Computing

### *3.1.1 MCNP*

The simulations carried out in this study were performed using a Monte Carlo code that was developed and is maintained by Los Alamos National Laboratory. The Monte Carlo N-Particle software package (MCNP) is a general purpose, continuous-energy, generalized-geometry, time-dependent, coupled neutron/photon/electron Monte Carlo transport code [25]. It can be used to simulate numerous particle transport scenarios across a wide array of energies and geometries. For photons, MCNP is capable of modeling coherent and incoherent scatter, fluorescent emission after photoelectric absorption, and absorption via pair production; it also provides extensive secondary particle tracking [25]. The Monte Carlo method relies on random number generation to sample the experimentally derived probability distributions that govern these events in order to accurately simulate the true behavior of the system in question. During an MCNP run particles originating from the user-defined source are followed through their entire lifetime in the system, and any secondary particles created by the primary particles can also be followed to extinction [25]. In this manner the Monte Carlo method can accurately simulate physical interactions through the tracking and scoring of source particles in the system.

To run an MCNP simulation the user must first create an input file that defines the required simulation parameters. The MCNP input file is comprised of three main sections (surfaces, cells, and data) commonly referred to as blocks. Each block is separated by a blank line in the input file and contains a specific set of simulation parameters. The surface block contains a numbered list of geometrical shapes

(planes, spheres, cones, cylinders, etc.) located in three-dimensional Cartesian coordinate system [23]. The surfaces defined in the surface block form the skeleton of the simulation, and they can be used in combination to define complex geometries. The cell block contains a numbered list of three-dimensional cells bounded by one or more surfaces. The cells can be assigned materials and densities within the cell block, or they can be left void. The cell block defines the composition and final shape of the simulation by filling-in potential spaces defined by the surface block. The third and final block, the data block, contains a variety of simulation parameters including source specification, source position, material definitions, tally specification, tally locations, physics specifications, and a number of other useful features of MCNP [23]. The data block contains the majority of the information about the simulation other than geometry, and it contains a diverse set of simulation options that make MCNP an adaptable radiation transport code.

To execute a simulation in MCNP, the user creates an input file that contains the simulation parameters like geometry, materials, source type, source position, tally specification, and variance reduction. The computing time necessary to run a simulation depends on its complexity and the amount of precision desired. In general, simulations can take anywhere from a few seconds to many hours to complete. When the simulation is complete, several output files are created that contain large amounts of detailed information about the simulated source particles. MCNP automatically tests the results of the user defined output tallies with ten statistical tests. These tests speak to the reliability of the results, as well as, provide information for improving the efficiency of the simulation. MCNP gives the user a variety of output tally options including flux, current, energy deposition, and track length. It also gives the user the ability to visualize and measure the particle flux throughout a 3D mesh superimposed over the simulation geometry [23]. Several versions of MCNP were available for use; for this study MCNP5 was chosen.

### *3.1.2 Computing Demands*

MCNP5 is capable of providing all of the necessary details and output information that was required for this study. MCNP5 allows the user to easily utilize multiple cores of a CPU's processor. The most recent release of the software, MCNPX, requires additional setup to execute multi-core processing which is part of the reason it was not chosen. The computer used for this simulation campaign contains 8GB of RAM and an Intel Core i7-3630QM processor rated at 2.4 GHz per core. As computing time was a limiting factor in the number of simulations that could be executed it was very important to maximize the speed at which simulations could be completed. MCNP5 was able to run the simulations through four threads utilizing each core of the processor equally. Simulations typically operated at total processing speeds of about 3.2 GHz. In addition to the high computational load on the processor, the computer's memory was highly utilized during simulations due to nature of high resolution mesh tallies. Single simulations typically required about 90 minutes to run and produced 500-600 Mb of data.

### *3.1.3 MCNPX Visual Editor*

The MCNPX Visual Editor is a piece of software delivered from RSICC with the MCNP5/MCNPX package that enables 2D and 3D visualizations of the MCNP5 input geometry, source position, and source particle tracks. Although MCNP5 itself contains geometry plotting capabilities, the Visual Editor has a relatively simple GUI and is provided with a helpful user's manual. The Visual Editor was used extensively while constructing and validating the simulation geometry and every simulated shield design. The 3D plotting capabilities were used to capture images and investigate and design the simulation geometry. The Visual Editor was also used to verify every photon source position and to insure that the source direction biasing vectors were performing as intended before any final simulations were conducted.

The Visual Editor has the ability to identify fatal errors and other problems with the input file structure, and this feature was used to scan for input file errors while building MCNP5 input files.

### *3.1.4 Microsoft Visual Studio*

Microsoft Visual Studio was used to build, manage, and manipulate the MCNP5 input files. Due to the nature of this work it was necessary to produce over 100 similar but slightly different input files. One useful feature is that Visual Studio highlights areas where changes have been made to a .txt file. This feature aided in making many error free manipulations of the input files. The MCNPX Visual Editor was not well suited for this task because it creates and saves additional files to the input file location, however Microsoft Visual Studio allowed for the efficient manipulation and sorting of all of the MCNP5 input files.

### *3.1.5 Solid Works*

Solid Works was used to make 3D models of all of the shield designs simulated in this study. This program has the ability to change the appearance of an object to more closely resemble a clear material. This feature made it possible for the user to see what the shield designs would possibly look like and to troubleshoot any design issues like unrealistic shapes or sharp edges. Solid Works also can calculate the volume and surface area of complex continuous volumes like those of the eye shields; this capability was used to determine the volume and surface area of each of the shield designs.

## 3.2 Simulation Geometry and Materials

### *3.2.1 Head and Eye Model*

The results of this study rely heavily on the head and eye geometry and composition. It is essential that the simulated phantom accurately models the geometry of the head and eyes in order to assure that the results can be applied to real world scenarios. The head and eye geometry for this study was largely adopted from Behrens et al [20-21]. In their recent papers Behrens et al analyzed dose conversion coefficients for photon and electron exposure to the human eye lens using computer simulated models. The head and eye models used in this work were recently developed specifically to address dose to the human lens, and this made them ideal for use in this study. The geometry and materials of the Behrens et al model are based on information adopted internationally by the ICRP [20].

### *3.2.2 Geometry and Materials of the Head*

The geometry and materials of the head were taken from Behrens et al [20]. This head geometry was adapted from Kramer et al [27], however instead of using elliptical surfaces to define the model geometry, Behrens et al modeled the geometry of the head with intersecting cylinders and spheres. This simplification closely matches the elliptical geometry while streamlining the implementation of the model in MCNP5. The dimensions of the head model are defined as the mean value between the ADAM and EVA phantoms with the intention of using a model that represents both genders [20]. The material of the head consists of ICRU four-element tissue with a density of 1.11 g/cm$^3$. Behrens et al deduced this mean density from ICRP 103 [20]. Table 3.1 lists the exact elemental mass fraction values that were used in MCNP5 to define the material and density of the head. The head is modeled as homogenous tissue and does not contain bones or other details because

this simplification did not create any systematic deviation with anthropomorphic phantoms according to Behrens et al [20].

Table 3.1: Material and Density of the Head

| Density ($g/cm^3$) | 1.11 |
|---|---|
| Element | Mass Fraction (%) |
| H | 10.1 |
| C | 11.1 |
| N | 2.6 |
| O | 76.2 |

The Behrens et al head model was selected for this work for several reasons. 1) The model was initially developed specifically to study eye lens dose in humans, and this made it suitable for use as the model on which to test radiation shielding eyewear. 2) The model geometry and materials are based in the scientific literature and have been used to publish recent scientific studies [20-21]. 3) As seen in Figure 3.1, the head model has sufficient facial details, like eye sockets and a protrusion which resembles a nose, to model the eye shields. 4) It was possible to build the head model in MCNP5 with basic surfaces like spheres, cylinders, planes, and cones.

The geometry of the head is made up of four sections including the upper head, the middle head, the lower head, and the eye sockets. Implementation of the head model in MCNP5 followed the following citation from Behrens et al [20].

- Upper part of the head: two quarter spheres connected with a half cylinder, z > 84.5 cm.

Midpoints of the two spheres: (x, y, z) = (0 cm , ±1.95 cm , 84.5 cm)

Radii of the two spheres: r = 7.2 cm. Valid values for y: |y| > 1.95 cm

Cylinder along the y-axis: r = 7.2 cm. Valid values for y: |y| ≤ 1.95 cm.

- Middle part of the head: three intersecting cylinders along the z-axis.
  Only the region that is covered by all three cylinders is taken as the volume, 71.6 cm < z ≤ 84.5 cm.
  Two cylinders: midpoints and radii: (x , y) = (±3.036 cm , 0 cm) and r = 10.79 cm
  Third cylinder: midpoint and radius: (x , y) = (0 cm , 0 cm) and r = 9.7 cm
- Lower part of the head: 68 cm < z ≤ 71.6 cm.
  The rear part is constructed in the same way as the middle part of the head; however, only values for y > 0 cm are valid.
  The front part consists of one cylinder:
  midpoint and radius: (x , y) = (0 cm , −0.79 cm) and r = 7.79 cm; only values for y ≤ 0 cm are valid.
- The centers of the eyeballs are located at the following positions in the head: (x, y, z) = (±3 cm, −7.4 cm, 81.25 cm). In order to represent the eye sockets, a section of the head in the form of a cone made of vacuum is cut out in front of each eye.
  The cones are defined as follows:
  Apexes: (x, y, z) = (±3 cm, −5.4 cm, 81.25 cm). The axes lie parallel to the y-axis.
  Opening angle: $30^0$. Only values for y < −7.4 cm are taken.

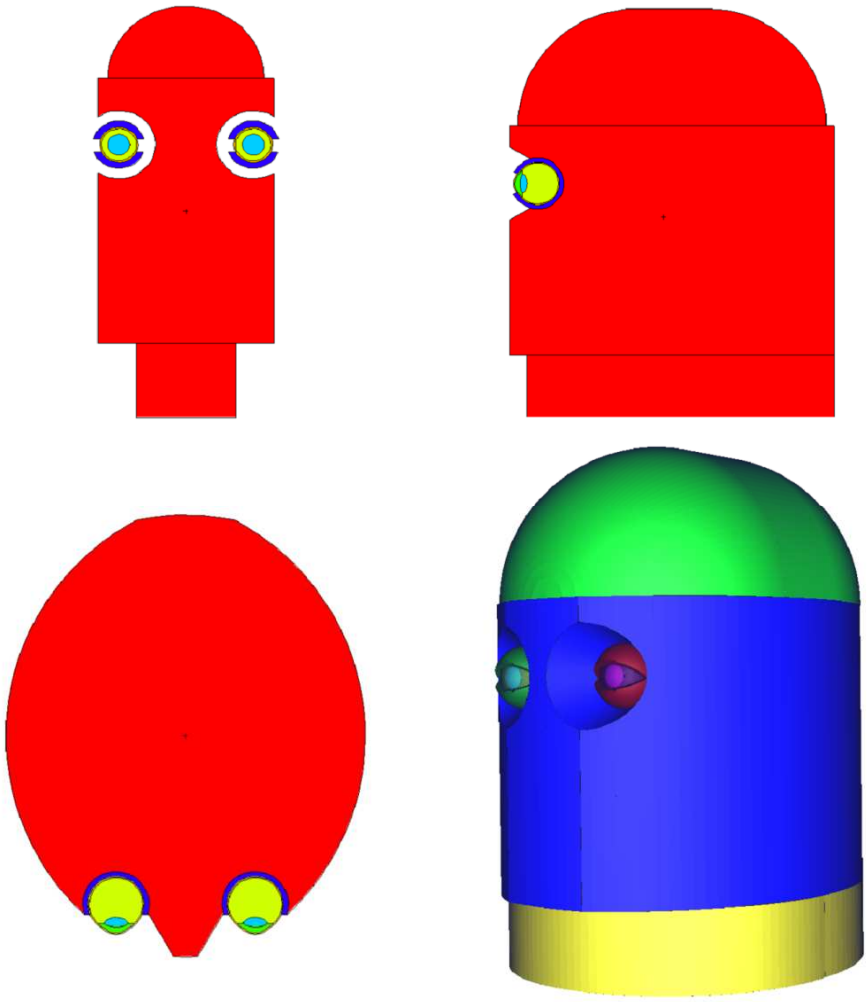

Figure 3.1: Four views head and eye model used in MCNP5 created with Visual Editor. Top Left: view of the model in the x/z plane through the center of the eyes. Top Right: view of the model in the y/z plane through the center of the left eye. Bottom Left: view of the model in the x/y plane through the center of the eyes. Bottom Right: three-dimensional view of the model showing the different pieces of the head and the eye within the eye socket

The head model and eye model used for this study are just part of a model that describes an entire person including legs, arms, and a torso. These additional pieces of the model were not included during this simulation campaign because they were not viewed as providing significant scatter contribution to eye lens dose. The average mean free path of the source photons used in the simulation ranged from 3.6 to 3.9 cm in the head. This made it unlikely that photons would scatter from the torso or the limbs to the lens of the eye. Several test simulations of this assumption were conducted to verify that the removal of the torso, and limbs would not affect the results of this work. Included in these tests was the likelihood that the x-ray operator may be wearing 0.5-0.75mm Pb equivalent apron and/or a thyroid collar. It was determined that the torso, arms, and legs could be removed from the simulation without affecting the results. With the torso and limbs removed from the simulation, it became possible for source photons to strike the underside of the head where the torso would have connected to the head. To account for this, a very thin cell (0.1mm) was defined extending from the bottom of the head to remove photons from the simulation that struck the bottom of the head. In this manner, no photon interactions occurring beneath the head were allowed in the simulations.

### *3.2.3 Geometry and Materials of the Eyes*

The geometry and materials of the eye were taken from Behrens et al [21]. This eye geometry was first developed by Charles and Brown [28] and was later adopted by the ICRP in 2002 [21]. The eye model includes five cells for each eye: the eye lens; cornea; vitreous humour; aqueous humour; and the eyelid. The volume of each eye lens is 0.2161 $cm^3$, and the mass is 0.2291 grams. The mean depth of the lens is 3.36mm which is very similar to the 3mm depth that the personal dose equivalent to the eye is measured [21]. Table 3.2 details the materials and densities of the eye model that were used in MCNP5. The materials and densities of the different components of the eye were compiled by Behrens et al and they are based on values

adapted from ICRU 1997 and ICRP 1975 [21]. The eye geometry in MCNP5 is defined by 24 surfaces (mostly spheres), and the left and the right eye are symmetrical. In Figure 3.2 the eye model used in MCNP5 is shown. In the 2D images of Figure 3.2 the lens is dark blue, the vitreous humour is light blue, the aqueous humour is green, the cornea is yellow, and the eye lid is orange. The eye socket and surrounding tissue are not shown.

Table 3.2: Materials and Densities of the Cells of the Eyes

| Density and Mass Fraction of the Materials of the Eye | | | | | |
|---|---|---|---|---|---|
| | Eye Lid | Lens | Aqueous Humour | Vitreous Humour | Cornea |
| Density ($g/cm^3$) | 1.09 | 1.06 | 1.003 | 1.0089 | 1.076 |
| Element | Mass Fraction (%) | | | | |
| H | 10 | 9.6 | 11.2 | 11.2 | 10.16 |
| C | 20.4 | 19.5 | | | 12.62 |
| N | 4.2 | 5.7 | | | 3.69 |
| O | 64.5 | 64.6 | 88.8 | 88.8 | 73.14 |
| Na | 0.2 | 0.1 | | | 0.07 |
| P | 0.1 | 0.1 | | | 0.07 |
| S | 0.2 | 0.3 | | | 0.2 |
| Cl | 0.3 | 0.1 | | | 0.07 |
| K | 0.1 | | | | |

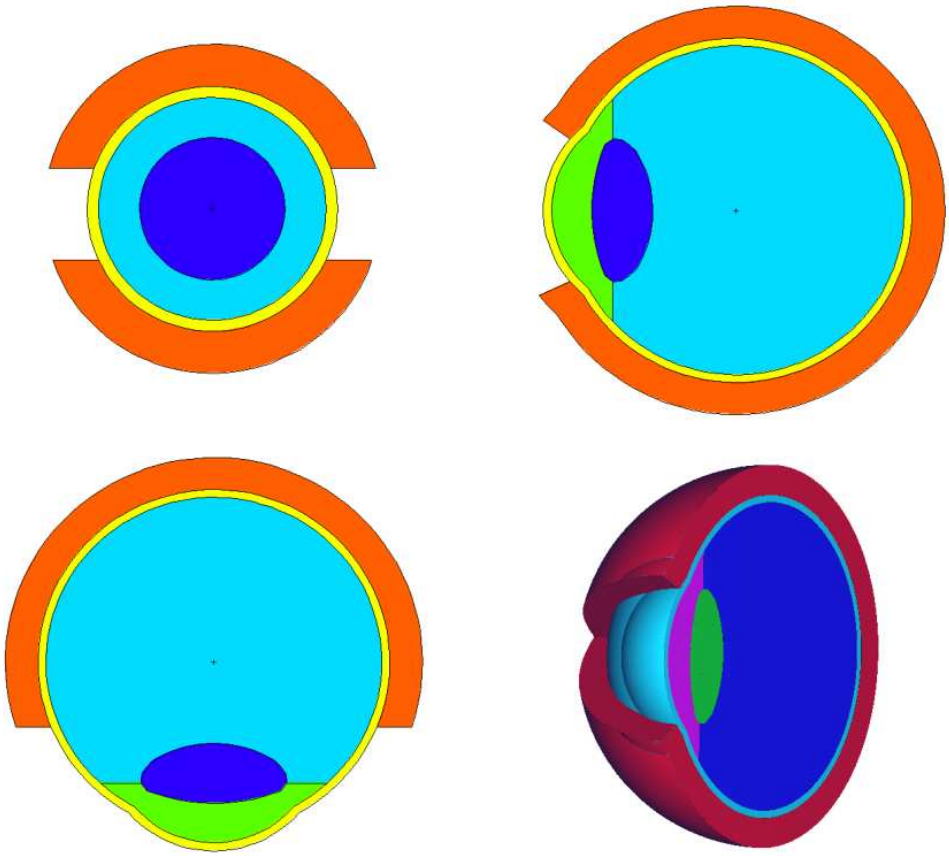

Figure 3.2: Four views of the eye model used in MCNP5 created with the Visual Editor. Top Left: view of the eye in the x/z plane through the center of the lens. Top Right: view of the eye in the y/z plane through the center of the lens. Bottom Left: view of the eye in the x/y plane through the center of the lens. Bottom Right: 3D view of the eye with half of the eye cut away to display the eye's interior structure

## 3.3 Photon Source Definition

### *3.3.1 MCNP5 Photon Spectrum*

The characteristics of the primary x-ray beam used during typical IC/IR procedures varies depending on procedure type, machine type, procedural factors, and a number of other considerations [8]. Consequently, there are a wide variety of x-ray machine voltages and filtrations used in practice. This study is not concerned with analyzing how different primary x-ray spectra affect the performance of varying eye shield designs. Therefore one x-ray voltage and filtration was chosen as a single representative for the many irradiation scenarios that are likely to be encountered. The ORAMED simulation campaign changed their simulated x-ray tube voltage from 60 to 110 kVp, and the filtrations from 3 to 6 mm Al and from 0 to 0.9 mm Cu [8]. Their simulation geometry included an x-ray machine, a patient phantom, and an image intensifier. However, simulating all of these components requires a significant amount of computing power and is not practical for running many slightly different simulations [8]. It is far less computationally expensive to directly input the scattered photon spectrum incident on the eye rather than the primary un-scattered x-ray beam into MCNP5 if this information is known. In 1996, Marshall et al [22] performed a series of scattered x-ray field measurements with a liquid nitrogen cooled planar germanium detector using a Picker Vector 70 x-ray generator. The scattered x-ray spectrum was measured at a distance of 50cm from an anthropomorphic pelvis phantom and at scatter angles of $90^0$ and $45^0$ to the incident x-ray beam. Marshal et al measured the scattered photon field from 12 individual x-ray tube configurations with tube voltages of 60-110 kVp and a filtration of 2.6mm of Al. The 85 kVp under-couch spectrum was selected from this data as the best representative for the photon source spectrum for this study. The 85 kVp scattered photon spectrum falls into the middle of tube voltages expected in IC/IR suites, and the under-couch geometry is more common than the over-couch

geometry [8]. Figure 3.3 shows a graph of both of the MCNP5 input photon spectra adapted from Marshal et al.

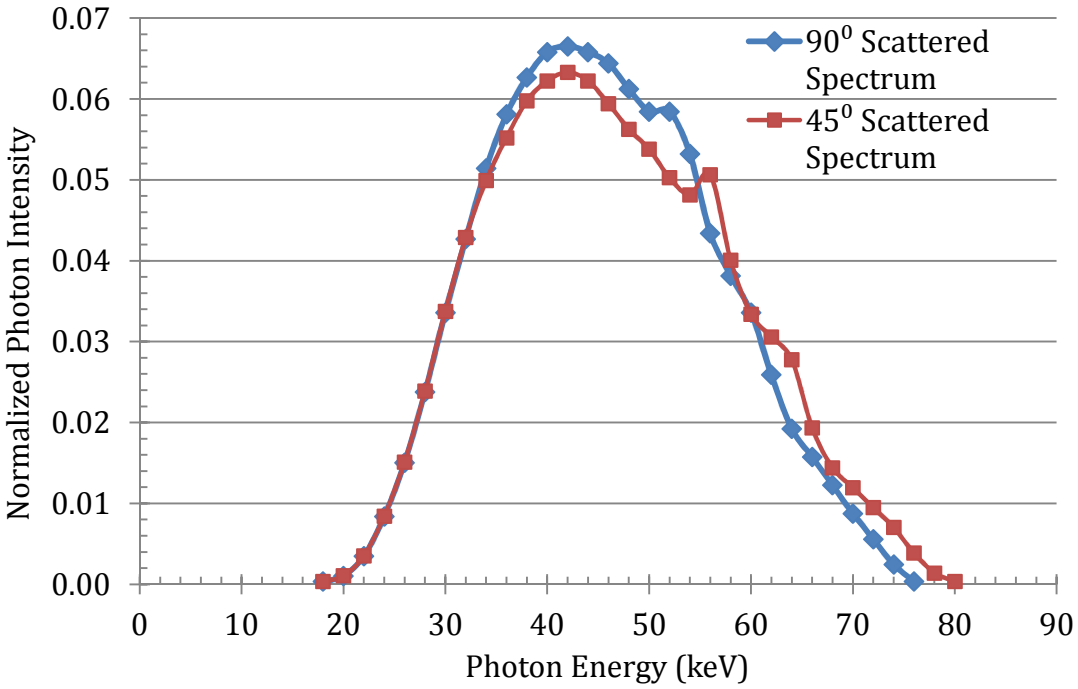


Figure 3.3: MCNP5 Photon Source Spectrum

*3.3.2 Source Distance, Angles, and Biasing*

Using the photon spectrum incident on the eye for the MCNP5 photon source greatly streamlined the simulation environment and allowed for quicker computing of the simulations. However, the spectral data taken from Marshal et al only had scattered photon data at a distance of 50cm from the phantom and scatter angles of $90^0$ and $45^0$. One goal of this work is to analyze how the irradiation angle of the head affects the performance of x-ray eye shields. Angular response is important to understanding how well an eye shield protects the eye from radiation. So to

adequately cover the irradiation angles likely in an IC/IR suite, eight evenly spaced photon source positions were chosen to analyze shield performance. The scattered photon spectrum from Marshal et al was modeled as a point source at a distance of 50cm from the center of the left eye lens. The photon source was moved radially about the left eye lens to eight separate source positions. The source positions are shown in Table 3.3 and correspond to positions at $0^0$, $30^0$, $60^0$, and $90^0$ in the x/y plane at the $90^0$ and $45^0$ irradiation angles.

For each shield design simulated with MCP5, eight separate input files were created to model the eight separate source positions. This could have created some time consuming input file manipulation if not managed properly. To streamline the production of MCNP5 input files the photon source was modeled as a point source rather than a volume or a plane source. With a point source in MCNP5 the source position and bias vector were the only two parameters that had to be changed in the input file to test a shield design at all eight source positions. For this study, a point source was determined to be an appropriate approximation and it aided in the efficient creation of over 100 MCNP5 input files.

MCNP5 allows the user to define the source energy distribution and frequency. The continuous 85 kVp spectrum data from Marshall et al was sampled for absolute frequency at every 2 keV. This method of sampling the continuous scattered photon spectrum yielded 30 photon energies for the $90^0$ scatter angle and 32 photon energies for the $45^0$ scatter angle. The 2 keV gap between sampled photon energies provided adequate resolution to account for the subtle peaks and valleys in the continuous photon spectrum. Each photon spectrum was normalized so that the individual photon emission frequencies totaled to one, and the values were entered into the MCNP5 input file according to which irradiation scenario was being tested.

Table 3.4 lists the source photon energies and frequencies for each irradiation angle. The source photons range from 18 to 80 keV with the most common photon energy being 42 keV for both the $45^0$ and $90^0$ scatter angles.

Table 3.3: MCNP5 Source Positions and Directional Bias Vectors

| Source Position Normal to the Left Lens | | | | Source Bias Vector | | |
|---|---|---|---|---|---|---|
| Lateral Angle | x | y | z | x | y | z |
| $0^0$ | 3 | -58.25 | 81.25 | 0.00 | 1.00 | 0.00 |
| $30^0$ | 28 | -51.55 | 81.25 | -1.00 | 1.73 | 0.00 |
| $60^0$ | 46.3 | -33.25 | 81.25 | -1.73 | 1.00 | 0.00 |
| $90^0$ | 53 | -8.25 | 81.25 | -1.00 | 0.00 | 0.00 |

| Source Position $45^0$ below the Left Lens | | | | Source Bias Vector | | |
|---|---|---|---|---|---|---|
| Lateral Angle | x | y | z | x | y | z |
| $0^0$ | 3 | -43.61 | 45.89 | 0.00 | 1.00 | 1.00 |
| $30^0$ | 20.68 | -38.87 | 45.89 | -0.58 | 1.00 | 1.16 |
| $60^0$ | 33.62 | -25.93 | 45.89 | -1.00 | 0.58 | 1.16 |
| $90^0$ | 38.36 | -8.25 | 45.89 | -1.00 | 0.00 | 1.00 |

Table 3.4: MCNP5 Source Photon Spectra

| 85 kVp Beam Scattered at $90^0$ | | | 85 kVp Beam Scattered at $45^0$ | | |
|---|---|---|---|---|---|
| X-ray energy (KeV) | relative intensity | normalized intensity | X-ray energy (KeV) | relative intensity | normalized intensity |
| 18 | 0.005 | 0.0004 | 18 | 0.005 | 0.0004 |
| 20 | 0.015 | 0.0011 | 20 | 0.015 | 0.0011 |
| 22 | 0.050 | 0.0035 | 22 | 0.050 | 0.0035 |
| 24 | 0.120 | 0.0084 | 24 | 0.120 | 0.0084 |
| 26 | 0.215 | 0.0151 | 26 | 0.215 | 0.0151 |
| 28 | 0.340 | 0.0238 | 28 | 0.340 | 0.0239 |
| 30 | 0.480 | 0.0336 | 30 | 0.480 | 0.0338 |
| 32 | 0.610 | 0.0427 | 32 | 0.610 | 0.0429 |
| 34 | 0.735 | 0.0515 | 34 | 0.71 | 0.0499 |
| 36 | 0.830 | 0.0581 | 36 | 0.785 | 0.0552 |
| 38 | 0.895 | 0.0627 | 38 | 0.850 | 0.0598 |
| 40 | 0.940 | 0.0658 | 40 | 0.885 | 0.0622 |
| 42 | 0.950 | 0.0665 | 42 | 0.900 | 0.0633 |
| 44 | 0.940 | 0.0658 | 44 | 0.885 | 0.0622 |
| 46 | 0.920 | 0.0644 | 46 | 0.845 | 0.0594 |
| 48 | 0.875 | 0.0613 | 48 | 0.800 | 0.0563 |
| 50 | 0.835 | 0.0585 | 50 | 0.765 | 0.0538 |
| 52 | 0.835 | 0.0585 | 52 | 0.715 | 0.0503 |
| 54 | 0.760 | 0.0532 | 54 | 0.685 | 0.0482 |
| 56 | 0.620 | 0.0434 | 56 | 0.720 | 0.0506 |
| 58 | 0.545 | 0.0382 | 58 | 0.570 | 0.0401 |
| 60 | 0.480 | 0.0336 | 60 | 0.475 | 0.0334 |
| 62 | 0.370 | 0.0259 | 62 | 0.435 | 0.0306 |
| 64 | 0.275 | 0.0193 | 64 | 0.395 | 0.0278 |
| 66 | 0.225 | 0.0158 | 66 | 0.275 | 0.0193 |
| 68 | 0.175 | 0.0123 | 68 | 0.205 | 0.0144 |
| 70 | 0.125 | 0.0088 | 70 | 0.170 | 0.0120 |
| 72 | 0.080 | 0.0056 | 72 | 0.135 | 0.0095 |
| 74 | 0.035 | 0.0025 | 74 | 0.100 | 0.0070 |
| 76 | 0.005 | 0.0004 | 76 | 0.055 | 0.0039 |
| | | | 78 | 0.020 | 0.0014 |
| | | | 80 | 0.005 | 0.0004 |

MCNP5 allows isotropic point sources to be directionally biased in order to direct more source particles towards the region of interest, in this case the lens of the eye. The source photons are weighted according to their initial direction so as to allow all tallies to maintain units per source particle [23]. Due to the relatively large distance (50cm) between the point source and the area of interest a large directional biasing factor was introduced. By doing this the simulation can score more tally information while using fewer particles than if no biasing was introduced. Source particles emitted in directions of more importance to the tally values are emitted with a higher frequency, but with a compensating lower weight than are the less important source particles [23]. This technique was employed to shorten run times and keep the relative error of the lens tallies as low as possible. The user can define source biasing based on several spatial particle distributions. For this study, source direction biasing was sampled from an exponential probability density function $p(\mu) = Ce^{K\mu}$, where C is a norming constant equal to $K/(e^{K}-e^{-K})$ and $\mu=\cos\theta$ where $\theta$ is an angle relative to the biasing vector [25]. The exponential biasing parameter K was set to 3.5. When K=3.5, about 50% of the source particles will be emitted from the source in a cone of $37^{0}$ about the biasing vector [26]. For every source position, the source directional biasing vector was defined to point the source directly at the left eye lens. Source particles are weighted according to their initial direction as to keep the tally values consistent with an isotropic point source value. In this manner, more source particles are likely to interact with the area of interest and the simulation will be able to provide better precision with fewer source particles and less computing time.

## 3.4 MCNP5 Tallies

### *3.4.1 *F8 Tally for the Lenses*

There were two MCNP5 output tallies considered for determining the dose to the eye lens, the F6 tally and the *F8 tally. The F6 tally gives the dose (MeV/g) deposited in a user defined cell. However, the F6 tally may not be appropriate for small cells like the lens of the eye. The F6 tally assumes that all electrons created locally in the tally cell deposit all of their energy locally [25]. This assumption makes a basic physics approximation and consequently allows for shorter simulation times. In contrast to the F6 tally, the *F8 (MeV) tally follows each secondary electron created until it completes its path length. No assumptions are made about where the electrons deposit their energy. The F6 tally can be thought of as a simplification of the *F8 tally. For this work the *F8 tally was chosen due to the fact that it offers a more detailed physics simulation for small volume tally cells. Since both lenses have the same volume and mass, the energy deposited in each lens is proportional to the lens dose. The *F8 tally is appropriate to use when taking ratios ($d_0/d$) to determine the protection factor of different shield designs. A *F8 tally was defined in MCNP5 for the left and the right lenses separately for every simulation, and every shield design yielded 16 *F8 data points for comparison against the other designs (eight source positions times two lenses).

### *3.4.2 Photon Flux Mesh Tally*

The *F8 tally data is important to quantifying how well a shield performs, but it is not well suited for visualizing the simulations and making iterative design modifications for future shield designs. It became apparent early on in the simulation campaign that visualizations of the shield simulations were necessary to fully understand the irradiation scenarios and identify the weaknesses of the eye

shield in question. MCNP5 allows the user to superimpose a 3D mesh on top of the simulation geometry to create a mesh of cells from which to gather data. The user can define the three-dimensional position of the mesh as well as the number of mesh cells in each direction (x, y, z). MCNP5 only allows the mesh tally to measure particle flux through the mesh cells so the mesh tally was defined to provide the photon flux through each cell of the mesh. The photon flux data taken by the mesh tally can be plotted with the MCPLOT command in MCNP5 once the simulation is completed. The mesh tally plots provide color-scaled visualizations of the photon flux throughout the simulation geometry. In particular, the mesh tally data offers the ability to visualize areas of high and low photon flux throughout the head and shield geometry. These mesh tally images were used to make changes to the shield design according to these observations. A large and fine mesh tally requires a large amount of computer memory, and this was a limiting factor to the resolution that the mesh tally could provide. The mesh used for all simulations in this study contained over 3.7 million mesh cells and utilized well over half of the available memory on the computer while simulations were running. The output mesh tally files (MCTAL) are also very large (up to 800Mb) once the simulation is complete because they contain detailed flux data for every one of the mesh tally cells.

Immediately after every simulation run was completed, MCNP5 prompted the user for mesh tally plotting commands. For every shield design and every source angle four images were taken of the mesh tally flux data for analysis. Two images were taken in the y/z plane centered on the lens of the left and the right eye respectively. One image was taken in the x/y plane intersecting the center of both lenses, and one image was taken in the x/z plan intersecting the center of both lenses. These images were analyzed carefully and used to identify weaknesses in shield designs and make subsequent changes to the shields. The mesh tally visualizations were vital to the ability to qualitatively observe the performance of the varying shields designs.

## 3.5 Shield Design Methodology

### *3.5.1 Material of the Shields*

Eye shields used for protecting the human eye lens from scattered x-rays are typically made of leaded glass and usually have a lead equivalency of 0.50-0.75mm [11]. For this study it was necessary to model several shield designs and thicknesses for their shielding abilities. The material used for the shield in the MCNP5 simulations was selected to be elemental lead. By selecting lead as the shield material instead of leaded glass, leaded acrylic, or a combination of materials allowed all of the shield thicknesses to be compared with each other without introducing error due to the use of different shielding materials. In short, rather than using complex materials to model a shield with a certain lead equivalency in MCNP5, lead was used as the shield material at the desired thickness of lead equivalence.

Figure 3.4: Image of the pair of safety glasses used to model the classic eye shield

### *3.5.2 Shielding Scenarios for Comparison*

For this study several standard shielding scenarios were conducted in order to compare the later shield designs to some basic irradiation scenarios. The first standard simulation was the unshielded scenario where MCNP5 was executed without an eye shield defined in the geometry. The data from this scenario were used in the calculations of the protection factors and used to analyze how the lens dose changes with irradiation angle when no shield is present. Secondly, a commonly used style of protective eyewear (Figure 3.4) was modeled in MCNP5 to compare results with a recent study [11], as well as to determine how the other shield designs compared to a common eye shield with 0.75mm lead equivalent lenses and 0.35 mm lead-equivalent side shields. The third standard scenario referred to as the "Full Face" was modeled as a full-face shield of 0.10mm lead to determine the maximum amount of protection a material of 0.10mm lead equivalence can provide to the wearer.

### *3.5.3 Iterative Shield Design*

An iterative design methodology was employed for the design and testing of the subsequent shield models in MCNP5. Iterative design involves steady manipulations of design parameters based on simulation performance from previous iterations of the design, and it is a useful technique for developing new or previously untested ideas [29]. To properly apply the fundamentals of an iterative design methodology to radiation shielding eyewear it was necessary to follow a structured approach. As a shield design was completed it was simulated in MCNP5 at all eight source positions. The results of the simulation were compared with the unshielded lens dose data, the classic shield, and the big shield; and the flux mesh tally images were investigated for any shielding weaknesses. Once the previous shield had been thoroughly analyzed a new shield design was produced. The new shield was

designed to address specific issues or weaknesses observed in the previous design, or to explore a new solution. In this manner, all of the shields were designed, simulated with MCNP5, analyzed for results, redesigned, and tested etc. until the desired shielding result was achieved.

## 3.6 Metrics for Shield Analysis

### *3.6.1 Protection Factor*

To numerically evaluate the shielding capabilities of each shield design, an average protection factor (APF) was calculated for each shield at every source angle. The protection factor has been defined as the ratio of the unshielded lens dose to the shielded lens dose. For each shield design there were eight source angles and thus sixteen separate protection factors (one for each lens in each simulation). For the sake of having an overall shield rating it was necessary to combine these protection factors into a single rating for the total performance of the shield. The APF was taken as the average of the 16 individual protection factors for each shield design. This protection factor describes the performance of the eye shield under circumstances where each source position is encountered with the same frequency. The individual protection factors were also analyzed for more information about the total APF.

### *3.6.2 Weighted Protection Factor*

The average protection factor does not account for the fact that certain source positions contribute more lens dose to the total dose than other positions in the unshielded configuration. This means that source positions that do not largely contribute to the eye lens dose are considered to be of equal importance to eye shield performance according to the average protection factor. To address the

assumption of equal dose contribution that the APF makes, a Weighted Protection Factor (WPF) was also calculated. The WPF is calculated similarly to the average PF except that instead of averaging the sixteen individual PF measurements, they are weighted according to the unshielded dose contribution associated with each individual source position. In this way, the individual protection factors can be combined to form a single metric that evaluates the shield according to its dose-weighted importance.

Both the average APF and the WPF assume that the head is irradiated from all source positions equally. This is most likely not the case in practice, however it is an appropriate way to rate shields against one another as to their performance in a radiation field from all eight source positions.

### *3.6.3 Qualitative Analysis*

In addition to the quantitative protection-factor calculations, there was a significant amount of information to analyze in the form of flux mesh tally images. For every simulation run, four images were captured that were used in conjunction with the *F8 tally data to critique the performance of each shield design. The numerical data was useful to scale and rank the shields, but it did not provide much information about why a shield performed poorly in a certain area; this is where the mesh tally images were very useful. They showed color-scaled images of the photon flux in each irradiation scenario. The images were analyzed for areas where unshielded photons could interact with the eye, areas where the eye shield had insufficient coverage, and areas where the eye shield adequately shielded the incident photons.

# CHAPTER 4 – RESULTS AND DISCUSSION

For the purpose of clarity, the following terminology will be used when referencing the eight individual source positions used in this study (Figure 4.1). There were two vertical source positions used for the simulations. Relative to the lens of the left eye, the first is located in the x/y plane at a $90^0$ source angle, and the second is located at a $45^0$ source angle. For both of these vertical positions there are four lateral source positions which move around the head from the front at $0^0$, $30^0$, $60^0$, and $90^0$. Every source position is located 50cm from the center of the left eye lens. For example, the source position located 50cm directly in front of the left eye lens is located in the $90^0$ vertical position and the $0^0$ lateral position, and it is referred to as the 90-0 source position. The source position located $45^0$ below the left lens and all the way to the side of the head is referred to as the 45-90 source position. All source positions between these examples are referenced using a similar nomenclature.

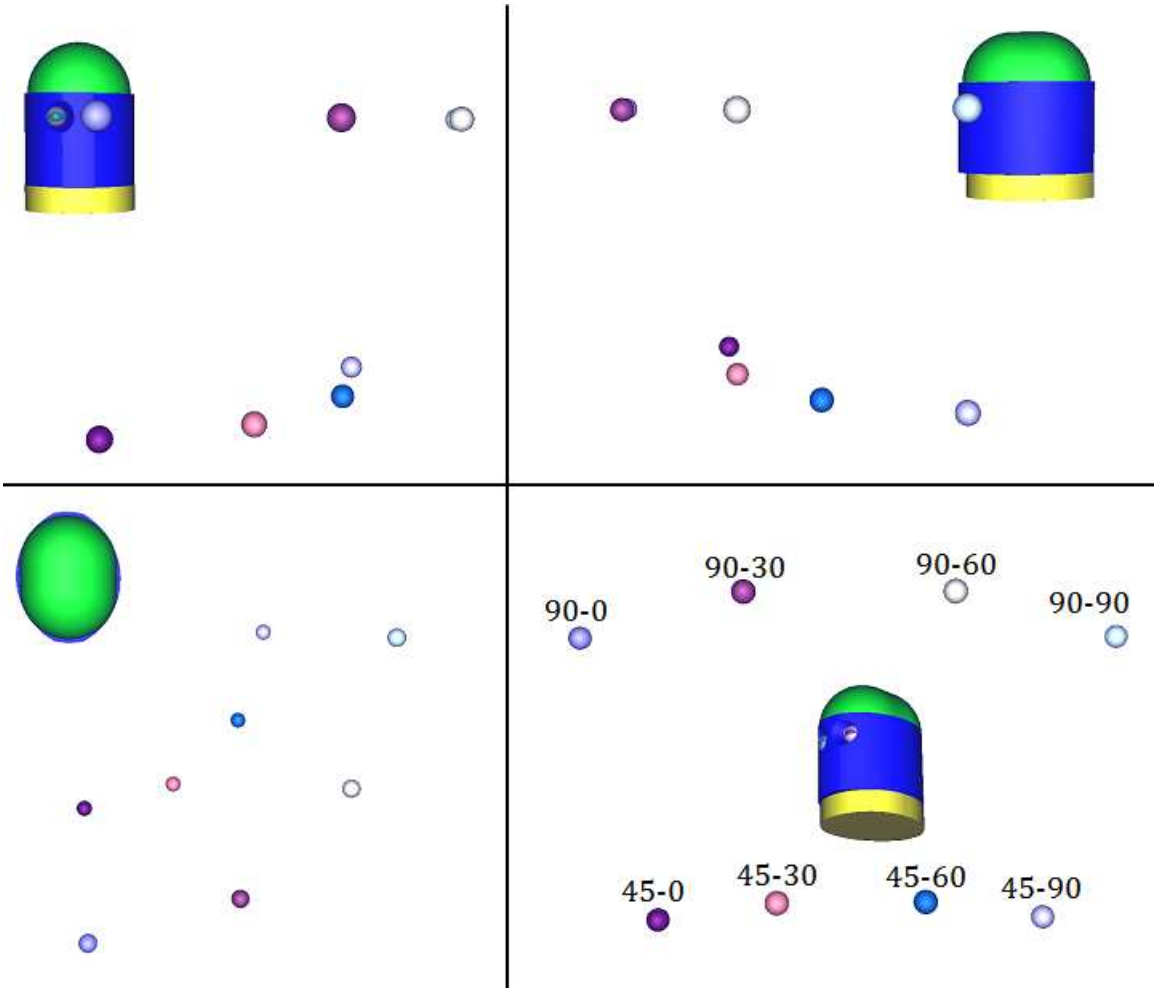


Figure 4.1: Source positions

## 4.1 No Shield

With the head and eyes in an unshielded configuration, several characteristics and trends in the energy deposition to the lens can be observed (Table 4.1). Dose to the left lens remains relatively constant at all eight source positions, and the left lens dose decreases only slightly as the source is moved from the front of the head to the side. However, dose to the left lens is slightly higher for the $90^0$ source positions than for the $45^0$ source positions. Dose to the right lens is comparable to that of the

left lens when the source is located in front of the head, but it quickly decreases as the source is moved around the head. As the photon source is positioned around the left side of the head, the head shields the right lens from photons and decreases the likelihood that they will reach the right lens.

Table 4.1: Energy deposited in the eye lenses in units of MeV in an unshielded configuration

| | $45^0$ Source Angle | | | |
|---|---|---|---|---|
| | Right Lens | Relative Error | Left Lens | Relative Error |
| $0^0$ | 2.51E-08 | 1.92% | 2.48E-08 | 1.90% |
| $30^0$ | 2.18E-08 | 2.03% | 2.53E-08 | 1.89% |
| $60^0$ | 1.08E-08 | 2.94% | 2.42E-08 | 1.94% |
| $90^0$ | 3.74E-09 | 5.01% | 2.10E-08 | 2.06% |
| | $90^0$ Source Angle | | | |
| | Right Lens | Relative Error | Left Lens | Relative Error |
| $0^0$ | 2.64E-08 | 1.87% | 2.62E-08 | 1.85% |
| $30^0$ | 2.30E-08 | 2.00% | 2.65E-08 | 1.83% |
| $60^0$ | 1.66E-08 | 2.34% | 2.56E-08 | 1.87% |
| $90^0$ | 6.63E-09 | 3.69% | 2.39E-08 | 1.93% |

| Total | Total Relative Error |
|---|---|
| 3.32E-07 | 0.52% |

## 4.2 Classic Shield

### *4.2.1 Classic Shield Design*

The "Classic Shield" was modeled after a commonly used style of radiation shielding eyewear (Figure 3.4 and 4.2). This shield design is typically manufactured with leaded glass lenses of 0.75mm lead equivalence, and it is available with optional 0.35mm lead equivalent side shields. The optional side shields are incorporated into

the MCNP5 model for the Classic Shield. The shield was placed as close as possible to the head without touching it. The side shields are modeled as a single piece with the front of the shield. No part of the frame was modeled. The total shield volume including the side shields is 4.51cm$^3$. The purpose for including this shield in the study was to model a commonly used shield design for performance comparisons to the subsequent shield designs. Appendix B contains exact geometry specifications contained within the MCNP5 input files for the Classic Shield, as well as every other shield design.

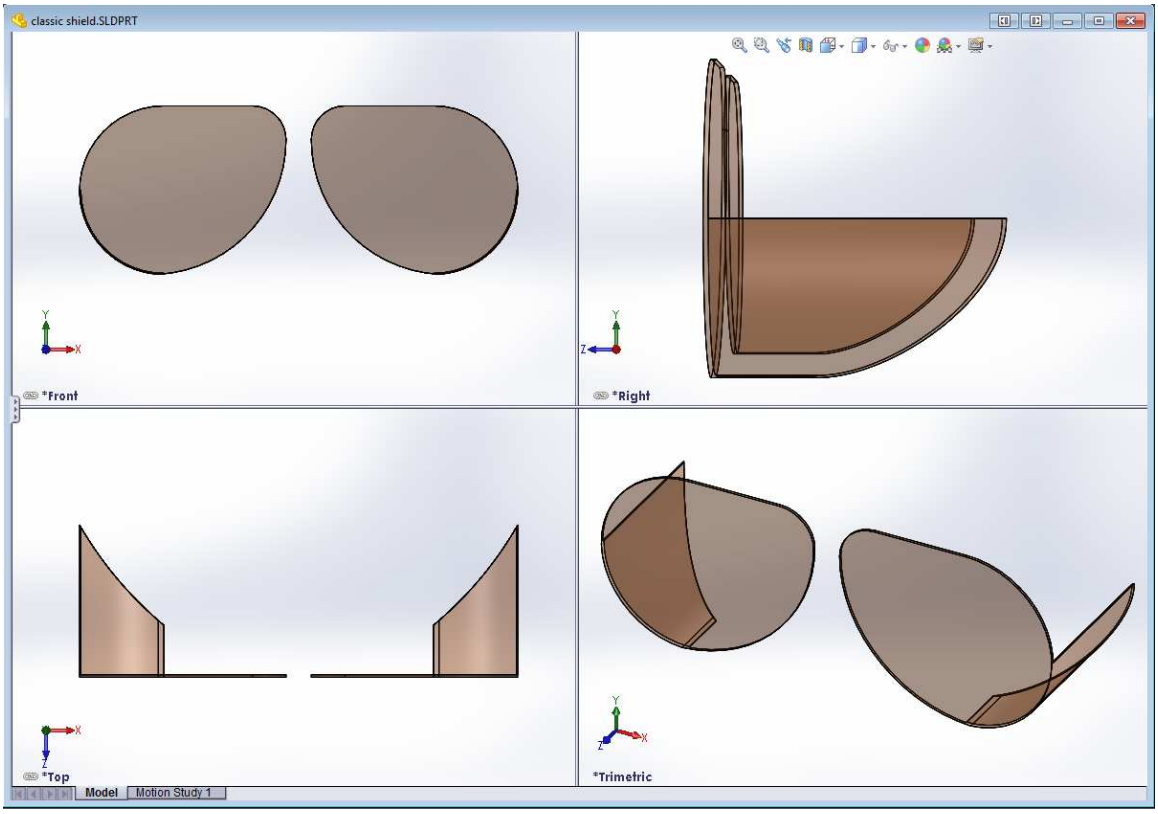


Figure 4.2: Image of the Classic Shield

*4.2.2 Classic Shield Performance*

In general, the Classic Shield performs very well when the source is located directly in front of the face; however, when the source is positioned where the shield has inadequate coverage of the eyes, the lenses are naturally less protected. In particular, the Classic Shield displays shielding weaknesses when the source is positioned to the side of the head in the 45-30, 45-60, 90-60, and 90-90 source positions (Table 4.2). At the 45-30, 45-60, and 90-60 source positions the right lens is left unprotected from photons passing through the nose opening. At the 90-90 source position, the side shields are unable to attenuate photons coming from the side of the head, and the left lens is essentially unshielded. The photon flux images for these source positions, as well as every flux image taken for the entire study can be found in Appendix A.

Table 4.2: Energy deposited in the eye lenses in units of MeV when the Classic Shield is modeled

| $45^0$ Source Angle | | | | |
|---|---|---|---|---|
| | Right Lens | Relative Error | Left Lens | Relative Error |
| $0^0$ | 3.99E-09 | 4.78% | 3.89E-09 | 4.85% |
| $30^0$ | 8.52E-09 | 3.28% | 3.65E-09 | 5.05% |
| $60^0$ | 1.04E-08 | 3.01% | 4.54E-09 | 4.55% |
| $90^0$ | 3.61E-09 | 3.69% | 5.12E-09 | 1.93% |
| $90^0$ Source Angle | | | | |
| | Right Lens | Relative Error | Left Lens | Relative Error |
| $0^0$ | 3.29E-09 | 5.30% | 3.11E-09 | 5.44% |
| $30^0$ | 3.27E-09 | 5.33% | 3.15E-09 | 5.22% |
| $60^0$ | 1.25E-08 | 2.71% | 4.57E-09 | 4.39% |
| $90^0$ | 6.18E-09 | 3.81% | 2.25E-08 | 1.99% |

| Total | Total Relative Error |
|---|---|
| 1.02E-07 | 0.92% |

## 4.3 Full Face Shield

### *4.3.1 Full Face Design*

The Full Face Shield (Figure 4.3) was simulated to determine how much protection a 0.1mm lead shield can be expected to provide with optimal shielding geometry. This geometry was determined to be a Full Face Shield that extends from the bottom of the head all the way to the top of the face, and extends half way around the head. The Full Face Shield is defined by two cylinders of 8.1cm and 8.11cm radius respectively. It was placed as close to the head as possible without touching it. The volume of shielding material is $3.74cm^3$, and the surface area is approximately $374cm^2$. Like the Classic Shield, the Full Face Shield was modeled for the purpose of making performance comparisons to the subsequent shield designs.

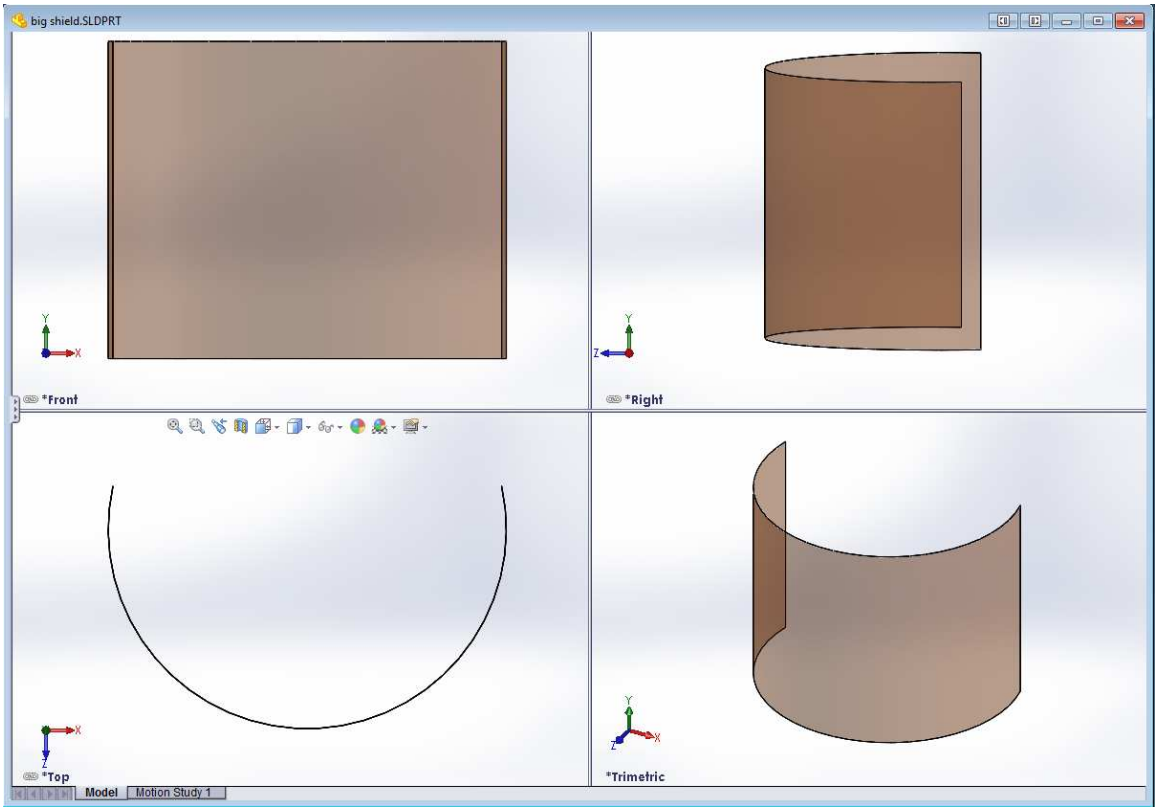


Figure 4.3: Scale image of the Full-Face shield

### *4.3.2 Full Face Performance*

The Full Face Shield was the most consistent shield tested at every source angle, and the dose trends across all source positions follow the unshielded dose trends. This shield performs especially well at the 45-60 source position due to the full coverage across the face which allows it to shield photons that could have passed through a nose opening. The large surface area of the Full Face Shield allows the shield to attenuate photons directed at the eyes from every source position. Dose values (Table 4.3) show the maximum amount of shielding performance that can be reasonably expected from a 0.1mm thick lead equivalent eye shield.

Table 4.3: Energy deposited in the eye lenses in units of MeV when the Full Face Shield is modeled

| $45^0$ Source Angle | | | | |
|---|---|---|---|---|
| | Right Lens | Relative Error | Left Lens | Relative Error |
| $0^0$ | 4.42E-09 | 4.57% | 5.04E-09 | 4.30% |
| $30^0$ | 2.91E-09 | 5.64% | 5.27E-09 | 4.17% |
| $60^0$ | 1.57E-09 | 7.74% | 4.74E-09 | 4.35% |
| $90^0$ | 9.21E-10 | 10.35% | 3.12E-09 | 5.23% |
| $90^0$ Source Angle | | | | |
| | Right Lens | Relative Error | Left Lens | Relative Error |
| $0^0$ | 7.40E-09 | 3.61% | 7.78E-09 | 3.45% |
| $30^0$ | 4.87E-09 | 4.50% | 8.26E-09 | 3.35% |
| $60^0$ | 2.70E-09 | 5.74% | 6.96E-09 | 3.61% |
| $90^0$ | 1.88E-09 | 7.21% | 5.00E-09 | 4.32% |

| Total | Total Relative Error |
|---|---|
| 7.28E-08 | 1.13% |

## 4.4 Shield #1

### *4.4.1 Shield #1 Design*

Shield #1 was designed with adaptability and simplicity as important design considerations (Figure 4.4). The general form of Shield #1 represents a very basic one-piece eye shield, and it lends itself to simple manipulations such as extending certain dimension, modifying the nose opening, or changing its position on the head. This shield was the initial design after which all subsequent eye shields were modeled. The nose opening was modeled to match the nose shape of the head model, and to be similar in shape to the Classic Shield nose cutout. Shield #1 has total volume of 4.24 $cm^3$ and a surface area of approximately 84.8 $cm^2$. The shield is 0.5mm of lead thick, 5 cm tall, and is defined by two cylinders of 8.1cm and 8.15cm in radius. The 0.5mm thickness was chosen to represent a shielding thickness

similar to currently available eyewear, and to investigate how different shield thicknesses affect shield performance.

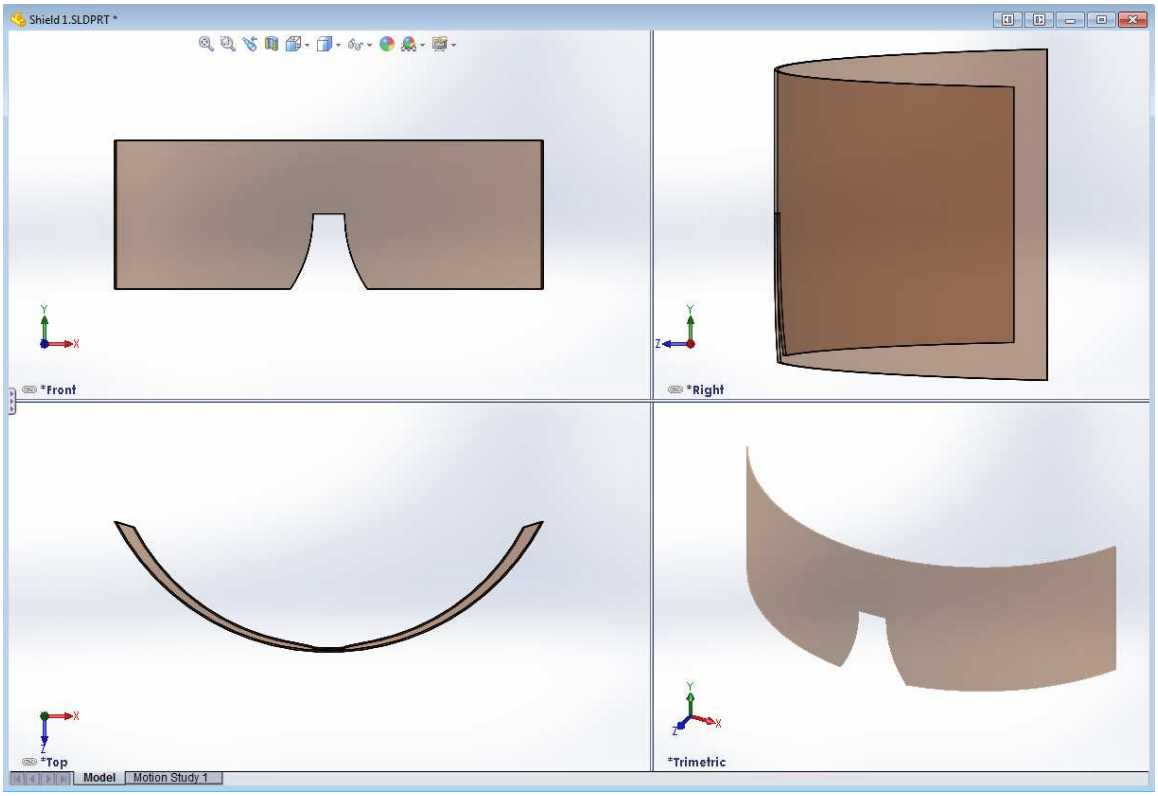


Figure 4.4: Images of Shield #1

### *4.4.2 Shield #1 Performance*

Dose data for Shield #1 (Table 4.4) shows that it has weaknesses at the 45-60, 45-90, and 90-60 source positions. These three source positions were responsible for lens doses about three times higher than at the other source positions for Shield #1. The 45-60 and 90-60 source position weaknesses are due to unshielded photons travelling through the nose opening and penetrating the face and eyes, and the photon flux images of the 45-90 source position showed insufficient coverage of the

shield on the side of the head below the eye. The photons were able to penetrate the head underneath the shield and travel through a thin layer of tissue before entering the lens of the eye.

Additional analysis of the photon flux images (see Appendix A) showed that the square-edged nose opening was larger than necessary and allowed a large amount of photons to pass through it. It is also likely that this design would not be very comfortable for the user. Additionally, the square-edged nose opening was positioned higher than the centerline of the lenses. This allowed photons to penetrate the head very near, if not directly in, the eyes at the 45-60 and 90-60 source positions, and this increased the right lens dose at these positions.

Table 4.4: Energy deposited in the eye lenses in units of MeV when Shield #1 is modeled

| $45^0$ Source Angle | | | | |
|---|---|---|---|---|
| | Right Lens | Relative Error | Left Lens | Relative Error |
| $0^0$ | 3.56E-09 | 3.58% | 3.51E-09 | 3.59% |
| $30^0$ | 3.56E-09 | 4.96% | 3.61E-09 | 5.09% |
| $60^0$ | 1.01E-08 | 3.05% | 3.69E-09 | 5.06% |
| $90^0$ | 3.93E-09 | 4.83% | 9.16E-09 | 3.17% |
| $90^0$ Source Angle | | | | |
| | Right Lens | Relative Error | Left Lens | Relative Error |
| $0^0$ | 2.74E-09 | 5.86% | 2.68E-09 | 5.88% |
| $30^0$ | 2.47E-09 | 6.09% | 2.83E-09 | 5.57% |
| $60^0$ | 6.74E-09 | 3.68% | 2.61E-09 | 5.86% |
| $90^0$ | 1.56E-09 | 7.68% | 3.22E-09 | 5.37% |

| Total | Total Relative Error |
|---|---|
| 6.59E-08 | 1.15% |

## 4.5 Shields #2 and #3

### *4.5.1 Shields #2 and #3 Design*

The design for Shield #2 (Figure 4.5) incorporated several changes from Shield #1. The curve of the shield was modeled to more closely fit the sides of the head. Shield #2 is defined by two cylinders of 7.1cm and 7.15cm radius. This allows the shield material to cover the face more effectively while reducing the shield volume. Rather than having excess material far away from the face, it is placed nearer to the head to have the greatest chance of shielding photons that would have otherwise entered the eyes. Shield #2 does not extend as far around the head as Shield #1. Although this will allow more photons to penetrate the side of the head near the eyes, it was observed in the flux images of Shield #1 that there was excess material on the side of the head. A weakness of Shield #1 is shown for the 45 degree source angles; it was clear that Shield #2 had to extend lower on the face in order to attenuate more photons that were contributing to lens dose. To implement this change, Shield #2 was made taller in the center and tapered upwards toward the side of the head. The shape of the nose opening was also changed slightly in an attempt to shield more photons from penetrating the center of the head. This included a rounded nose opening and a slightly larger nose opening radius to narrow the nose opening towards the bottom of the shield. The biggest change to the nosepiece was to lower the bridge by 1.25cm. This change was made to eliminate the high dose to the right lens in the 90-60 source position for Shield #1. The shield was placed lower on the face over all because the upper shielding material of Shield #1 was observed to be unnecessary, and the top of the shield was moved down by 1cm. The total shield volume of Shield #2 is 3.17$cm^3$ and the surface area is approximately 63.4 $cm^2$.

Shield #3 has the same overall shape as Shield #2, but the thickness has been reduced from 0.5mm to 0.1mm of lead. After the results of Shield #2 had been

analyzed it was determined that Shield #2 was a good candidate to investigate the effect of shield thickness on shield performance. Additionally, all of the shields simulated after Shield #2 had a thickness of 0.1mm of lead because it is possible to manufacture a 0.1mm lead equivalent eye shields out of leaded acrylic. The total shield volume of Shield #3 is 0.634 $cm^3$ and the surface area is approximately 63.4 $cm^2$.

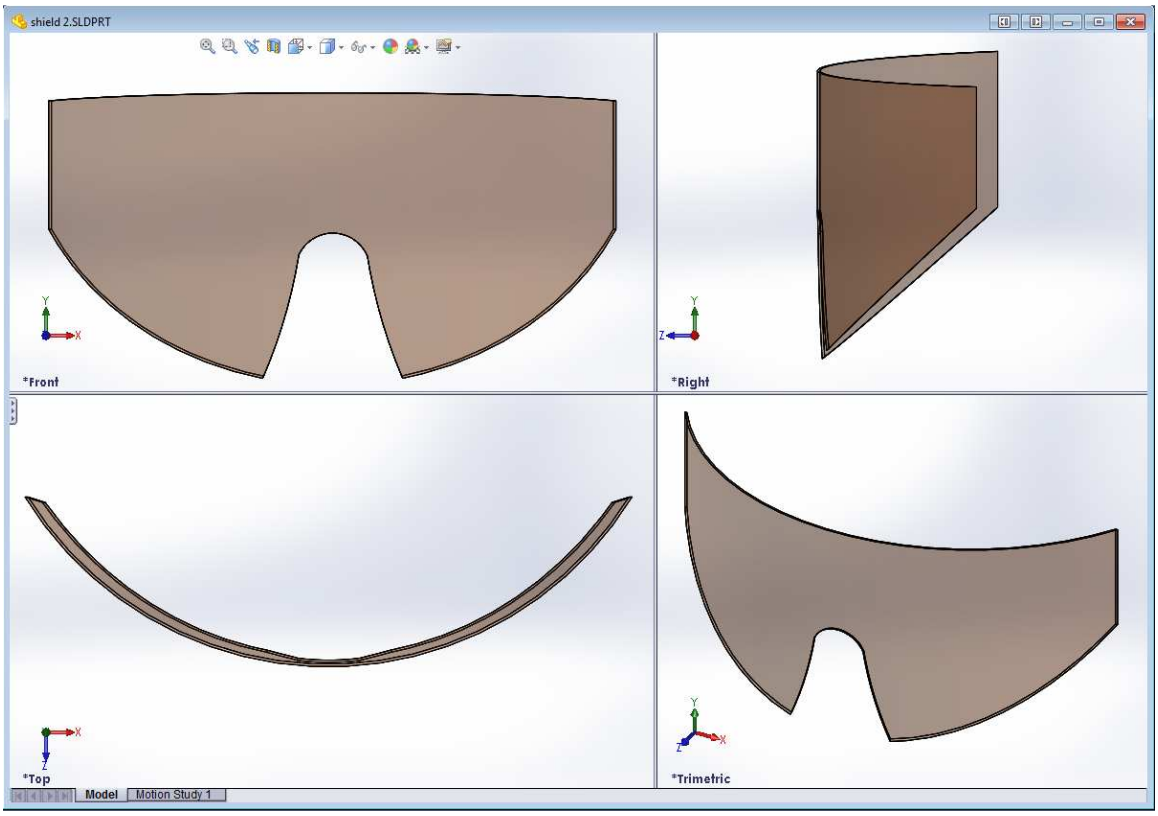


Figure 4.5: Images of Shields #2 and #3

*4.5.2 Shields #2 and #3 Performance*

The design changes made for Shields #2 and #3 performed well and somewhat as intended. Shield #2 provided about a 15% reduction in total eye lens dose while using 25% less material than Shield #1. This represents an excellent improvement in shielding performance, as well as optimization of the use of shielding material. Shield material that was deemed to be superfluous was removed from the design, and areas that appeared to require more shielding material were supplemented. The ability to reduce the amount of shielding material stems directly from the qualitative information gained from observing the photon flux images. The best shielding improvements over Shield #1 occurred at the 45-90 and 90-60 source positions. The lowered nose bridge allowed Shield #2 to effectively shield the photons that had previously directly entered the right eye lens in the 90-60 source position. The small position change made to the bridge lowered the right lens dose in this position by over 70% compared to Shield #1. In the 45-90 source position, the photon flux images revealed that Shield #2 adequately shielded photons from interacting in the left lens, and this reduced the dose from this source position by over 50%. The most pronounced weakness of Shield #2 is the 45-60 source position because the source photons are able to directly irradiate the right eye without any shielding, and this weakness is shared with the Classic Shield and Shield #1.

Shield #3 was modeled with the same shape as Shield #2 and 80% less shield thickness, yet it still provided good protection. The strengths and weaknesses of Shield #3 match Shield #2 except that Shield #3 allows higher lens dose due to its lower thickness. However, Shield #3 provides nearly half of the shielding performance of Shield #2 while utilizing just 20% of the shielding thickness, and it is clear that reducing shield thickness from 0.5 mm to 0.10 mm does not drastically reduce shield performance.

Table 4.5: Energy deposited in the eye lenses in units of MeV when Shield #2 is modeled

| | $45^0$ Source Angle | | | |
|---|---|---|---|---|
| | Right Lens | Relative Error | Left Lens | Relative Error |
| $0^0$ | 2.72E-09 | 5.73% | 2.98E-09 | 5.58% |
| $30^0$ | 2.68E-09 | 5.70% | 3.11E-09 | 5.45% |
| $60^0$ | 9.72E-09 | 3.10% | 3.52E-09 | 5.15% |
| $90^0$ | 3.52E-09 | 5.11% | 4.18E-09 | 4.60% |
| | $90^0$ Source Angle | | | |
| | Right Lens | Relative Error | Left Lens | Relative Error |
| $0^0$ | 2.95E-09 | 5.63% | 3.16E-09 | 5.43% |
| $30^0$ | 2.33E-09 | 6.24% | 3.41E-09 | 5.06% |
| $60^0$ | 1.85E-09 | 7.00% | 3.40E-09 | 5.10% |
| $90^0$ | 1.89E-09 | 6.85% | 4.36E-09 | 4.60% |

| Total | Total Relative Error |
|---|---|
| 5.58E-08 | 1.28% |

Table 4.6: Energy deposited in the eye lenses in units of MeV when Shield #3 is modeled

| | $45^0$ Source Angle | | | |
|---|---|---|---|---|
| | Right Lens | Relative Error | Left Lens | Relative Error |
| $0^0$ | 6.02E-09 | 3.90% | 6.72E-09 | 3.69% |
| $30^0$ | 4.62E-09 | 4.39% | 7.26E-09 | 3.56% |
| $60^0$ | 9.97E-09 | 3.06% | 7.16E-09 | 3.57% |
| $90^0$ | 3.55E-09 | 5.10% | 6.17E-09 | 3.77% |
| | $90^0$ Source Angle | | | |
| | Right Lens | Relative Error | Left Lens | Relative Error |
| $0^0$ | 8.66E-09 | 3.32% | 9.01E-09 | 3.20% |
| $30^0$ | 5.92E-09 | 4.05% | 9.92E-09 | 3.03% |
| $60^0$ | 3.56E-09 | 4.99% | 8.66E-09 | 3.21% |
| $90^0$ | 2.88E-09 | 5.64% | 7.79E-09 | 3.43% |

| Total | Total Relative Error |
|---|---|
| 1.08E-07 | 0.92% |

## 4.6 Shield #4

### *4.6.1 Shield #4 Design*

The design of Shield #4 (Figure 4.6) is very similar to the shape of Shield #2 and #3 except for a few small changes. These changes were motivated by photon flux image observations of Shields #2 and 3, and were made to the sides and bottom of the shield. The nose opening, the upper plane of the shield, and the shield position on the head remain unchanged from previous designs. Shield #4 was modeled with slightly less material on the sides and slightly more on the bottom of the shield. The bottom edge of the shield was modeled using a round surface rather than a plane (like Shields #2 and #3), and the sides of the shield were moved back by 2.5mm each. These small changes were implemented in an attempt to limit the amount of photons that can penetrate the head directly below the shield from the $45^0$ source positions, as well as to shield more photons striking the side of the head. The volume and surface area are slightly higher than Shield #3 due to these subtle changes, and are $0.65cm^3$ and $65cm^2$, respectively. The shield thickness is 0.1mm of lead. The design of Shield #4 incorporated very small changes to the previous design to investigate how these small changes to shielding coverage can affect shield performance.

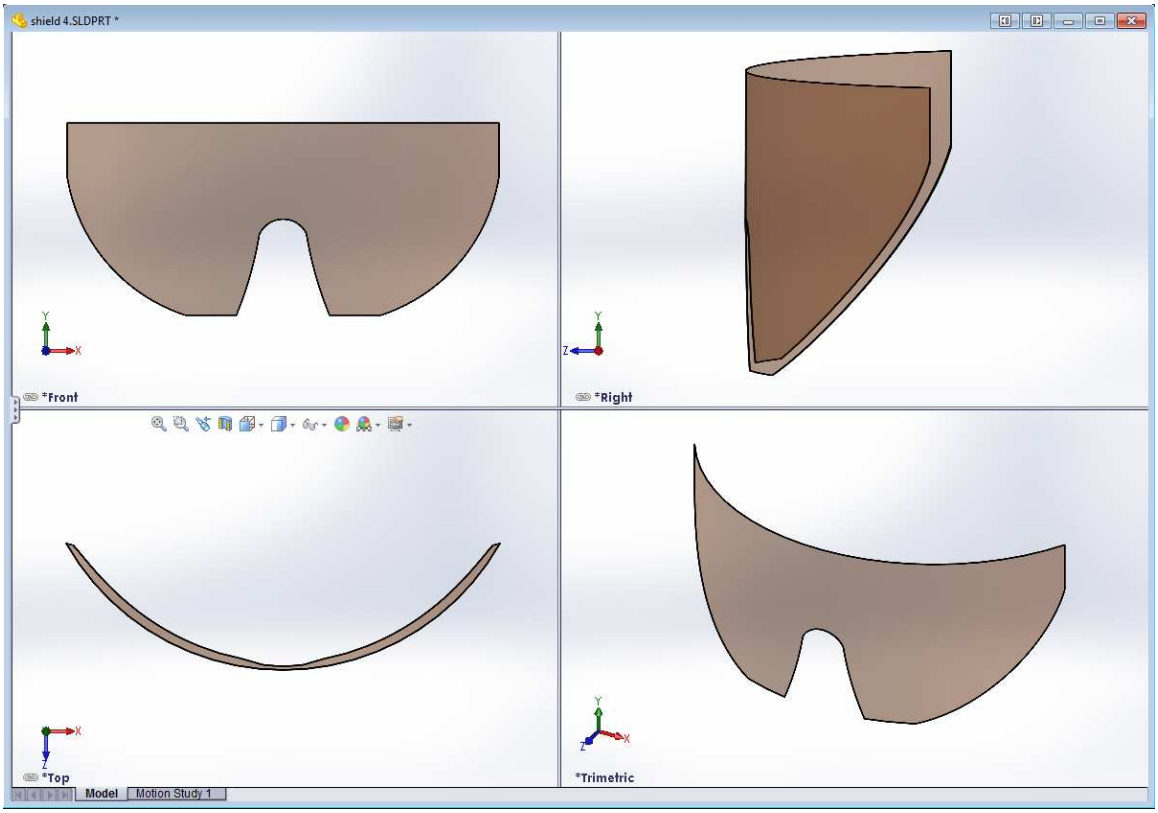


Figure 4.6: Images of Shield #4

*4.6.2 Shield #4 Performance*

The small changes that were reflected in the design of Shield #4 resulted in no significant change to the total eye lens dose when compared with the results of Shield #3. In addition, there are no source positions where the Shield #4 performance differs significantly from Shield #3. Shield #4 has a similar weakness to the previous shields at the 45-60 source position for the right lens.

Table 4.7: Energy deposited in the eye lenses in units of MeV when Shield #4 is modeled

| | $45^0$ Source Angle | | | |
|---|---|---|---|---|
| | Right Lens | Relative Error | Left Lens | Relative Error |
| $0^0$ | 5.96E-09 | 3.92% | 6.65E-09 | 3.71% |
| $30^0$ | 4.60E-09 | 4.40% | 7.23E-09 | 3.56% |
| $60^0$ | 9.94E-09 | 3.06% | 6.93E-09 | 3.61% |
| $90^0$ | 3.54E-09 | 5.10% | 6.04E-09 | 3.82% |
| | $90^0$ Source Angle | | | |
| | Right Lens | Relative Error | Left Lens | Relative Error |
| $0^0$ | 8.63E-09 | 3.33% | 8.99E-09 | 3.20% |
| $30^0$ | 5.92E-09 | 4.05% | 9.83E-09 | 3.04% |
| $60^0$ | 3.56E-09 | 4.99% | 8.71E-09 | 3.20% |
| $90^0$ | 2.91E-09 | 5.62% | 7.75E-09 | 3.44% |

| Total | Total Relative Error |
|---|---|
| 1.07E-07 | 0.92% |

## 4.7 Shield #5

### *4.7.1 Shield #5 Design*

Shield #5 (Figure 4.7) was designed and tested to explore the shielding behavior of an eye shield defined by spherical surfaces. The radius of the outer surface of the spherical shield is 7.11cm, and the inner surface radius is 7.1cm. This shape was developed by manipulating several spherical radii and positions until one was established that was positioned similarly on the face to the previous shields. The nose opening is defined by the same surfaces as those used in Shields #2-4. The side coverage was again moved back slightly compared to Shield #4. Due to the spherical nature of the shield, the top, bottom, and sides of the shield fit very close to the face, while the shield protrudes away from the face in the center. The protruding center of the shield has the effect of narrowing the nose opening at high angles of incidence

where previous shields have struggled to attenuate an adequate quantity of source photons. The volume and surface area of Shield #5 are 0.95cm$^3$ and 95cm$^2$, respectively, and the shield thickness is 0.1mm of lead.

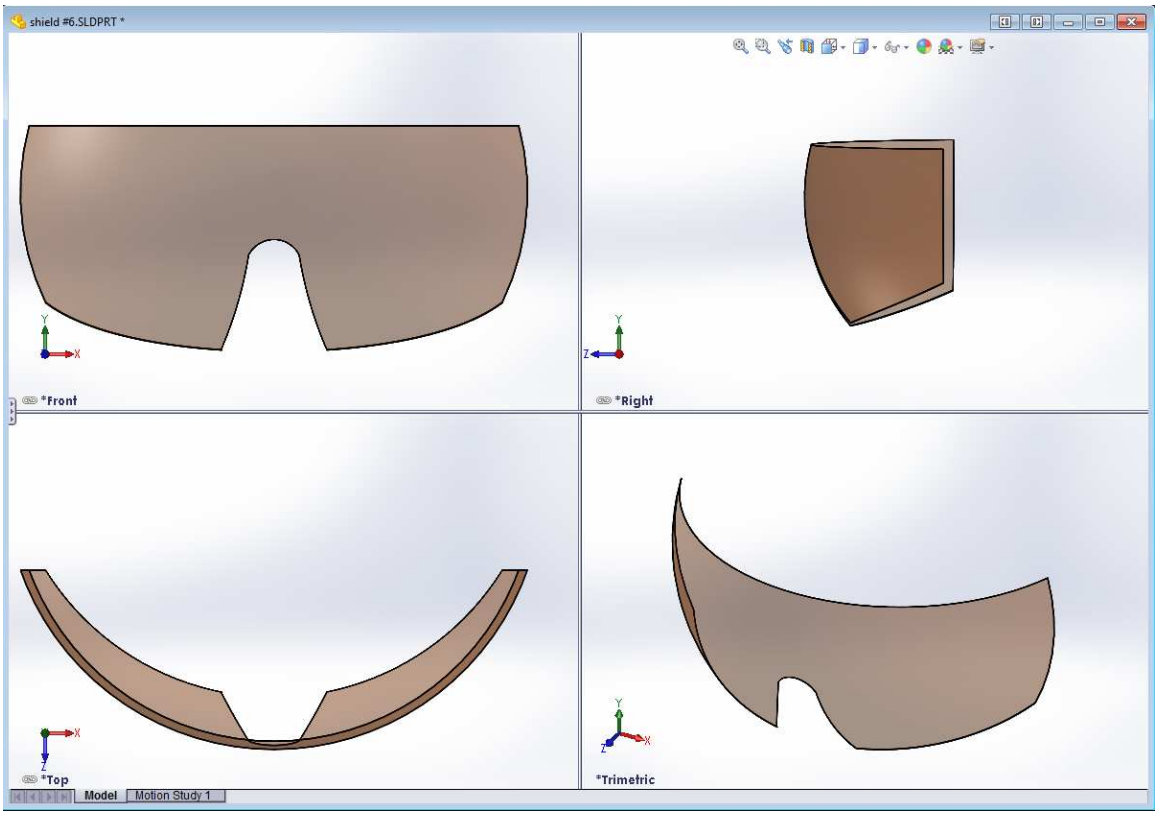


Figure 4.7: Images of Shield #5

*4.7.2 Shield #5 Performance*

Shield #5 performed slightly worse than Shields #3 and #4 with regard to total eye lens dose even though Shield #5 uses about a third more shielding material. In general, Shield #5 displays similar shielding performance across all source angles, and at the 45-60 source position Shield #5 protects the right lens slightly better

than Shields #3 and #4. The narrow nose opening appears to have had the desired result, but the performance at other source positions was not improved.

Table 4.8: Energy deposited in the eye lenses in units of MeV when Shield #5 is modeled

| | $45^0$ Source Angle | | | |
|---|---|---|---|---|
| | Right Lens | Relative Error | Left Lens | Relative Error |
| $0^0$ | 6.97E-09 | 3.62% | 7.39E-09 | 3.52% |
| $30^0$ | 9.18E-09 | 3.18% | 7.64E-09 | 3.46% |
| $60^0$ | 9.38E-09 | 3.17% | 7.49E-09 | 3.48% |
| $90^0$ | 3.60E-09 | 5.04% | 7.18E-09 | 3.52% |
| | $90^0$ Source Angle | | | |
| | Right Lens | Relative Error | Left Lens | Relative Error |
| $0^0$ | 8.31E-09 | 3.38% | 8.56E-09 | 3.28% |
| $30^0$ | 6.28E-09 | 4.50% | 8.98E-09 | 4.09% |
| $60^0$ | 4.26E-09 | 4.58% | 8.49E-09 | 3.24% |
| $90^0$ | 3.06E-09 | 5.53% | 8.14E-09 | 3.35% |

| Total | Total Relative Error |
|---|---|
| 1.15E-07 | 0.92% |

## 4.8 Shield #6

### *4.8.1 Shield #6 Design*

Shield #6 (Figure 4.8) utilizes the same shape as Shield #5 except for an additional piece designed around the nose opening. Due to the spherical shape of the shield, there is room between the shield and the face to model additional shielding around the nose opening. This additional material is intended to further reduce the size of the opening at high angles of incidence in an attempt to reduce the right lens dose at the 45-60 source position. The additional material around the nose does not touch

the face. In fact it is no closer to the face than Shield #2 and #3. The material is simply an extension of the nose opening towards the face, and it has a thickness of 0.1mm.

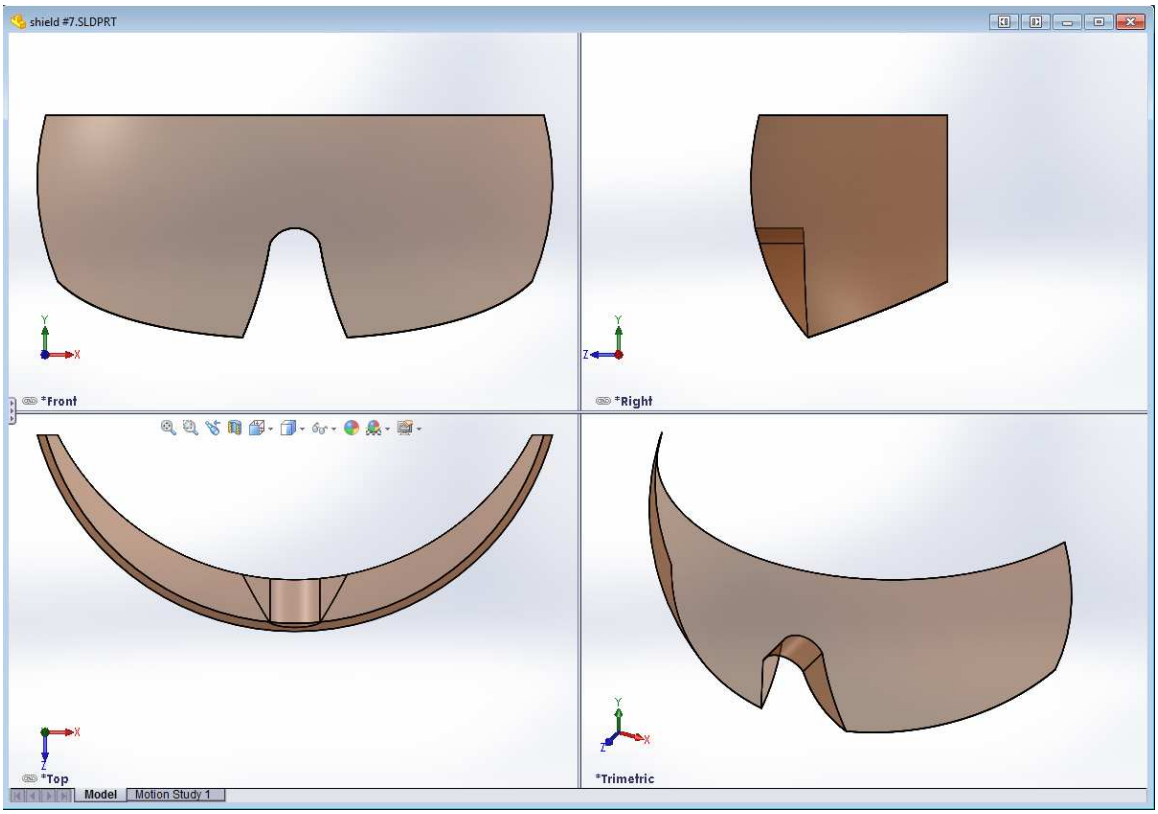


Figure 4.8: Images of Shield #6

*4.8.2 Shield #6 Performance*

The additional shielding material in the nose opening of Shield #6 did not contribute to significant dose reduction compared to Shield #5 except for the right lens dose at the 45-30 source angle (Table 4.9). The additional material worked as expected by shielding photons from the angled source positions, but it only had an effect on the

right lens at the 45-30 source position and not the 45-60 position. The photon flux images still show photons passing through the nose opening at these positions, and without completely covering this opening, as with the Full Face Shield, it is unlikely that a large fraction of the photons can be shielded with a conventional shield design.

Table 4.9: Energy deposited in the eye lenses in units of MeV when Shield #6 is modeled

| | $45^0$ Source Angle | | | |
|---|---|---|---|---|
| | Right Lens | Relative Error | Left Lens | Relative Error |
| $0^0$ | 6.70E-09 | 3.70% | 7.25E-09 | 3.56% |
| $30^0$ | 5.91E-09 | 3.94% | 7.58E-09 | 3.47% |
| $60^0$ | 9.20E-09 | 3.20% | 7.48E-09 | 3.48% |
| $90^0$ | 3.51E-09 | 5.13% | 7.18E-09 | 3.52% |
| | $90^0$ Source Angle | | | |
| | Right Lens | Relative Error | Left Lens | Relative Error |
| $0^0$ | 8.30E-09 | 3.38% | 8.50E-09 | 3.29% |
| $30^0$ | 6.11E-09 | 3.95% | 9.26E-09 | 3.16% |
| $60^0$ | 4.24E-09 | 4.60% | 8.48E-09 | 3.24% |
| $90^0$ | 3.06E-09 | 5.53% | 8.14E-09 | 3.35% |

| Total | Total Relative Error |
|---|---|
| 1.11E-07 | 0.91% |

## 4.9 Eye Lens Energy Deposition Profiles

For each shield there are 16 data points presented in this section that reflect the data in Tables 4.1-4.9. The data are divided into four charts depicting the left and right lenses for each vertical source position ($45^0$ and $90^0$). The smoothed lines connecting the data points were included to aid in the visualization of the shield performance, but they are not based on additional data between the data points. Error bars are presented only for the No Shield scenario because all other error bars were at least as small. The numerical energy deposition error data can be found in Tables 4.1-4.9.

### *4.9.1 Right Lens for the $45^0$ Source Positions*

Figure 4.8 depicts the right lens energy deposition profiles for the $45^0$ source positions. The unshielded lens dose trends quickly downwards as the photon source is moved around to the opposite side of the head at the 45-90 source position. At the 45-60 and 45-90 source positions, every shield offered little or no protection over the unshielded dose, except for the Full-Face Shield. For the 45-60 source position the shields are unable to perform well because they allow photons to pass through the nose opening directly into the eye. Significant modification to the area around the nose opening would be necessary to adequately shield the right lens from this source position. Shields #5 and #6 were the best performers, other than the Full-Face for this source position because their spherical designs slightly narrow the nose opening. For the 45-90 source position, the majority of the shielding of the right lens is provided by the head, and the shields did not differentiate themselves significantly. The Full-Face shield is able to outperform the other shields at the 45-60 and 45-90 because it has superior coverage over the entire face, and it does not have a nose opening.

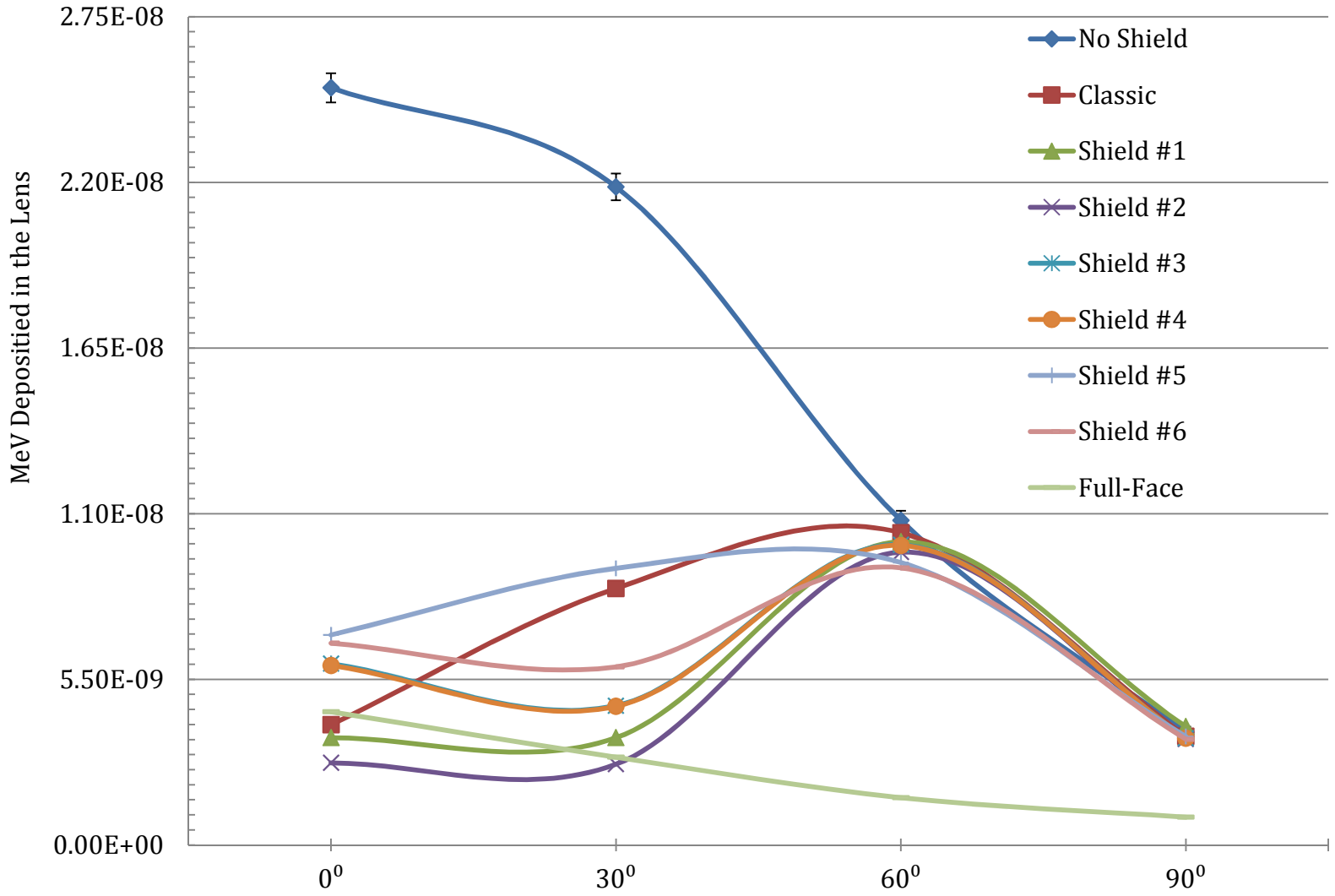


Figure 4.9: Energy deposition profiles for the right lens for all shields at all $45^0$ source positions

*4.9.2 Left Lens for the $45^0$ Source Positions*

Figure 4.9 depicts the left lens energy deposition profiles for the $45^0$ source positions. The unshielded dose remains relatively constant across all lateral source angles except for a slight dip at the 45-90 source position. In general, every shield follows this trend. The 0.1mm thick Shields #3-6 all perform similarly with only slight deviations at the 45-0 and 45-90 source positions. The Full Face Shield performs better than the other 0.1mm thick shields at every lateral source positions, and better than all shields at the 45-90 position. Again, this is due to its large surface area. Although the Classic Shield is 0.75mm thick, it performs consistently worse than the 0.5mm thick Shield #2. This suggests that optimal shield geometry can provide better shielding performance than high shield thickness alone. Shield #2 provides much better coverage on the face below the eyes where the $45^0$ source photons are likely to hit. The Classic Shield is thicker, but the shield cannot work on photons that never encounter its surface. For Shield #1, the relatively high lens dose for the 45-90 source position was due to inadequate coverage of the left eye from the side, and this weakness was addressed on subsequent shield design

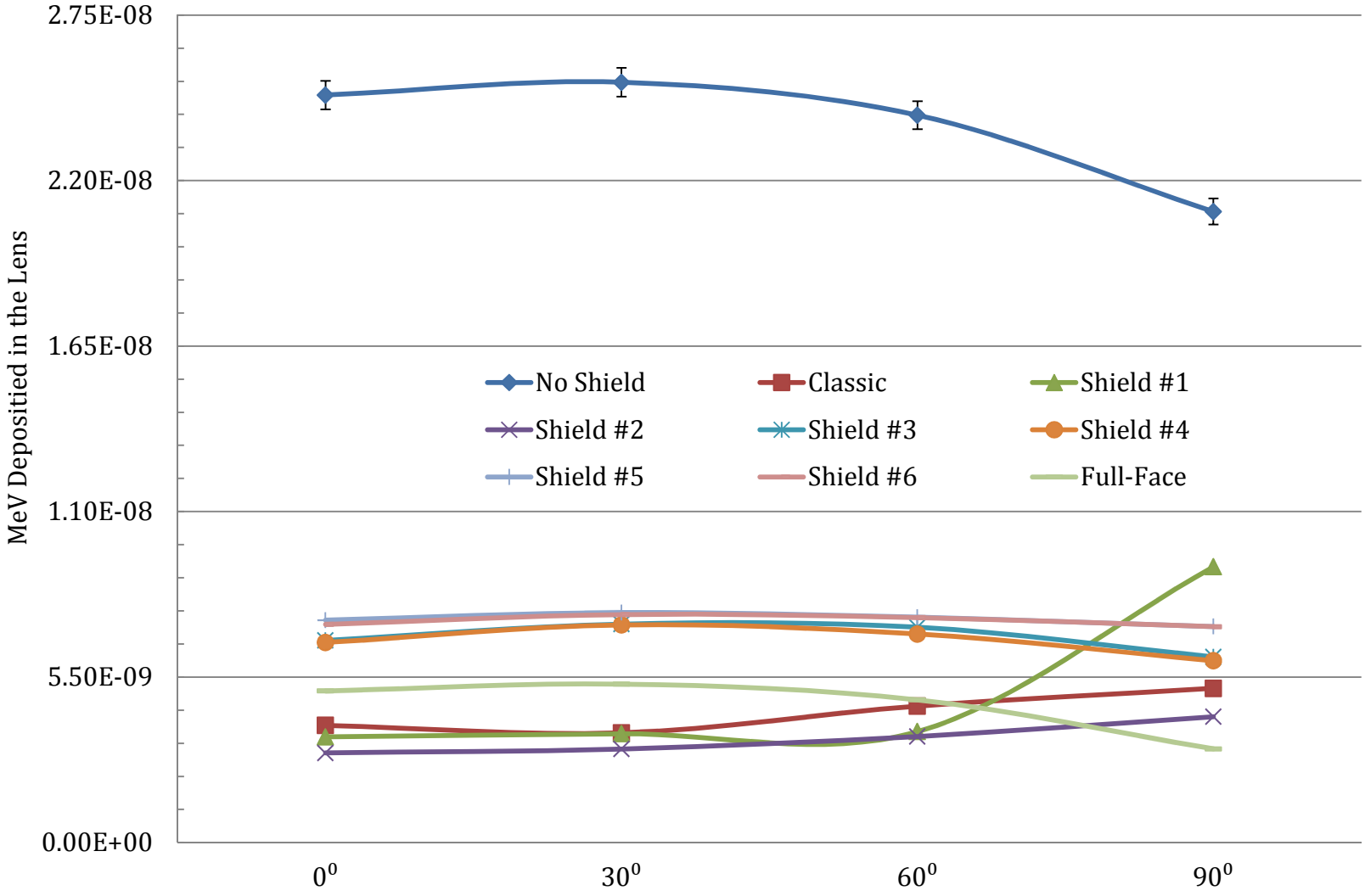


Figure 4.10: Energy deposition profiles for the left lens for all shield at all $45^0$ source positions

### *4.9.3 Right Lens for the $90^0$ Source Positions*

Figure 4.10 depicts the right lens energy deposition profiles for the $90^0$ source positions. The unshielded dose trends downward as the source is moved around the head in a similar fashion to the unshielded right lens dose for the $45^0$ source positions. The 0.1mm thick shields perform consistently across all lateral source positions with the Full Face Shield performing the best. The Classic Shield and Shield #1 display high doses for the 90-60 source position because both shields allow photons to pass through the nose opening and penetrate the right eye directly. Shield #2 is the best overall performer for these source positions. The $90^0$ source positions do not pose as serious of a challenge to the coverage of a shield, rather, shield thickness holds significant weight. Shield #2 possesses the best combination due to its 0.5mm thickness and good lateral coverage across all $90^0$ source positions.

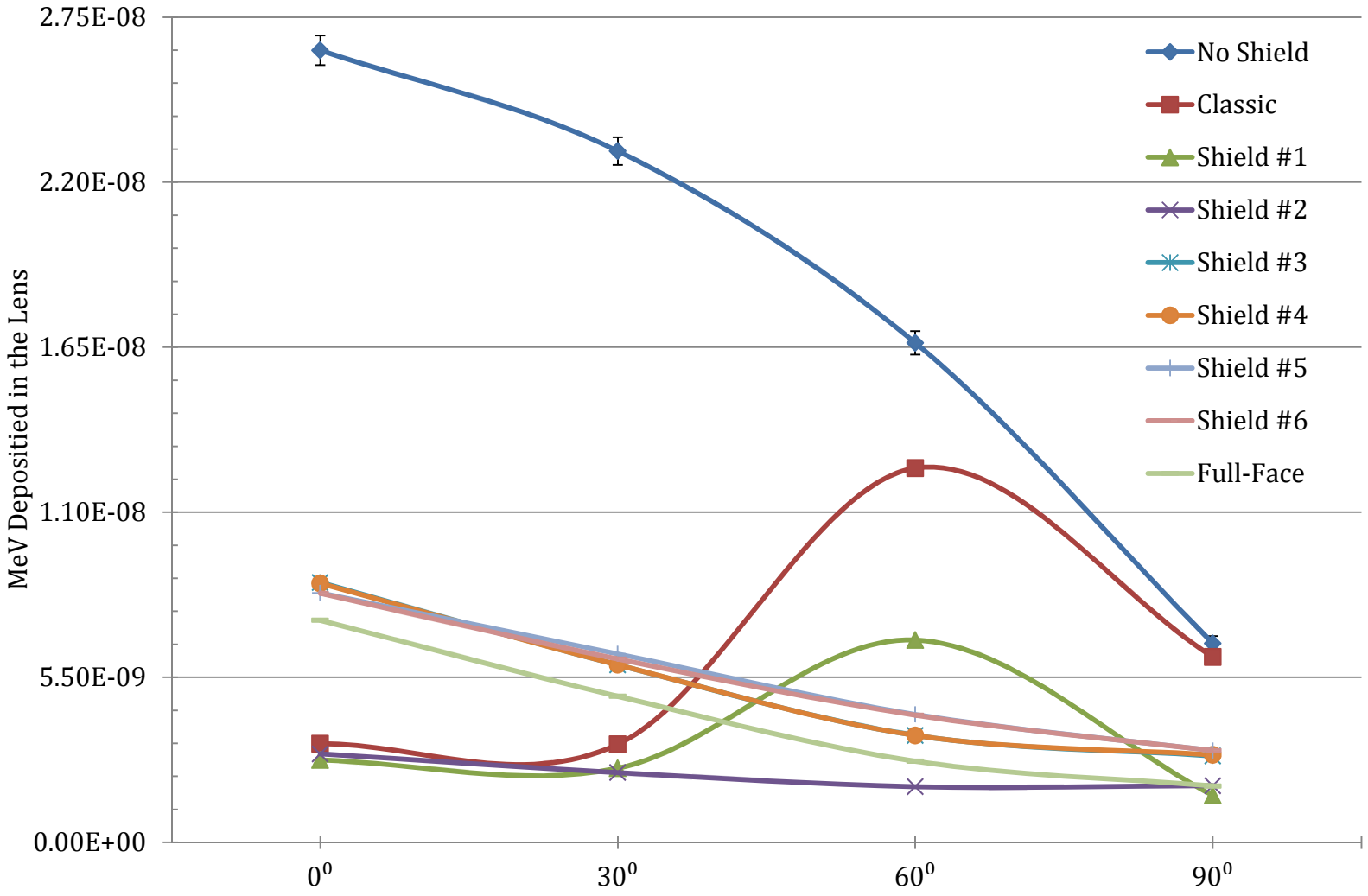


Figure 4.11: Energy deposition profiles for the right lens for all shields at all $90^0$ source positions

*4.9.4 Left Lens for the $90^0$ Source Positions*

Figure 4.11 depicts the left lens energy deposition profiles for the $90^0$ source positions. The unshielded dose remains relatively level across the lateral source positions with a slight downward slope. Again, the 0.1mm thick shields all display similar performance characteristics with the Full Face Shield performing the best. The Classic Shield (0.75mm) and Shields #1 and #2 (0.5mm) perform similarly in the 90-0, 90-30, and 90-60 source positions, but the Classic Shield displays a significant weakness at the 90-90 source position. The side shields of the Classic Shield were not high enough on the face to shield photons directed at the eye from the side, and this resulted in a minimal amount of protection to the left lens. This was the greatest weakness of the Classic Shield, but it could be easily remedied by modeling the side shields slightly higher on the face. This figure also suggests that at the $90^0$ source positions, shield thickness holds more importance to shield performance than the shield geometry.

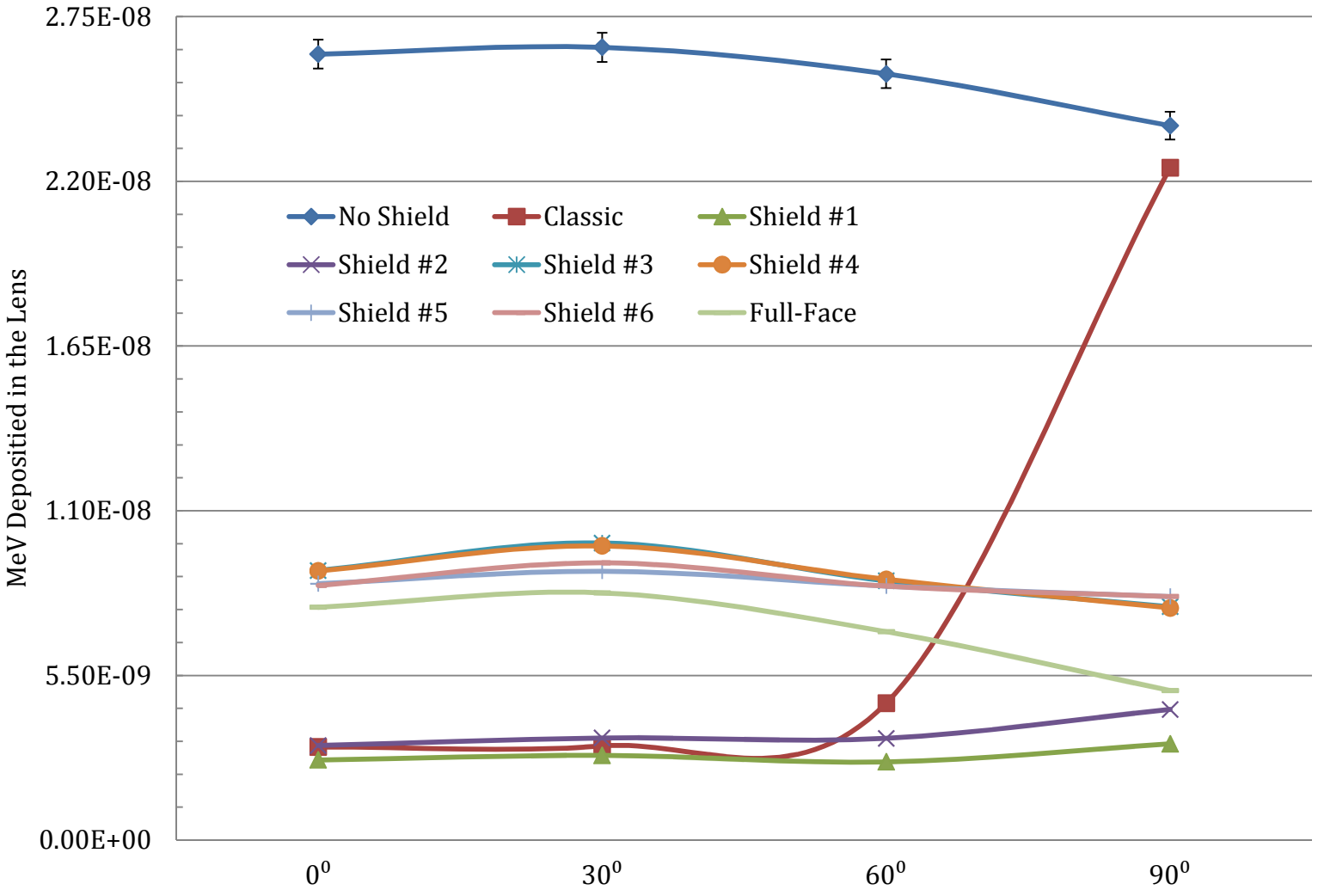


Figure 4.12: Energy deposition profiles for the left lens for all shields at all $90^0$ source positions

## 4.10 Shield Protection factors

A total protection factor was calculated for each shield in two ways. The Average Protection Factor (APF) was taken as the average of the individual protection factors for all 16 data points for every shield. The Weighted Protection Factor (WPF) was calculated similarly to the APF except that each individual protection factor was weighted by its fractional contribution to the total lens dose. Table 4.10 contains the WPF source position weighting factors. The APF and WPF are shown in Figure 4.12 and tabulated in Table 4.11. For all shields except the Full Face Shield, the WPF is greater than or equal to the APF. This occurs because the WPF reduces the importance of source positions that do not contribute significantly to total lens dose. Source positions 45-60, 45-90, and 90-90 are weighted low in the WPF calculations, and these source positions also correspond to poor performance and low protection factors for every shield except the Full Face shield.

Table 4.10: Fractional contributions to total lens dose for the right and the left lens from every source position

| Source Position | Right Lens | Left Lens |
|---|---|---|
| 45-0 | 7.58% | 7.49% |
| 45-30 | 6.59% | 7.62% |
| 45-60 | 3.25% | 7.29% |
| 45-90 | 1.13% | 6.32% |
| 90-0 | 7.96% | 7.91% |
| 90-30 | 6.95% | 7.98% |
| 90-60 | 5.02% | 7.72% |
| 90-90 | 2.00% | 7.19% |
| Sum | 100% | |

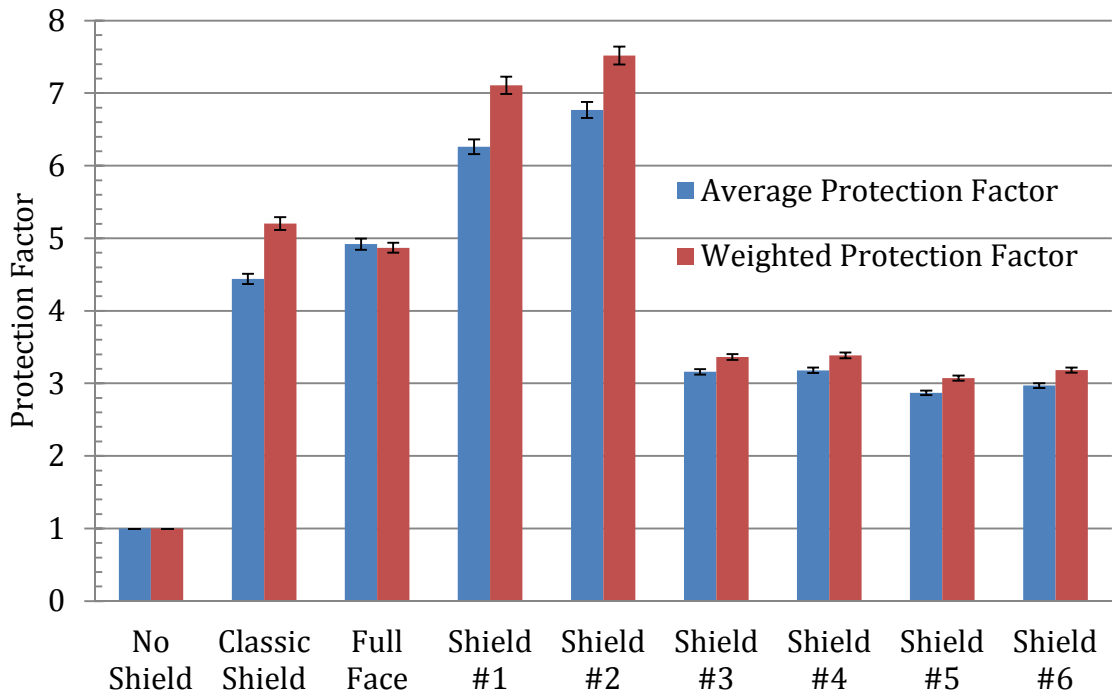


Figure 4.13: Protection factors for all shields

The protection factors (Figure 4.13) give an overall ranking to the shields simulated in this study. The Classic Shield and the Full Face Shield can be seen to have strikingly similar performance even though they are drastically different in design. The Classic Shield has superior shield thickness, but the Full Face Shield has superior shield geometry. This illustrates that thickness and geometry can both be important in the design of an eye shield, and they can be utilized individually or in combination to achieve a shielding goal. Shields #1 and #2 illustrate the increased shield performance that can be obtained when good shield geometry and sufficient shield thickness are used in combination; these two were the best performing shields simulated. However, there may be issues involved with the feasibility of such large and thick eye shields. Shields #3-6 illustrate the performance of several 0.1mm thick shield designs. Even though they represent several different shielding designs,

they all provide similar performance with overall protection factors of 2.9-3.4. They are able to provide protection factors approaching 55%-70% of the Classic and Full Face Shield while utilizing far less material.

Each shield has its own strengths and weaknesses at the eight simulated source positions. Even though a shield has an acceptable APF and/or WPF, it may not provide sufficient coverage at one or more of the individual source positions, and if a shield is used in a situation where it consistently encounters a source position for which it cannot provide sufficient shielding, the APF and WPF will not accurately describe the protection that the shield provides.

Table 4.11 Shield characteristics and performance

| Shield Number | Average Protection Factor (APF) | APF Absolute Error | Weighted Protection Factor (WPF) | WPF Absolute Error | Shield Volume ($cm^3$) | Shield Thickness (mm) |
|---|---|---|---|---|---|---|
| No Shield | 1.00 | 0.000 | 1.00 | 0.000 | 0.00 | 0.00 |
| Classic | 4.44 | 0.072 | 5.20 | 0.088 | 4.51 | 0.75 |
| Full Face | 4.92 | 0.077 | 4.87 | 0.068 | 3.74 | 0.10 |
| Shield #1 | 6.26 | 0.101 | 7.11 | 0.119 | 4.24 | 0.50 |
| Shield #2 | 6.77 | 0.110 | 7.52 | 0.124 | 3.17 | 0.50 |
| Shield #3 | 3.16 | 0.037 | 3.36 | 0.039 | 0.63 | 0.10 |
| Shield #4 | 3.18 | 0.038 | 3.39 | 0.040 | 0.65 | 0.10 |
| Shield #5 | 2.87 | 0.032 | 3.07 | 0.035 | 0.95 | 0.10 |
| Shield #6 | 2.97 | 0.033 | 3.18 | 0.035 | 1.01 | 0.10 |

# CHAPTER 5 - CONCLUSIONS

The recent reductions to the international dose limit recommendations for the lens of the eye have renewed interest in radiation protection strategies in occupational settings where eye-lens radiation exposure occurs frequently. One such setting, interventional fluoroscopy, has significant potential for over-exposure of the lens especially if protective measures are not taken. Some common radiation protection equipment in fluoroscopy suites include leaded aprons, ceiling-suspended shields, leg shields, and radiation shielding eyewear. Although these items have been shown to provide the lenses of the eyes some protection, the quantity of protection depends on many factors. Protective eyewear in particular has the potential to control and reduce eye lens dose in interventional fluoroscopy rooms; however the amount of protection they provide can vary greatly.

The main objectives of this research were to investigate how shielding scenario variables affect the performance of radiation shielding eyewear, to test the feasibility and performance of eye shields constructed of 0.1 mm lead equivalent material, and to develop a method to quantify the overall protection provided by different eye shields.

The eight separate shielding scenarios tested show some interesting trends. In order to quantify how well the shields performed, two rating methods were devised to evaluate the shield performance across all source angles, the Average Protection Factor and the Weighted Protection Factor. The two shields that were modeled after commercially available eyewear (Classic and Full Face) performed similarly with total protection factors around 5. Even though these shields represent very different designs, they can provide similar protection. This also illustrates that shield

thickness should not be the most important shield design consideration; the shape of the shield is also very important. The two shields modeled with 0.5 mm of lead and large surface areas provided weighted protection factors of more than 7, and these were the best performing shields of the study. They performed so well because their design combined adequate coverage with substantial shield thickness. The highest protection factor that can be reasonably expected from a 0.1 mm thick lead shield (Full Face Shield) was determined to be 4.9. Additional shield designs constructed of 0.1 mm lead equivalent material, but smaller in size, provided consistent protection factors of around 3. Small changes to the design of these shields made equally small changes to the shield performance. Most importantly, shield performance at the individual source positions is not always consistent; some source positions pose significant shielding geometry problems for the shields. When shields are positioned incorrectly, have inadequate coverage, or large gaps to the face, they may not provide the protection that is expected by the wearer.

The results of this study suggest that relatively thin (0.1 mm lead equivalent) eye shields could provide good overall protection in interventional fluoroscopy rooms. However, more work is needed developing methods of rating the amount of protection eye shield can provide. Although the protection factors described here provide some idea of overall shield performance, they do not account for the likelihood that, in practice, an eye shield will be exposed to radiation from certain angles more than others. A survey of the most common irradiation angles observed in fluoroscopy rooms could be used to develop a more accurate rating method for different eye shields. If certain angles are more common than others, certain shield designs that perform well at those angles could be used in practice, and the protection factor provided by that shield could be used more confidently when making dosimetry estimates for the operator.

# BIBLIOGRAPHY


[1] Rehani, Madan M et al. “Radiation and Cataract.” *Radiation protection dosimetry* 147.1-2 (2011): 300–304.

[2] International Commission on Radiological Protection (ICRP). Recommendations of the International Commission on Radiological Protection. Publication103. Ann. ICRP 37 (1–332) Elsevier (2007).

[3] Worgul, B V et al. “Cataracts Among Chernobyl Clean-up Workers: Implications Regarding Permissible Eye Exposures.” *Radiation research* 167.2 (2007): 233–243.

[4] Chodick, Gabriel et al. “Risk of Cataract After Exposure to Low Doses of Ionizing Radiation: A 20-Year Prospective Cohort Study Among US Radiologic Technologists.” *American Journal of Epidemiology* 168.6 (2008): 620–631.

[5] Minamoto A, Taniguchi H, Yoshitani N, Mukai S, Yokoyama T, Kumagami T, et al. Cataract in atomic bomb survivors. *Int J Radiat Biol* 2004;80(5):339-45.

[6] ICRP. “ICRP Issues Statement Lowering Threshold for Eye Lens.” 2011. Web. 31 Jan. 2013.

[7] FDA. "Radiation-Emitting Products." *Fluoroscopy*. FDA, 20 May 2013.

[8] Vanhavere, F et al. “ORAMED: Optimixation of Radiation Protection of Medical Staff.” EURADOS Report 2012-2. Braunschweig, April 2011.

[9] Fetterly, Kenneth A. et al. “Effective Use of Radiation Shields to Minimize Operator Dose During Invasive Cardiology Procedures.” *JACC: Cardiovascular Interventions* 4.10 (2011): 1133–1139.

[10] Geber, T., M. Gunnarsson, and S. Mattsson. “Eye Lens Dosimetry for Interventional procedures–Relation Between the Absorbed Dose to the Lens and Dose at Measurement Positions.” *Radiation Measurements* 46.11 (2011): 1248–1251.

[11] Sturchio, Glenn M. et al. “Protective Eyewear Selection for Interventional Fluoroscopy.” *Health Physics* 104 (2013): S11–S16.

[12] Ainsbury, E. A. et al. “Radiation Cataractogenesis: A Review of Recent Studies.” *Radiation Research* 172.1 (2009): 1–9.

[13] Shore, Roy E., Kazuo Neriishi, and Eiji Nakashima. “Epidemiological Studies of Cataract Risk at Low to Moderate Radiation Doses:(not) Seeing Is Believing.” *Radiation research* 174.6b (2010): 889–894.

[14] "IAEA Activity on Retrospective Evaluation of Lens Injuries and Dose (RELID)." *IAEA Cataract Study*. IAEA, n.d. Web. 28 May 2013.

[15] *Radiation Measurement* 46.11 (2011): 1195-334. Print.

[16] Martin, James E. *Physics for Radiation Protection: A Handbook*. 2nd ed. Weinheim: Wiley-VCH, 2006. Print.

[17] Shultis, J. Kenneth., and Richard E. Faw. *Radiation Shielding*. Upper Saddle River, NJ: Prentice Hall PTR, 1996. Print.

[18] MarShield. *Lead X-Ray Glass vs. Lead Plastic Acrylic (Publication)*. Burlington: MarShield, n.d. *Marshield.com*. Web. 15 Feb. 2013.

[19] Martini, Frederic, and William C. Ober. “Fundamentals of Anatomy & Physiology”. San Francisco, CA: Pearson Benjamin Cummings, 2006. Print.

[20] Behrens, R, and G Dietze. “Dose Conversion Coefficients for Photon Exposure of the Human Eye Lens.” *Physics in Medicine and Biology* 56.2 (2011): 415–437.

[21] Behrens, R., G. Dietze, and M. Zankl. “Dose Conversion Coefficients for Electron Exposure of the Human Eye Lens.” *Physics in Medicine and Biology* 54 (2009): 4069.

[22] Marshall, N. W., K. Faulkner, and H. Warren. “Measured Scattered X-ray Energy Spectra for Simulated Irradiation Geometries in Diagnostic Radiology.” *Medical Physics* 23 (1996): 1271.

[23] Shultis, J. K., and R. E. Faw. “An MCNP Primer.” *Dept. of Mechanical and Nuclear* (2006).

[24] Charles M W and Brown N 1975 Dimensions of the human eye relevant to radiation protection *Phys. Med. Biol.* 20 202–18

[25] MCNP, X. *Monte Carlo Team, MCNP–A General Purpose Monte Carlo N-Particle Transport Code, Version 5*. LA-UR-03-1987, Los Alamos National Laboratory, April 2003.

[26] MCNP, X. *Monte Carlo Team, MCNP–A General Purpose Monte Carlo N-Particle Transport Code, Version 5*. LA-CP-03-0245, Los Alamos National Laboratory, April 2003.

[27] Kramer, R., and G. Drexler. "On the Calculation of the Effective Dose Equivalent." *Radiation Protection Dosimetry* 3.1-2 (1982): 13–24.

[28] Charles, M. W., and N. Brown. "Dimensions of the Human Eye Relevant to Radiation Protection (dosimetry)." *Physics in Medicine and Biology* 20.2 (1975): 202.

[29] Nielsen, J. "Iterative User-interface Design." *Computer* 26.11 (1993): 32–41.

# APPENDICES

# APPENDIX A

## Photon flux images from MCNP5

The following images were captured from the MCNP5 tally plotter after every simulation run. Each set of four images contains two images taken in the y/z plane centered on the lens of the left eye and the lens of the right eye (bottom left and bottom right respectively), one image was taken in the x/y plane intersecting the center of both lenses (top left), and one image was taken in the x/z plan intersecting the center of both lenses (top right). The flux colors do not represent the same photon flux from image to image, and some images were taken with limited extents

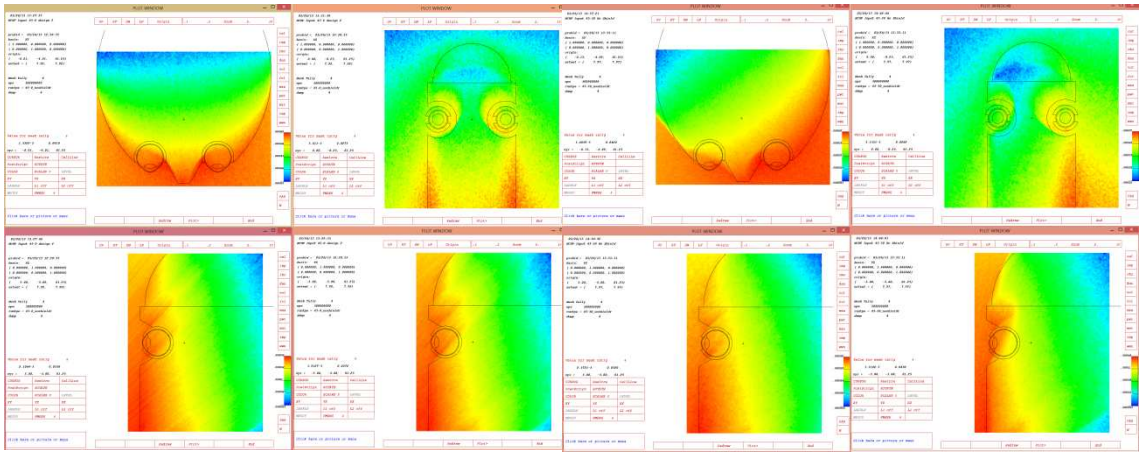

Figure A.1: No Shield 45-0



Figure A.2: No Shield 45-30

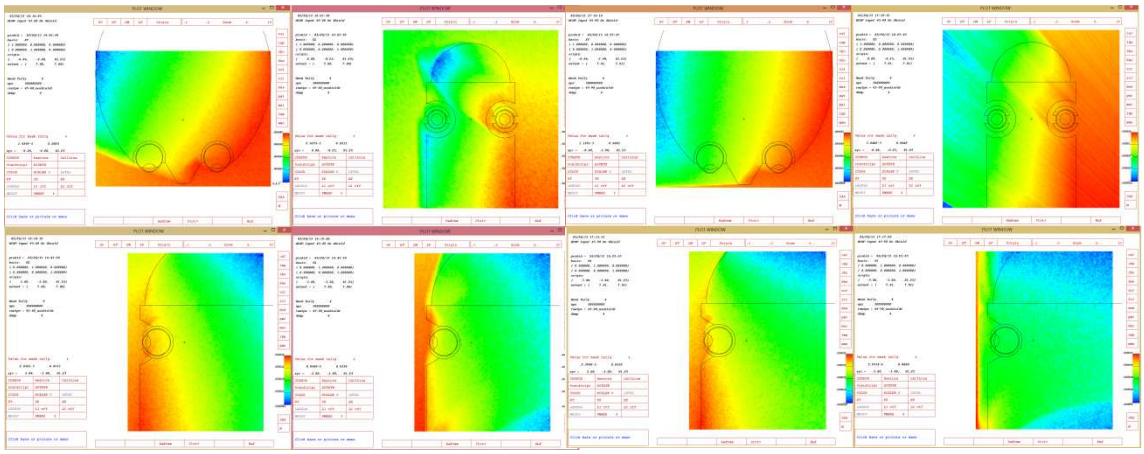

Figure A.3: No Shield 45-60



Figure A.4: No Shield 45-90

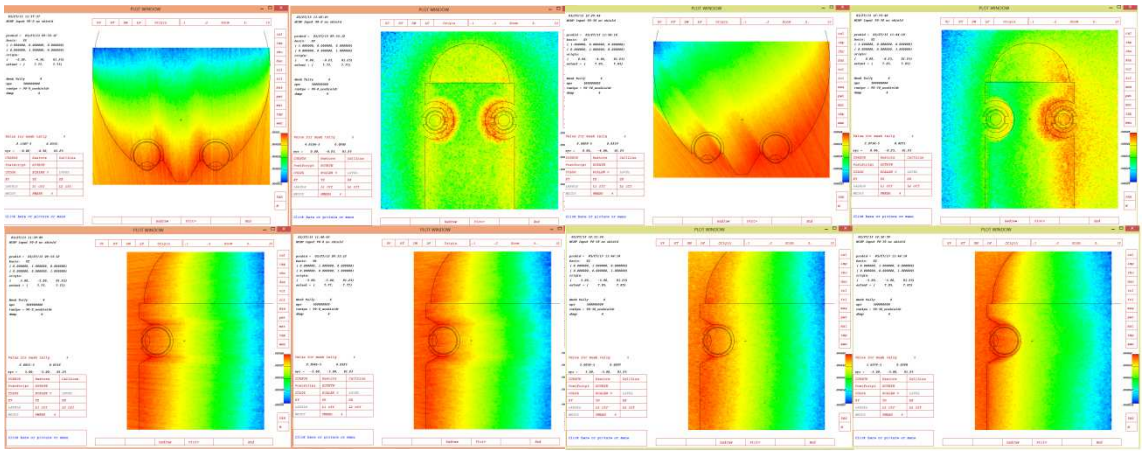

Figure A.5: No Shield 90-0



Figure A.6: No Shield 90-30

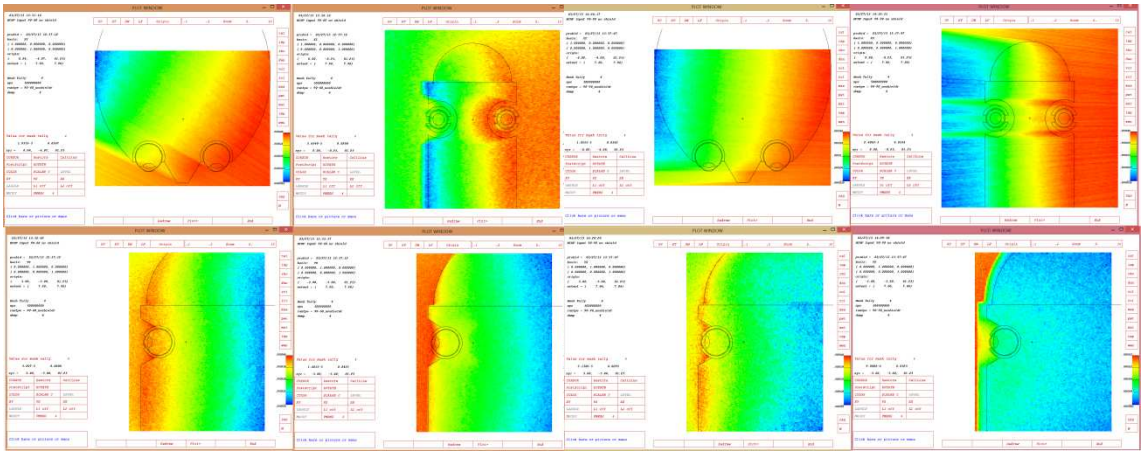

Figure A.7: No Shield 90-60

Figure A.8: No Shield 90-90

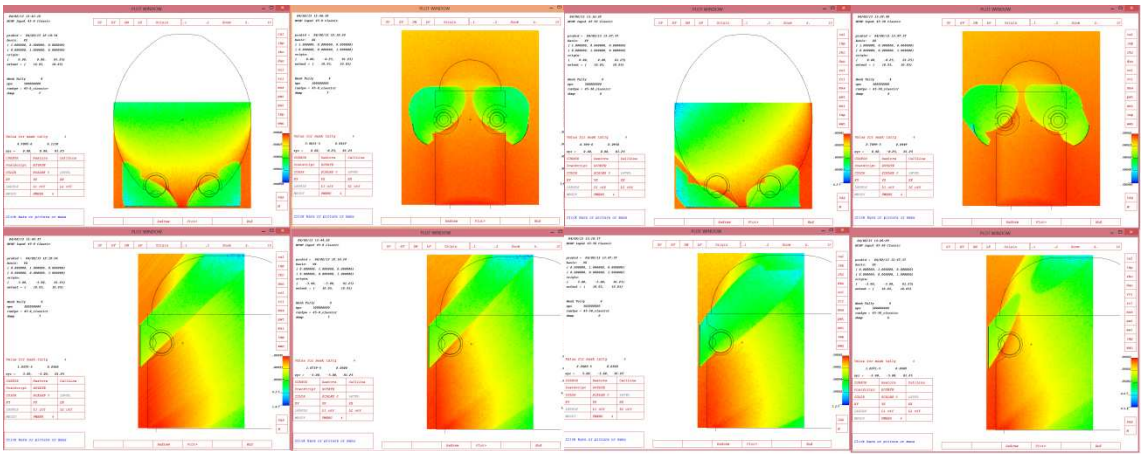

Figure A.9: Classic Shield 45-0

Figure A.10: Classic Shield 45-30

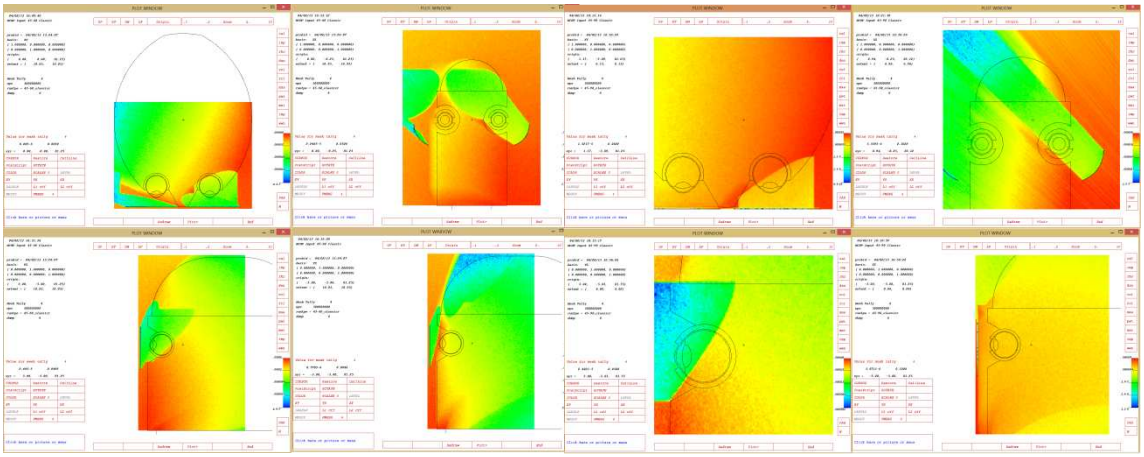

Figure A.11: Classic Shield 45-60

Figure A.12: Classic Shield 45-90

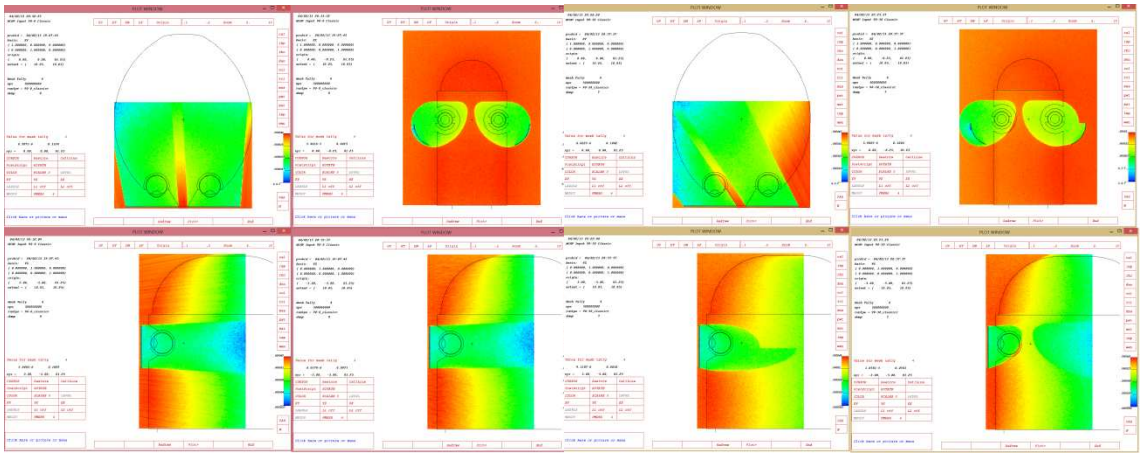

Figure A.13: Classic Shield 90-0



Figure A.14: Classic Shield 90-30

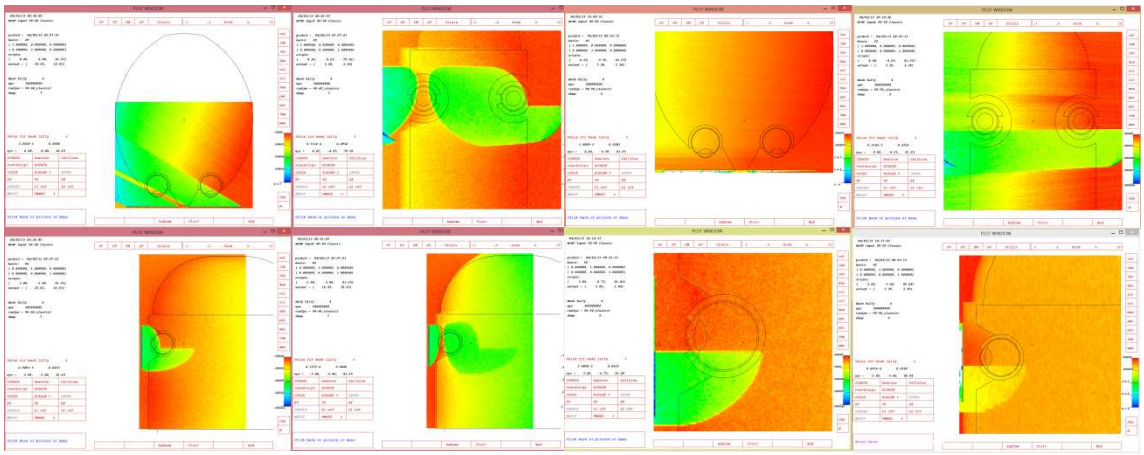

Figure A.15: Classic Shield 90-60



Figure A.16: Classic Shield 90-90

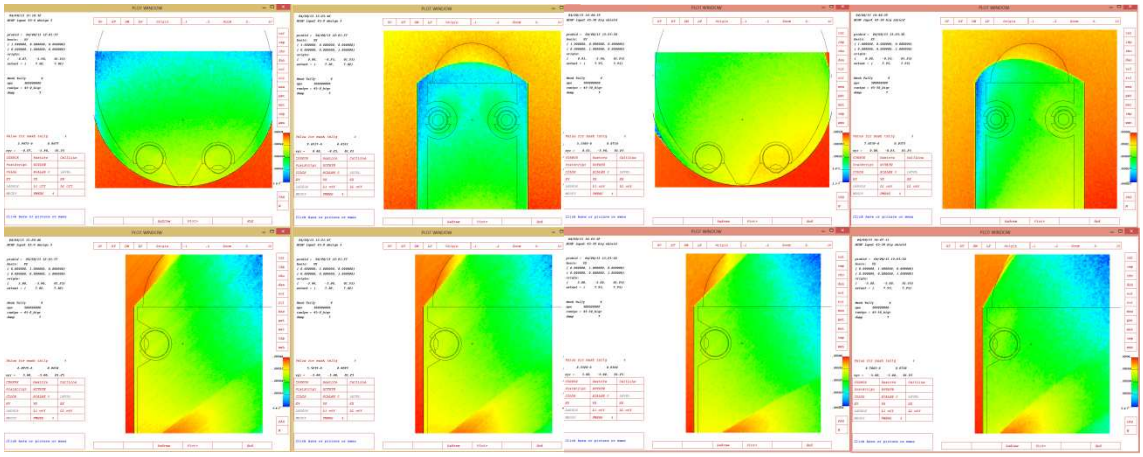

Figure A.17: Full Face Shield 45-0



Figure A.18: Full Face Shield 45-30

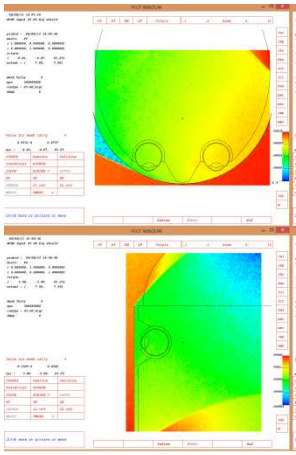

Figure A.19: Full Face Shield 45-60

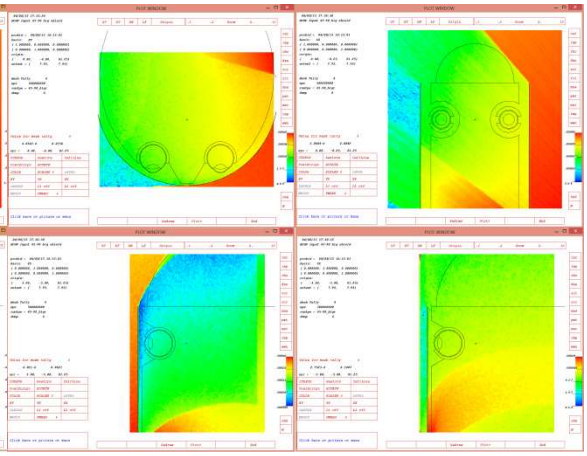

Figure A.20: Full Face Shield 45-90

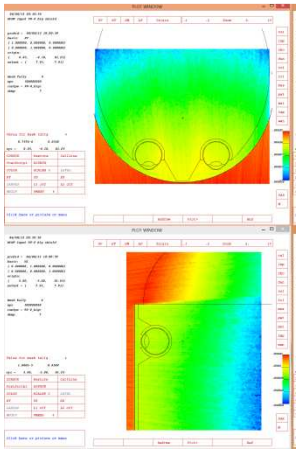

Figure A.21: Full Face Shield 90-0

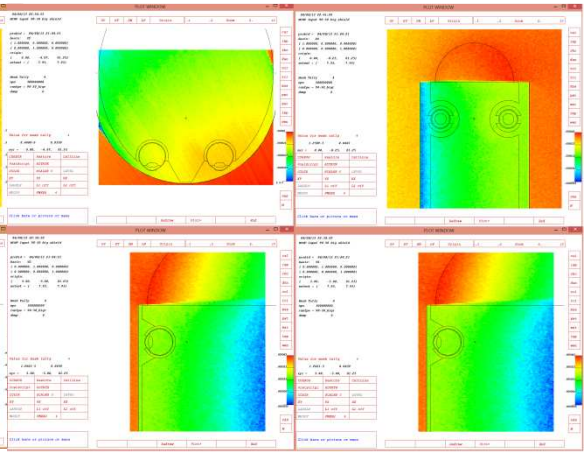

Figure A.22: Full Face Shield 90-30

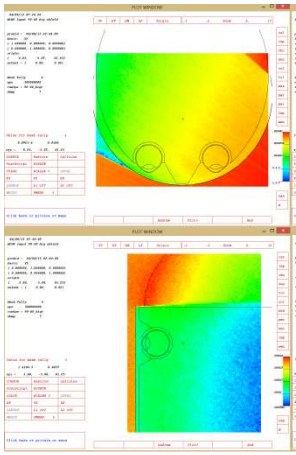

Figure A.23: Full Face Shield 90-60

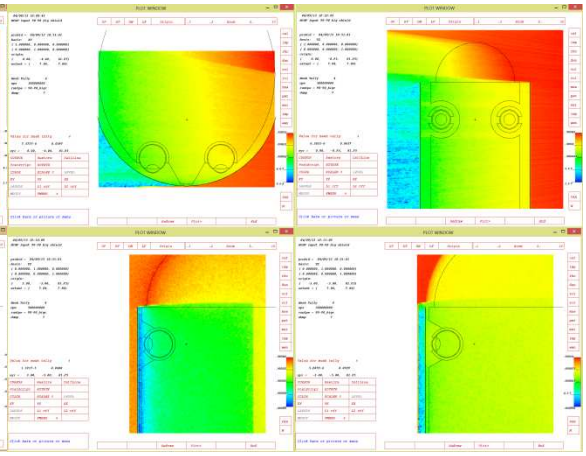

Figure A.24: Full Face Shield 90-90

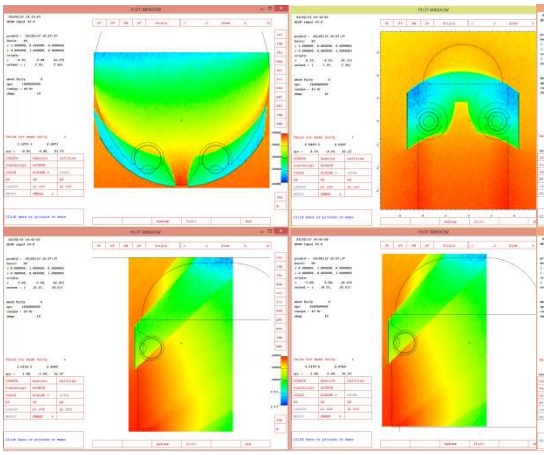

Figure A.25: Shield #1 45-0

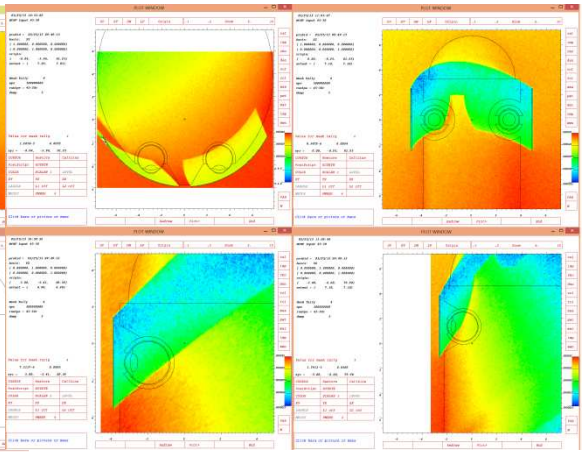

Figure A.26: Shield #1 45-30

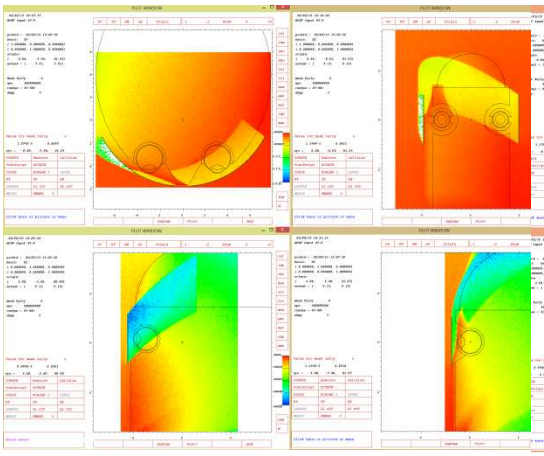

Figure A.27: Shield #1 45-60

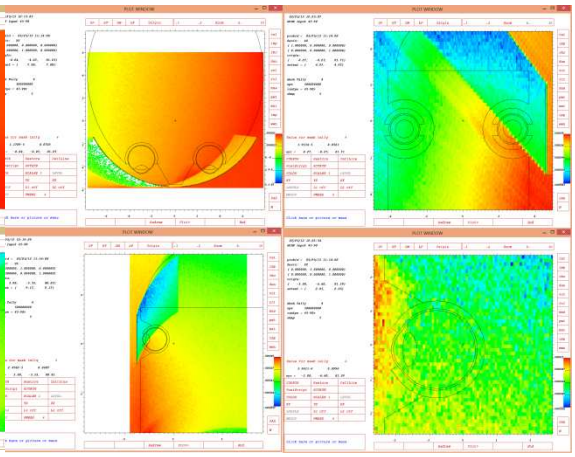

Figure A.28: Shield #1 45-90

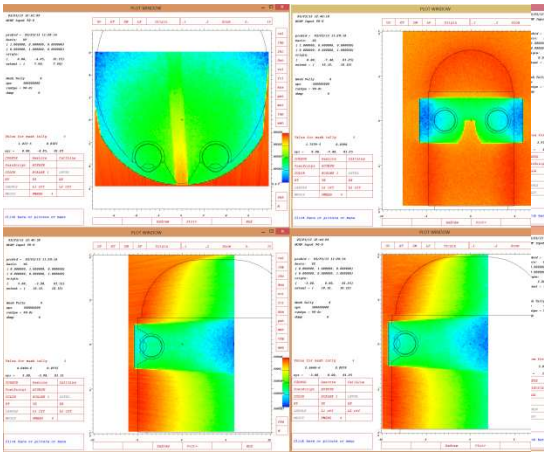

Figure A.29: Shield #1 90-0

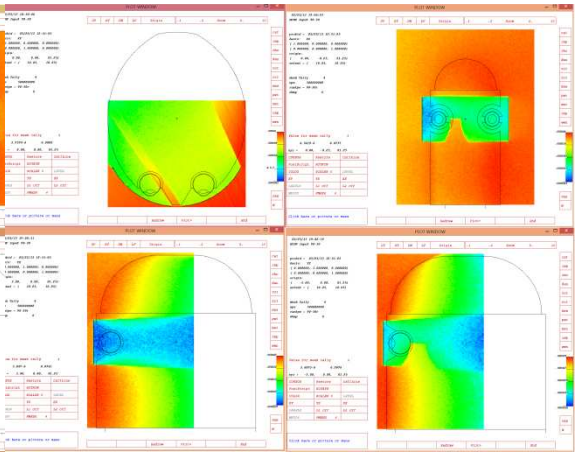

Figure A.30: Shield #1 90-30

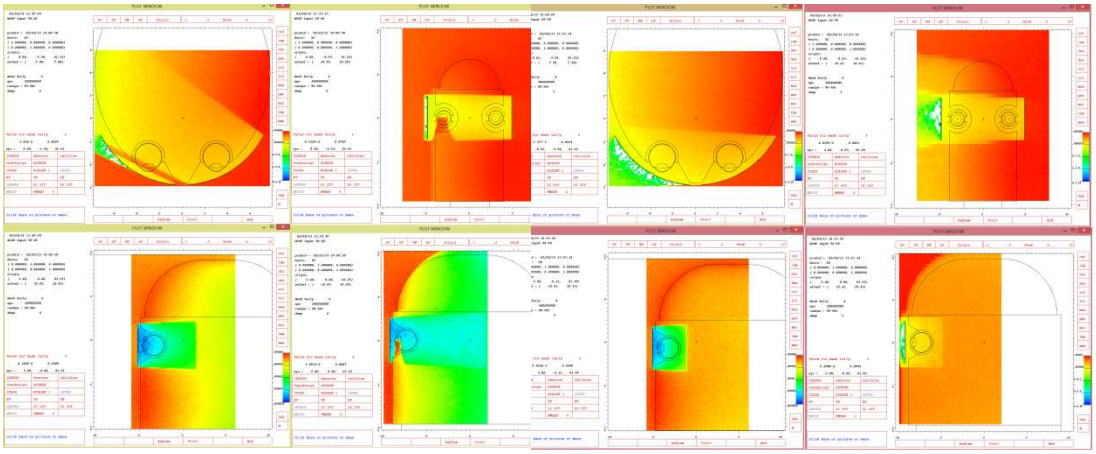

Figure A.31: Shield #1 90-60

Figure A.32: Shield #1 90-90

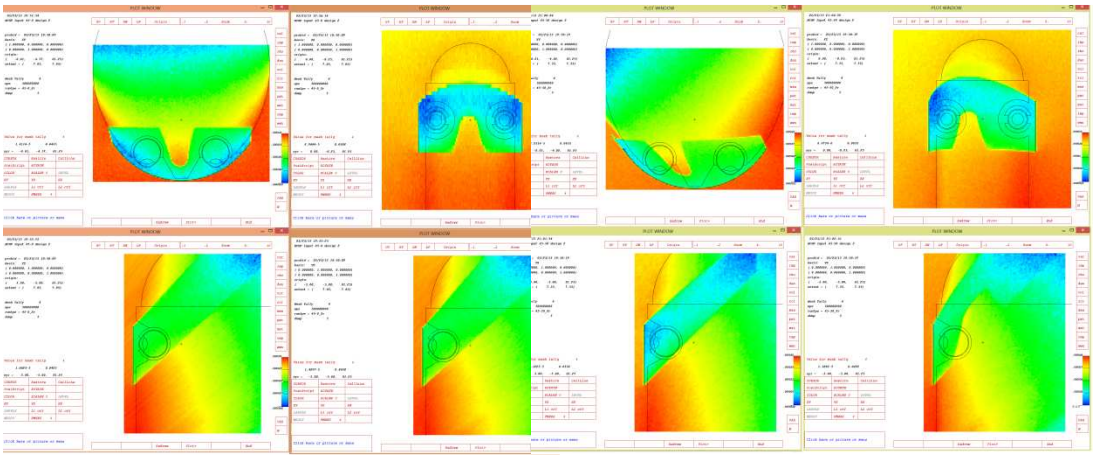

Figure A.33: Shield #2 45-0

Figure A.34: Shield #2 45-30

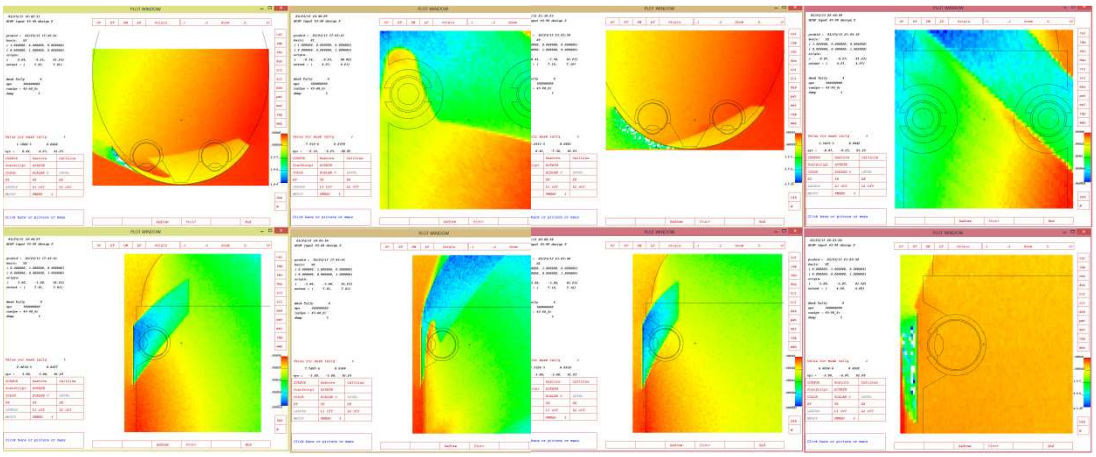

Figure A.35: Shield #2 45-60

Figure A.36: Shield #2 45-90

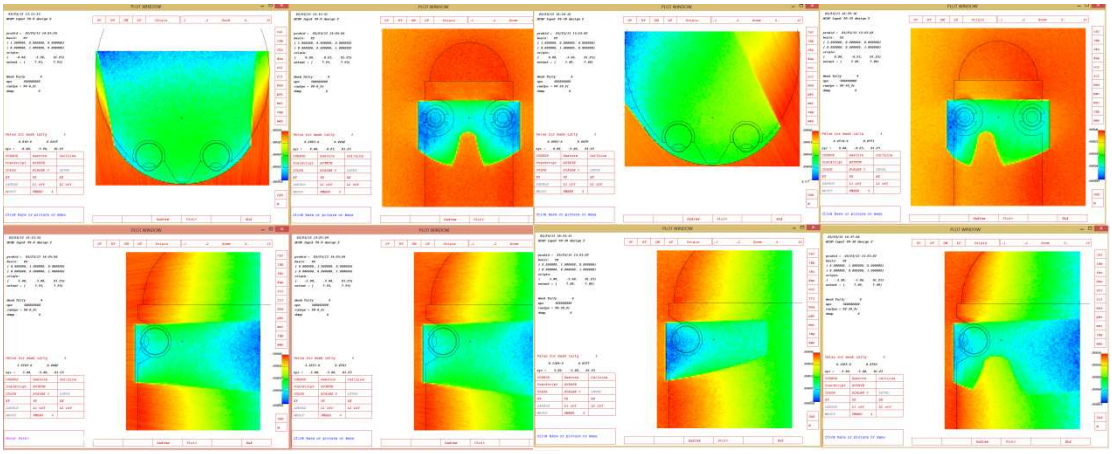

Figure A.37: Shield #2 90-0



Figure A.38: Shield #2 90-30

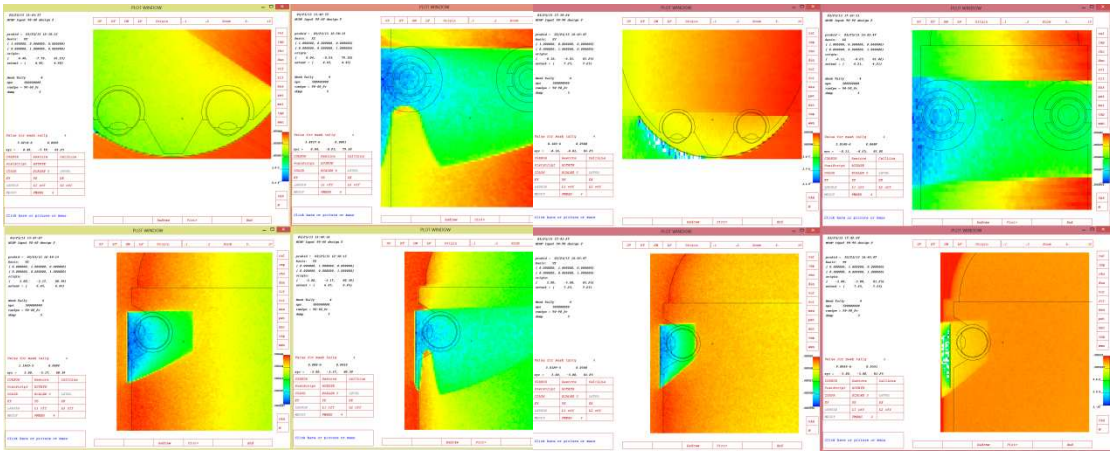

Figure A.39: Shield #2 90-60



Figure A.40: Shield #2 90-90

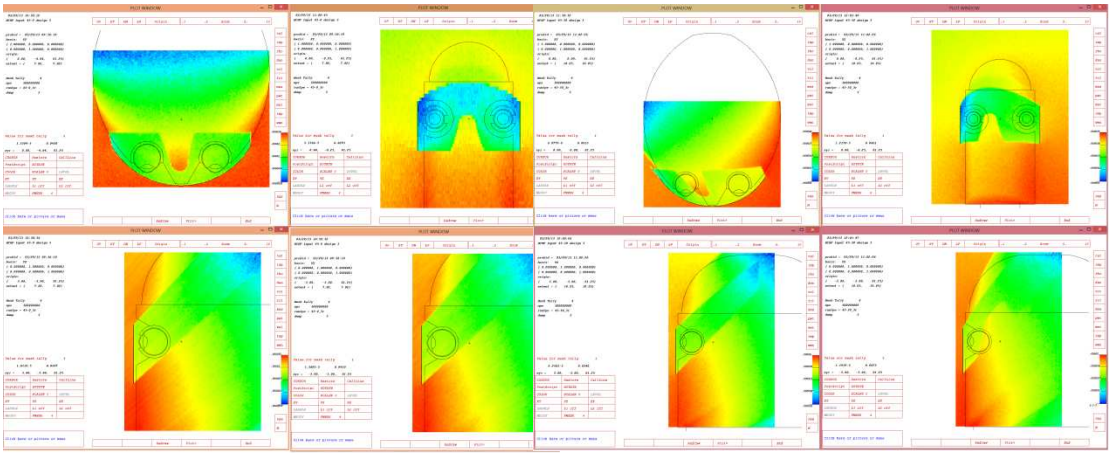

Figure A.41: Shield #3 45-0



Figure A.42: Shield #3 45-30

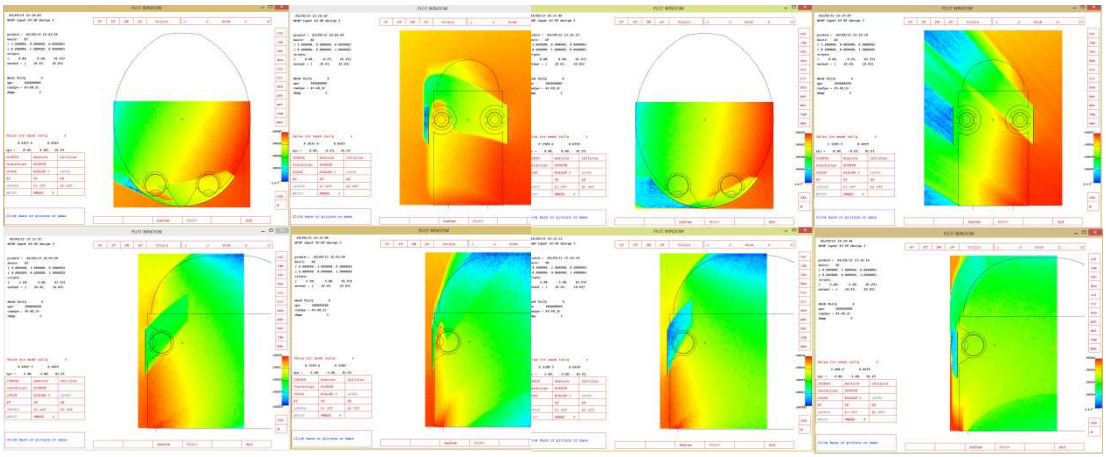

Figure A.43: Shield #3 45-60



Figure A.44: Shield #3 45-90

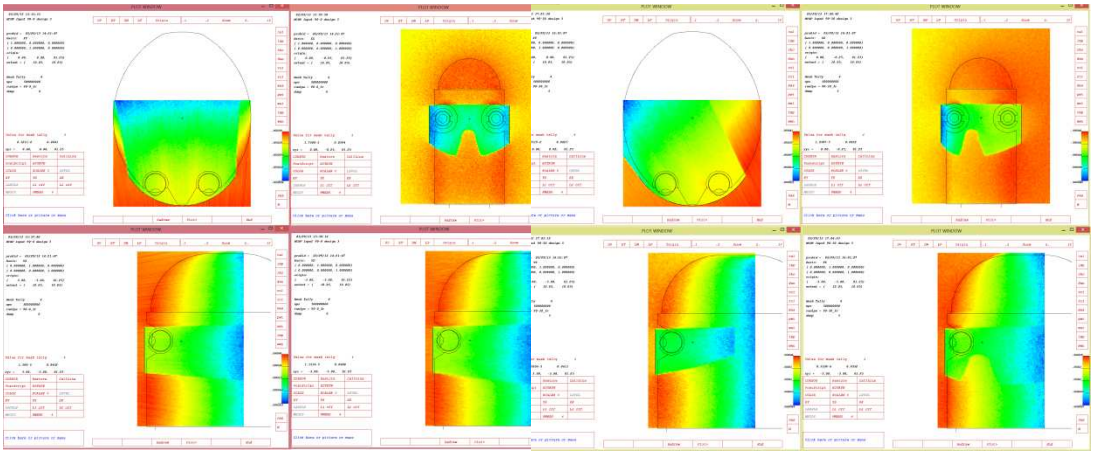

Figure A.45: Shield #3 90-0



Figure A.46: Shield #3 90-30

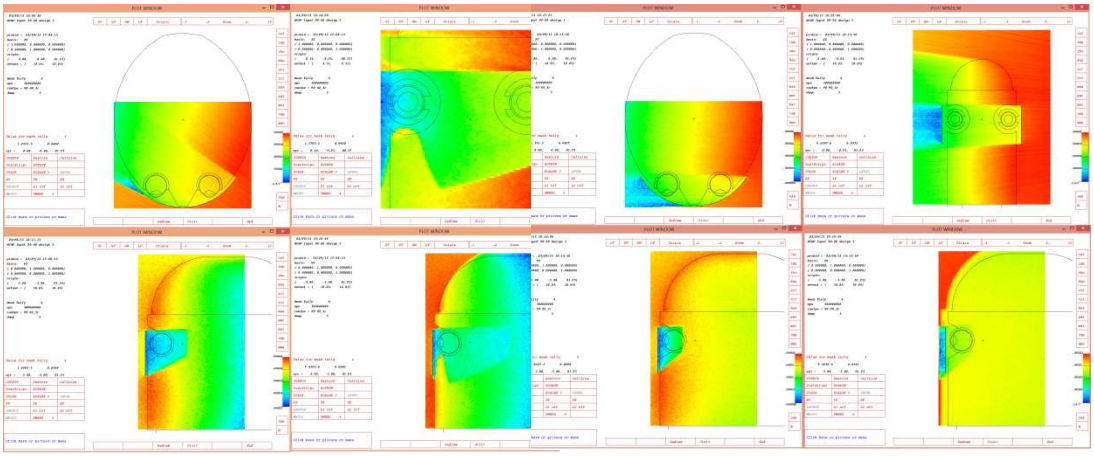

Figure A.47: Shield #3 90-60



Figure A.48: Shield #3 90-90

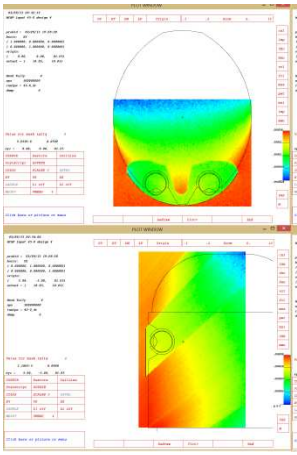

Figure A.49: Shield #4 45-0

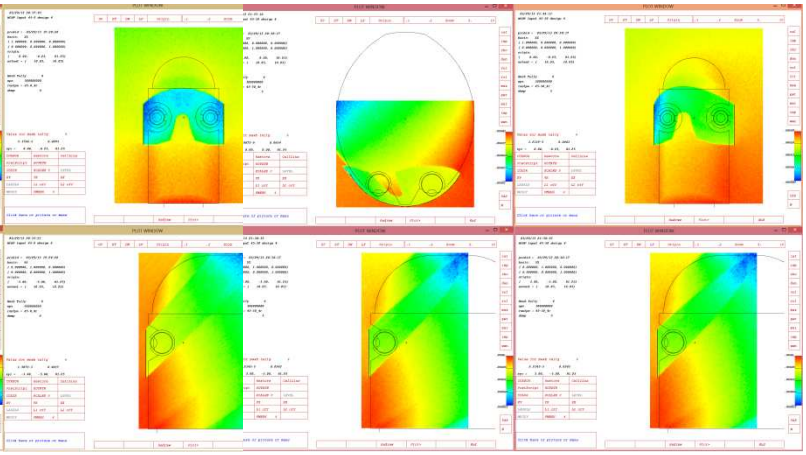

Figure A.50: Shield #4 45-30

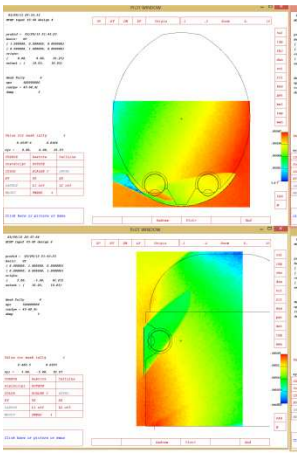

Figure A.51: Shield #4 45-60

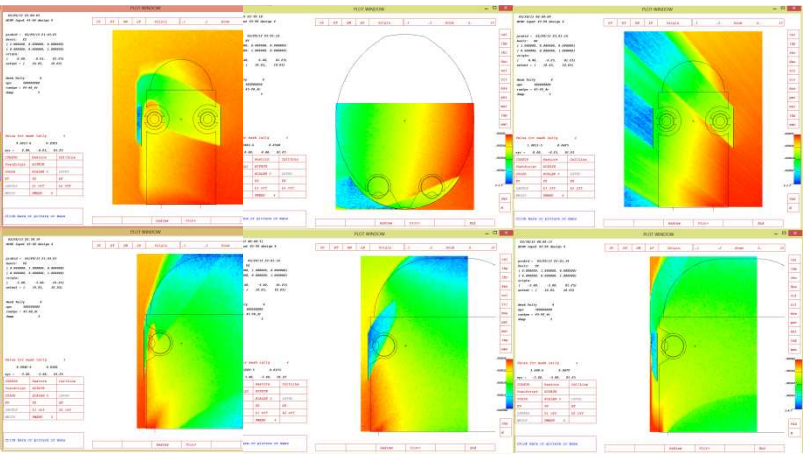

Figure A.52: Shield #4 45-90

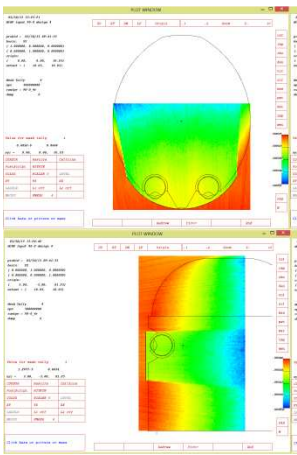

Figure A.53: Shield #4 90-0

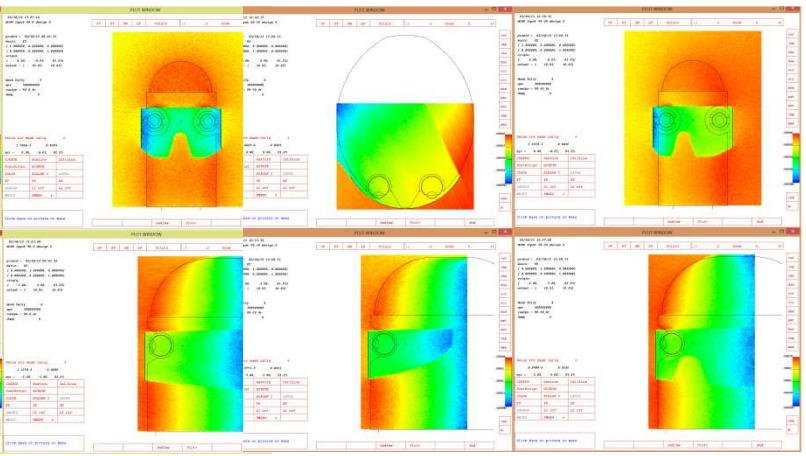

Figure A.54: Shield #4 90-30

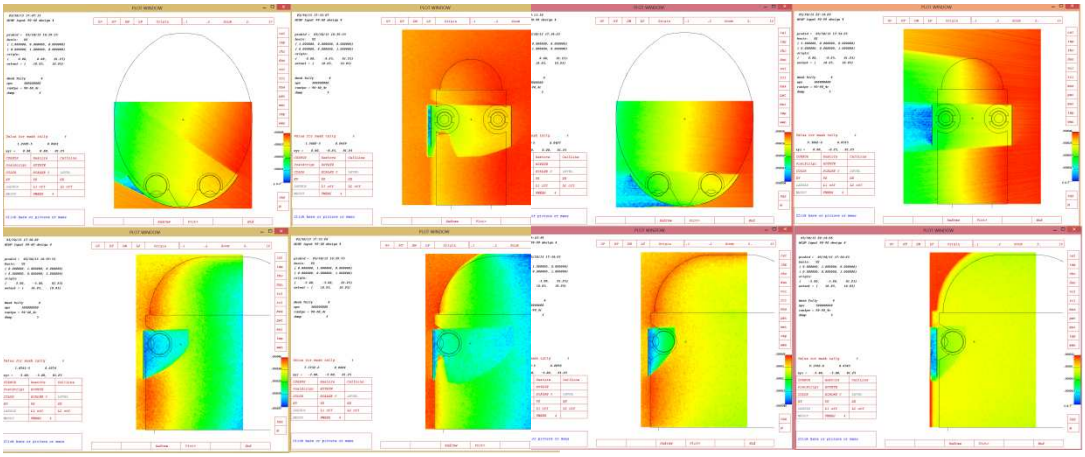

Figure A.55: Shield #4 90-30



Figure A.56: Shield #4 90-90

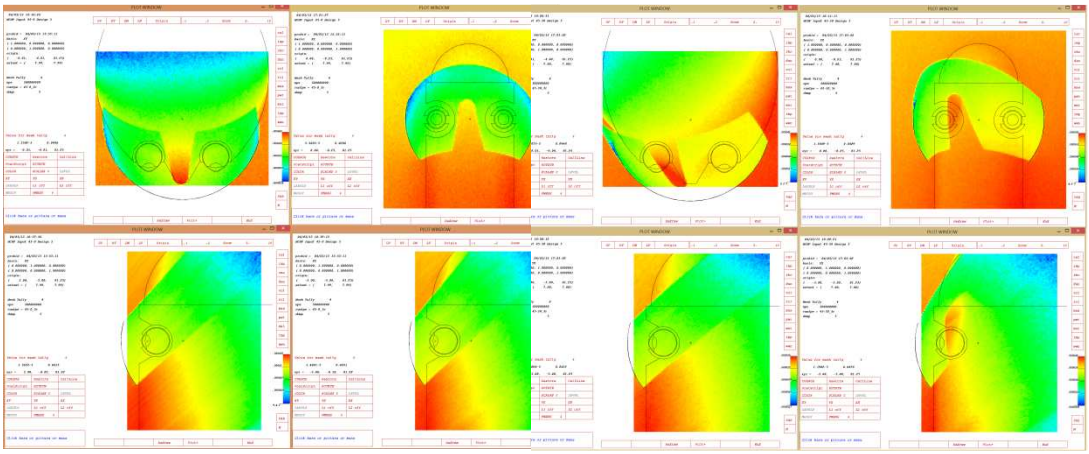

Figure A.57: Shield #5 45-0



Figure A.58: Shield #5 45-30

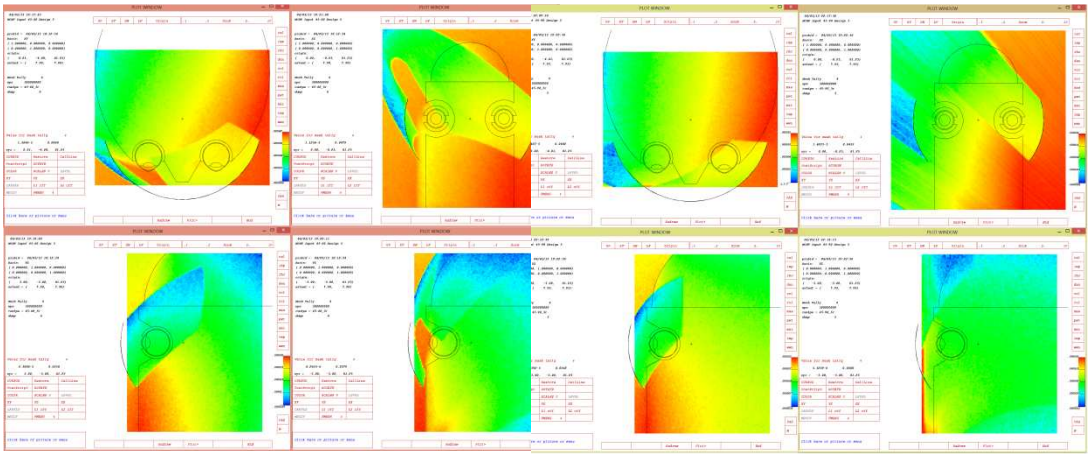

Figure A.59: Shield #5 45-60



Figure A.60: Shield #5 45-90

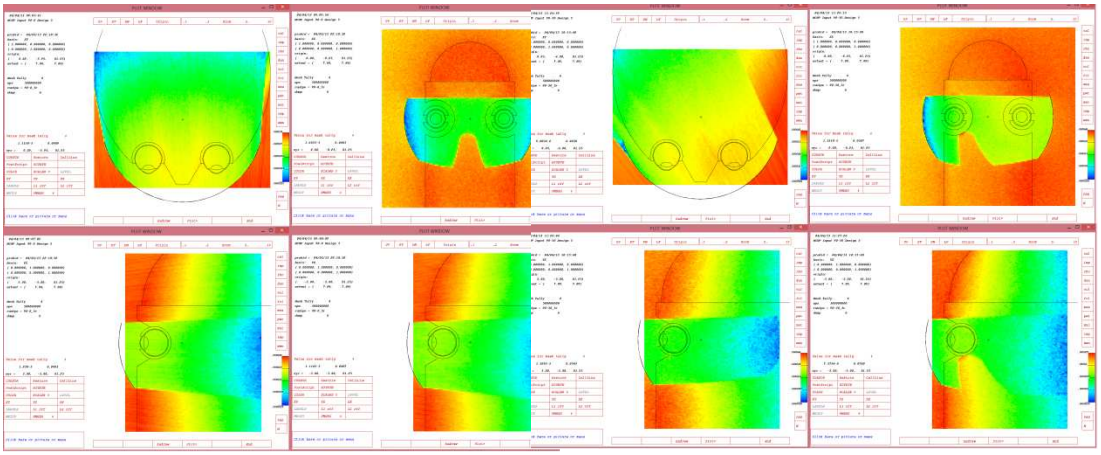

Figure A.61: Shield #5 90-0



Figure A.62: Shield #5 90-30

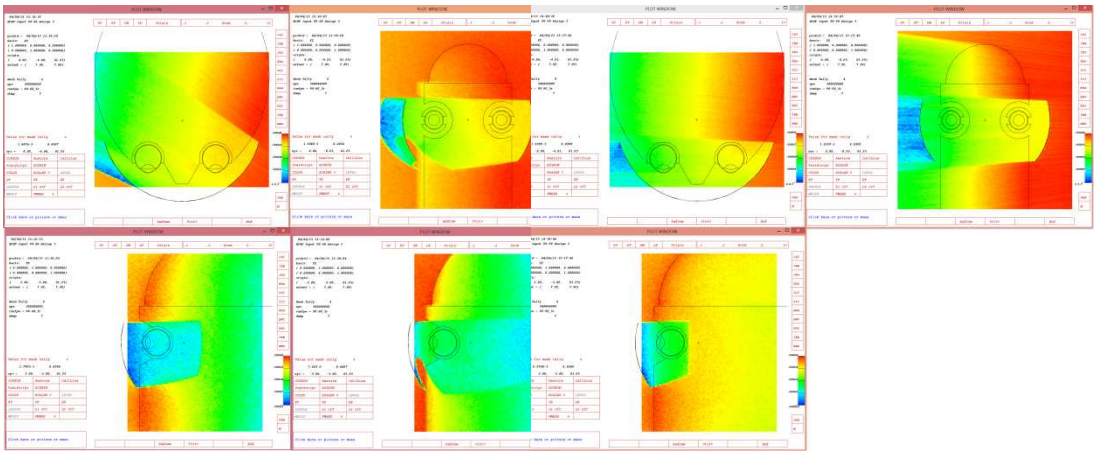

Figure A.63: Shield #5 90-30



Figure A.64: Shield #5 90-90

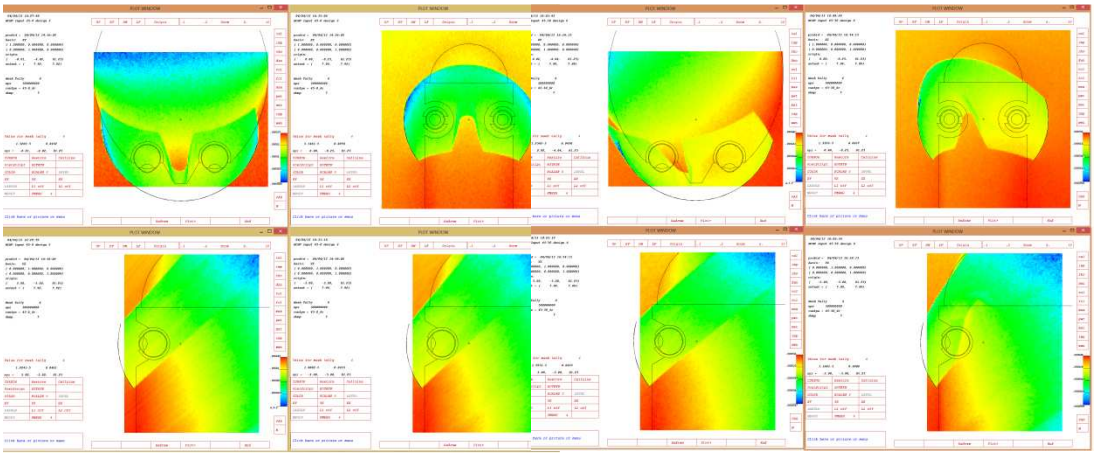

Figure A.65: Shield #6 45-0



Figure A.66: Shield #6 45-30

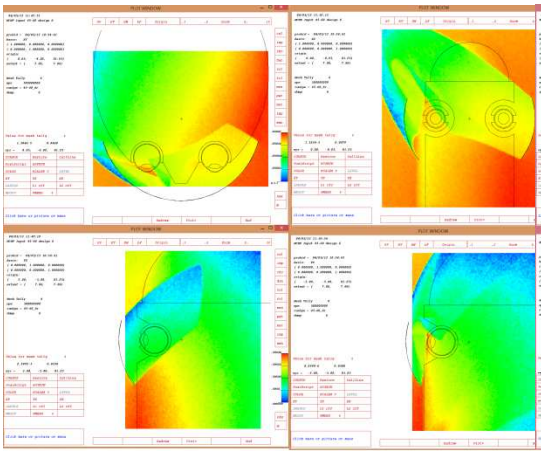

Figure A.67: Shield #6 45-60

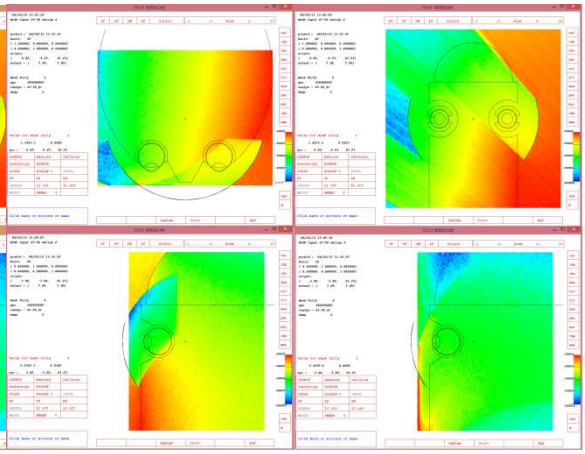

Figure A.68: Shield #6 45-90

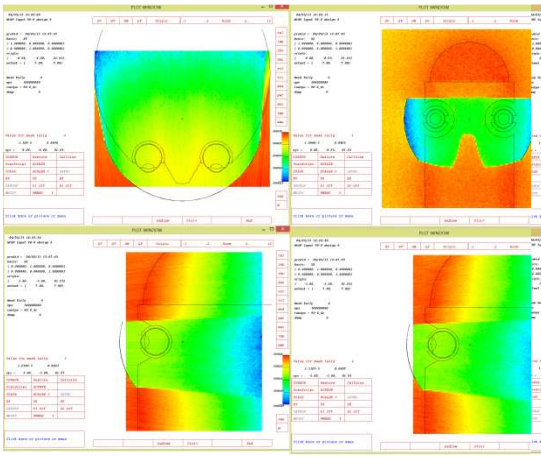

Figure A.69: Shield #6 90-0

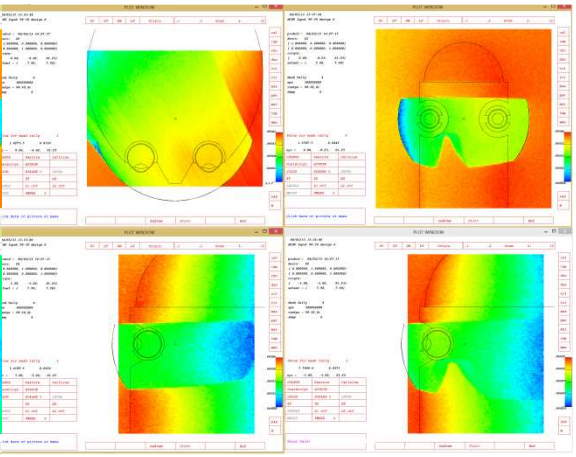

Figure A.70: Shield #6 90-30

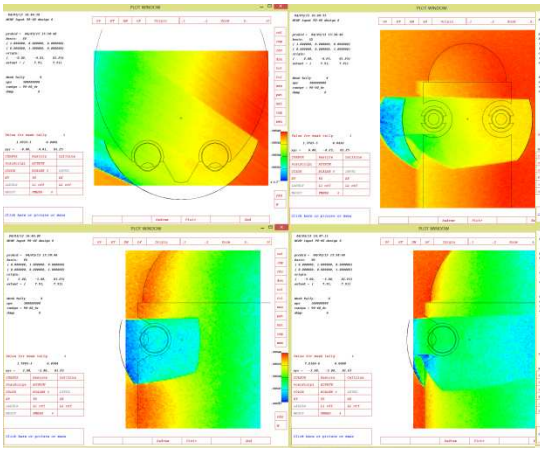

Figure A.71: Shield #6 90-60

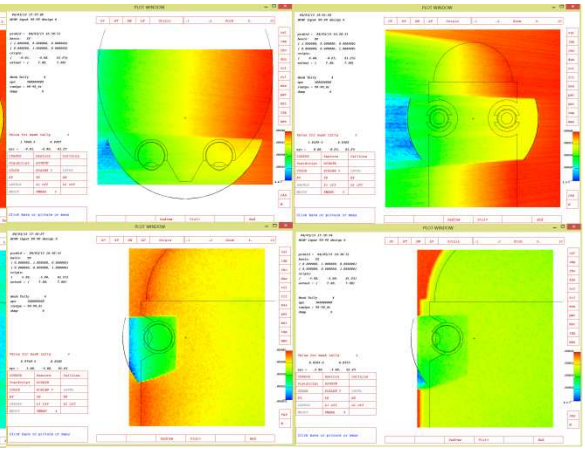

Figure A.72: Shield #6 90-90

# APPENDIX B

## MCNP5 Input Files

The following MCNP5 input files contain at least one example of every shield geometry and every source position and definition. Every input file used in this study can be constructed from these nine examples.

### B.1 No Shield 45-0

```
MCNP Input No Shield 45-0
c
c CELL BLOCK
c  cells of the eye
   1    2   -1.06 -4 -6 -8 -10 -12  $left lens
   2    2   -1.06 -5 -7 -9 -11 -13  $right lens
   3    4 -1.0089 -14 18 #1  $left vitreous humour
   4    4 -1.0089 -15 18 #2  $right vitreous humour
   5    3  -1.003 (-16 :-14 )-18 #1  $left aquous humour
   6    3  -1.003 (-15 :-17 )-18 #2  $right aqueous humour
   7    5  -1.076 (-22 :-19 )16 14  $left cornea
   8    5  -1.076 (-21 :-20 )17 15  $right cornea
   9    1   -1.09 (-23 :-25 )(-27 :28 )19 22  $left eyelid
  10    1   -1.09 (-24 :-26 )(-27 :28 )20 21  $right eyelid
c  cells of head
  20    6   -1.11 (32 -30 -33 ):(-29 32 34 ):(32 33 -34 -31 ) $upper head
  21    6   -1.11 (-32 -35 -36 -37 38 )(44 :46 )(45 :46 )23 24  $face
  22    6   -1.11 (-38 -39 -3 40 ):(-35 -36 -37 -38 3 40 ) $lower head
  23    0        (-40 -39 -3 58 ):(-35 -36 -37 -40 3 58 ) $bottom of head
c  cells of the world
  30    0        #1 #2 #3 #4 #5 #6 #7 #8 #9 #10 #20 #21 #22 $inside world
        #23 #40
  40    0        47 :-49 :48  $outside world

c SURFACES BLOCK
c  surfaces of the eye
   3       py 0
   4        s 3 -8.774 81.25 0.8
   5        s -3 -8.774 81.25 0.8
```

```
 6       s 3 -8.524 81.25 0.6
 7       s -3 -8.524 81.25 0.6
 8       s 3 -8.2419 81.25 0.5
 9       s -3 -8.2419 81.25 0.5
 10       s 3 -7.9289 81.25 0.595
 11       s -3 -7.9289 81.25 0.595
 12       s 3 -7.1439 81.25 1.25
 13       s -3 -7.1439 81.25 1.25
 14       s 3 -7.4 81.25 1.155
 15       s -3 -7.4 81.25 1.155
 16       s 3 -7.95 81.25 0.72
 17       s -3 -7.95 81.25 0.72
 18       py -8.252
 19       s 3 -7.4 81.25 1.21
 20       s -3 -7.4 81.25 1.21
 21       s -3 -7.9539 81.25 0.775
 22       s 3 -7.9539 81.25 0.775
 23       s 3 -7.4 81.25 1.435
 24       s -3 -7.4 81.25 1.435
 25       s 3 -7.9539 81.25 1
 26       s -3 -7.9539 81.25 1
 27       p 3 -8.546 80.75 3 -10.69051 79.75 2 -8.546 80.75
 28       p 3 -8.546 81.75 3 -9.92234 82.75 2 -8.546 81.75
c  surfaces of the head
 29       s 0 1.95 84.5 7.2
 30       s 0 -1.95 84.5 7.2
 31      c/y 0 84.5 7.2
 32       pz 84.5
 33       py -1.95
 34       py 1.95
 35      c/z 3.036 0 10.79
 36      c/z -3.036 0 10.79
 37       cz 9.7
 38       pz 71.6
 39      c/z 0 -0.79 7.79
 40       pz 68
 44      k/y -3 -5.4 81.25 0.33333 -1
 45      k/y 3 -5.4 81.25 0.33333 -1
 46       py -7.4
c surfaces of the graveyard
 47      c/z 3 -8.25 50.1
 48       pz 91.7
 49       pz 45.8
```

```
c surface for the bottom of the head
  58       pz 67.99

c DATA BLOCK
mode  p e
c MATERIALS
c eyelid skin
m1    1000.          -0.1
      6000.         -0.204 7000.         -0.042 8000.         -0.645
      11000.         -0.002 15000.         -0.001 16000.         -0.002
      17000.         -0.003 19000.         -0.001
c eye lens
m2    1000.          -0.096
      6000.         -0.195 7000.         -0.057 8000.         -0.646
      11000.         -0.001 15000.         -0.001 16000.         -0.003
      17000.         -0.001
c aqueous humour
m3    1000.          -0.112
      8000.         -0.888
c vitreous humour
m4    1000.          -0.112
      8000.         -0.888
c cornea
m5    1000.         -0.1016
      6000.         -0.1262 7000.         -0.0369 8000.         -0.7314
      11000.        -0.00065 15000.        -0.00065 16000.        -0.00195
      17000.        -0.00065
c ICRU 4-element tissue
m6    1000.          -0.101
      6000.         -0.111 7000.         -0.026 8000.         -0.762
c
imp:p   1 12r       0          1          0          $ 1, 40
imp:e   1 12r       0          1          0          $ 1, 40
c
c SOURCE
sdef pos=3 -43.61 45.89 par=2 erg=d1 vec=0 1 1 dir=d2
si1 L  .018  .020  .022  .024  .026  .028  .030  .032  .034  .036  .038
      .040  .042  .044  .046  .048  .050  .052  .054  .056  .058  .060
      .062  .064  .066  .068  .070  .072  .074  .076  .078  .080
sp1    .0004 .0011 .0035 .0084 .0151 .0239 .0338 .0429 .0499 .0552 .0598
      .0622 .0633 .0622 .0594 .0563 .0538 .0503 .0482 .0506 .0401 .0334
      .0306 .0278 .0193 .0144 .0120 .0095 .0070 .0039 .0014 .0004
sb2 -31 3.5
```

```
c
c TALLIES
prdmp 2j 1
*f18:p,e 1
fc18 ENERGY DEPOSITED IN THE LEFT LENS (MeV)
*f28:p,e 2
fc28 ENERGY DEPOSITED IN THE RIGHT LENS (MeV)
fmesh4:p origin -7.75 -10 71.6 imesh 7.75  iints 155
                    jmesh 2 jints 120
                    kmesh 91.7 kints 201
nps 500000000
```

B.2 Classic Shield 45-30

```
MCNP Input 45-30 Classic
c
c CELL BLOCK
c  cells of the eye
   1    2   -1.06 -4 -6 -8 -10 -12  $left lens
   2    2   -1.06 -5 -7 -9 -11 -13  $right lens
   3    4 -1.0089 -14 18 #1  $left vitreous humour
   4    4 -1.0089 -15 18 #2  $right vitreous humour
   5    3  -1.003 (-16 :-14 )-18 #1  $left aquous humour
   6    3  -1.003 (-15 :-17 )-18 #2  $right aqueous humour
   7    5  -1.076 (-22 :-19 )16 14  $left cornea
   8    5  -1.076 (-21 :-20 )17 15  $right cornea
   9    1   -1.09 (-23 :-25 )(-27 :28 )19 22  $left eyelid
  10    1   -1.09 (-24 :-26 )(-27 :28 )20 21  $right eyelid
c  cells of head
  20    6   -1.11 (32 -30 -33 ):(-29 32 34 ):(32 33 -34 -31 ) $upper head
  21    6   -1.11 (-32 -35 -36 -37 38 )(44 :46 )(45 :46 )23 24  $face
  22    6   -1.11 (-38 -39 -3 40 ):(-35 -36 -37 -38 3 40 ) $lower head
  23    0        (-40 -39 -3 58 ):(-35 -36 -37 -40 3 58 ) $bottom of head
c  cells of the world
  30    0        #1 #2 #3 #4 #5 #6 #7 #8 #9 #10 #20 #21 #22 $inside world
        #23 #40 #100 #101 #102 #103
  40    0        47 :-49 :48  $outside world
c   cells of the shield
 100    7  -11.35 ((-60 :-61 ):(60 61 -65 66 -67 68 ):(60 61 -62 66 -68 ))-63
        64 $left shield
 101    7  -11.35 ((-69 :-70 ):(69 70 -65 -72 73 68 ):
```

```
        (69 70 -71 -72 -68 ))-63 64 $right shield
 102    7  -11.35 -60 74 63 77 -66 -78 -3 $left side shield
 103    7  -11.35 -69 75 63 76 72 -78 -3 $right side shield

c SURFACES BLOCK
c  surfaces of the eye
   3      py 0
   4       s 3 -8.774 81.25 0.8
   5       s -3 -8.774 81.25 0.8
   6       s 3 -8.524 81.25 0.6
   7       s -3 -8.524 81.25 0.6
   8       s 3 -8.2419 81.25 0.5
   9       s -3 -8.2419 81.25 0.5
  10       s 3 -7.9289 81.25 0.595
  11       s -3 -7.9289 81.25 0.595
  12       s 3 -7.1439 81.25 1.25
  13       s -3 -7.1439 81.25 1.25
  14       s 3 -7.4 81.25 1.155
  15       s -3 -7.4 81.25 1.155
  16       s 3 -7.95 81.25 0.72
  17       s -3 -7.95 81.25 0.72
  18      py -8.252
  19       s 3 -7.4 81.25 1.21
  20       s -3 -7.4 81.25 1.21
  21       s -3 -7.9539 81.25 0.775
  22       s 3 -7.9539 81.25 0.775
  23       s 3 -7.4 81.25 1.435
  24       s -3 -7.4 81.25 1.435
  25       s 3 -7.9539 81.25 1
  26       s -3 -7.9539 81.25 1
  27       p 3 -8.546 80.75 3 -10.69051 79.75 2 -8.546 80.75
  28       p 3 -8.546 81.75 3 -9.92234 82.75 2 -8.546 81.75
c  surfaces of the head
  29       s 0 1.95 84.5 7.2
  30       s 0 -1.95 84.5 7.2
  31      c/y 0 84.5 7.2
  32       pz 84.5
  33       py -1.95
  34       py 1.95
  35      c/z 3.036 0 10.79
  36      c/z -3.036 0 10.79
  37       cz 9.7
  38       pz 71.6
```

```
  39      c/z 0 -0.79 7.79
  40       pz 68
  44      k/y -3 -5.4 81.25 0.33333 -1
  45      k/y 3 -5.4 81.25 0.33333 -1
  46       py -7.4
c surfaces of the graveyard
  47      c/z 3 -8.25 50.1
  48       pz 91.7
  49       pz 45.8
c surfaces of the shield lenses
  60      c/y -4 80.75 2.5
  61      c/y -1.375 82.25 1
  62      c/y -4.375 82.25 4
  63       py -9.75
  64       py -9.825
  65       pz 83.25
  66       px -4
  67       px -1.375
  68       pz 82.25
  69      c/y 4 80.75 2.5
  70      c/y 1.375 82.25 1
  71      c/y 4.375 82.25 4
  72       px 4
  73       px 1.375
c surfaces of the side shields
  74      c/y -4 80.75 2.465
  75      c/y 4 80.75 2.465
  76      c/z -3.036 0 11.39
  77      c/z 3.036 0 11.39
  78       pz 80.75
c surface for the bottom of the head
  58       pz 67.99

c DATA BLOCK
mode  p e
c MATERIALS
c eyelid skin
m1    1000.          -0.1
      6000.         -0.204 7000.         -0.042 8000.         -0.645
      11000.         -0.002 15000.         -0.001 16000.         -0.002
      17000.         -0.003 19000.         -0.001
c eye lens
m2    1000.          -0.096
```

```
     6000.          -0.195 7000.          -0.057 8000.          -0.646
     11000.         -0.001 15000.         -0.001 16000.         -0.003
     17000.         -0.001
c aqueous humour
m3   1000.          -0.112
     8000.          -0.888
c vitreous humour
m4   1000.          -0.112
     8000.          -0.888
c cornea
m5   1000.          -0.1016
     6000.          -0.1262 7000.         -0.0369 8000.         -0.7314
     11000.         -0.00065 15000.       -0.00065 16000.       -0.00195
     17000.         -0.00065
c ICRU 4-element tissue
m6   1000.          -0.101
     6000.          -0.111 7000.          -0.026 8000.          -0.762
c elemental lead
m7   82000.              1
imp:p   1 12r       0          1          0          1 3r        $ 1, 103
imp:e   1 12r       0          1          0          1 3r        $ 1, 103
c SOURCE
sdef pos=20.68 -38.87 45.89 par=2 erg=d1 vec=-0.577 1 1.155 dir=d2
si1 L  .018  .020  .022  .024  .026  .028  .030  .032  .034  .036  .038
     .040  .042  .044  .046  .048  .050  .052  .054  .056  .058  .060
     .062  .064  .066  .068  .070  .072  .074  .076  .078  .080
sp1    .0004 .0011 .0035 .0084 .0151 .0239 .0338 .0429 .0499 .0552 .0598
     .0622 .0633 .0622 .0594 .0563 .0538 .0503 .0482 .0506 .0401 .0334
     .0306 .0278 .0193 .0144 .0120 .0095 .0070 .0039 .0014 .0004
sb2 -31 3.5
c TALLIES
prdmp 2j 1
*f18:p,e 1
fc18 ENERGY DEPOSITED IN THE LEFT LENS (MeV)
*f28:p,e 2
fc28 ENERGY DEPOSITED IN THE RIGHT LENS (MeV)
fmesh4:p origin -7.75 -10 71.6 imesh 7.75  iints 232
                    jmesh 2     jints 180
                    kmesh 91.7  kints 301
nps 500000000
```

B.3 Full Face Shield 45-60

MCNP Input 45-60 Full Face

```
c
c CELL BLOCK
c  cells of the eye
   1    2   -1.06 -4 -6 -8 -10 -12  $left lens
   2    2   -1.06 -5 -7 -9 -11 -13  $right lens
   3    4 -1.0089 -14 18 #1  $left vitreous humour
   4    4 -1.0089 -15 18 #2  $right vitreous humour
   5    3  -1.003 (-16 :-14 )-18 #1  $left aquous humour
   6    3  -1.003 (-15 :-17 )-18 #2  $right aqueous humour
   7    5  -1.076 (-22 :-19 )16 14  $left cornea
   8    5  -1.076 (-21 :-20 )17 15  $right cornea
   9    1   -1.09 (-23 :-25 )(-27 :28 )19 22  $left eyelid
  10    1   -1.09 (-24 :-26 )(-27 :28 )20 21  $right eyelid
c  cells of head
  20    6   -1.11 (32 -30 -33 ):(-29 32 34 ):(32 33 -34 -31 ) $upper head
  21    6   -1.11 (-32 -35 -36 -37 38 )(44 :46 )(45 :46 )23 24  $face
  22    6   -1.11 (-38 -39 -3 40 ):(-35 -36 -37 -38 3 40 ) $lower head
  23    0        (-40 -39 -3 58 ):(-35 -36 -37 -40 3 58 ) $bottom of head
c  cells of the world
  30    0        #1 #2 #3 #4 #5 #6 #7 #8 #9 #10 #20 #21 #22 $inside world
        #23 #40 #99
  40    0        47 :-49 :48  $outside world
c   cells of the shield
  99    7  -11.35 -52 50 -32 38 -3  $x-ray eye shield

c SURFACES BLOCK
c  surfaces of the eye
   3       py 0
   4        s 3 -8.774 81.25 0.8
   5        s -3 -8.774 81.25 0.8
   6        s 3 -8.524 81.25 0.6
   7        s -3 -8.524 81.25 0.6
   8        s 3 -8.2419 81.25 0.5
   9        s -3 -8.2419 81.25 0.5
  10        s 3 -7.9289 81.25 0.595
  11        s -3 -7.9289 81.25 0.595
  12        s 3 -7.1439 81.25 1.25
  13        s -3 -7.1439 81.25 1.25
  14        s 3 -7.4 81.25 1.155
  15        s -3 -7.4 81.25 1.155
```

```
  16       s 3 -7.95 81.25 0.72
  17       s -3 -7.95 81.25 0.72
  18      py -8.252
  19       s 3 -7.4 81.25 1.21
  20       s -3 -7.4 81.25 1.21
  21       s -3 -7.9539 81.25 0.775
  22       s 3 -7.9539 81.25 0.775
  23       s 3 -7.4 81.25 1.435
  24       s -3 -7.4 81.25 1.435
  25       s 3 -7.9539 81.25 1
  26       s -3 -7.9539 81.25 1
  27       p 3 -8.546 80.75 3 -10.69051 79.75 2 -8.546 80.75
  28       p 3 -8.546 81.75 3 -9.92234 82.75 2 -8.546 81.75
c  surfaces of the head
  29       s 0 1.95 84.5 7.2
  30       s 0 -1.95 84.5 7.2
  31      c/y 0 84.5 7.2
  32       pz 84.5
  33       py -1.95
  34       py 1.95
  35      c/z 3.036 0 10.79
  36      c/z -3.036 0 10.79
  37       cz 9.7
  38       pz 71.6
  39      c/z 0 -0.79 7.79
  40       pz 68
  44      k/y -3 -5.4 81.25 0.33333 -1
  45      k/y 3 -5.4 81.25 0.33333 -1
  46       py -7.4
c surfaces of the graveyard
  47      c/z 3 -8.25 50.1
  48       pz 91.7
  49       pz 45.8
c surfaces of the shield
  50      c/z 0 -1.75 8.1
  52      c/z 0 -1.75 8.11
c surface for the bottom of the head
  58       pz 67.99

c DATA BLOCK
mode  p e
c MATERIALS
c eyelid skin
```

```
m1    1000.          -0.1
      6000.         -0.204 7000.         -0.042 8000.         -0.645
      11000.         -0.002 15000.         -0.001 16000.         -0.002
      17000.         -0.003 19000.         -0.001
c eye lens
m2    1000.          -0.096
      6000.         -0.195 7000.         -0.057 8000.         -0.646
      11000.         -0.001 15000.         -0.001 16000.         -0.003
      17000.         -0.001
c aqueous humour
m3    1000.          -0.112
      8000.         -0.888
c vitreous humour
m4    1000.          -0.112
      8000.         -0.888
c cornea
m5    1000.          -0.1016
      6000.         -0.1262 7000.         -0.0369 8000.         -0.7314
      11000.        -0.00065 15000.        -0.00065 16000.        -0.00195
      17000.        -0.00065
c ICRU 4-element tissue
m6    1000.          -0.101
      6000.         -0.111 7000.         -0.026 8000.         -0.762
c elemental lead
m7    82000.              1
c
imp:p   1 12r       0          1          0          1          $ 1, 99
imp:e   1 12r       0          1          0          1          $ 1, 99
c SOURCE
sdef pos=33.62 -25.93 45.89 par=2 erg=d1 vec=-1 0.577 1.155 dir=d2
si1 L  .018  .020  .022  .024  .026  .028  .030  .032  .034  .036  .038
      .040  .042  .044  .046  .048  .050  .052  .054  .056  .058  .060
      .062  .064  .066  .068  .070  .072  .074  .076  .078  .080
sp1    .0004 .0011 .0035 .0084 .0151 .0239 .0338 .0429 .0499 .0552 .0598
      .0622 .0633 .0622 .0594 .0563 .0538 .0503 .0482 .0506 .0401 .0334
      .0306 .0278 .0193 .0144 .0120 .0095 .0070 .0039 .0014 .0004
sb2 -31 3.5
c TALLIES
prdmp 2j 1
*f18:p,e 1
fc18 ENERGY DEPOSITED IN THE LEFT LENS (MeV)
*f28:p,e 2
fc28 ENERGY DEPOSITED IN THE RIGHT LENS (MeV)
```

```
fmesh4:p origin -7.75 -10 71.6 imesh 7.75  iints 155
                  jmesh 2 jints 120
                  kmesh 91.7 kints 201
nps 500000000
```

B.4 Shield #1 45-90

```
MCNP Input 45-90 Shield 1
c
c CELL BLOCK
c  cells of the eye
   1    2   -1.06 -4 -6 -8 -10 -12  $left lens
   2    2   -1.06 -5 -7 -9 -11 -13  $right lens
   3    4 -1.0089 -14 18 #1  $left vitreous humour
   4    4 -1.0089 -15 18 #2  $right vitreous humour
   5    3  -1.003 (-16 :-14 )-18 #1  $left aquous humour
   6    3  -1.003 (-15 :-17 )-18 #2  $right aqueous humour
   7    5  -1.076 (-22 :-19 )16 14  $left cornea
   8    5  -1.076 (-21 :-20 )17 15  $right cornea
   9    1   -1.09 (-23 :-25 )(-27 :28 )19 22  $left eyelid
  10    1   -1.09 (-24 :-26 )(-27 :28 )20 21  $right eyelid
c  cells of head
  20    6   -1.11 (32 -30 -33 ):(-29 32 34 ):(32 33 -34 -31 ) $upper head
  21    6   -1.11 (-32 -35 -36 -37 38 )(44 :46 )(45 :46 )23 24  $face
  22    6   -1.11 (-38 -39 -3 40 ):(-35 -36 -37 -38 3 40 ) $lower head
  23    0        (-40 -39 -3 58 ):(-35 -36 -37 -40 3 58 ) $bottom of head
c  cells of the world
  30    0        #1 #2 #3 #4 #5 #6 #7 #8 #9 #10 #20 #21 #22 $inside world
        #23 #40 #99
  40    0        47 :-49 :48  $outside world
c   cells of the shield
  99    7  -11.35 -53 54 -52 50 -51 (-56 :-57 :55 ) $x-ray eye shield

c SURFACES BLOCK
c  surfaces of the eye
   3       py 0
   4        s 3 -8.774 81.25 0.8
   5        s -3 -8.774 81.25 0.8
   6        s 3 -8.524 81.25 0.6
   7        s -3 -8.524 81.25 0.6
   8        s 3 -8.2419 81.25 0.5
```

```
 9       s -3 -8.2419 81.25 0.5
10        s 3 -7.9289 81.25 0.595
11        s -3 -7.9289 81.25 0.595
12        s 3 -7.1439 81.25 1.25
13        s -3 -7.1439 81.25 1.25
14        s 3 -7.4 81.25 1.155
15        s -3 -7.4 81.25 1.155
16        s 3 -7.95 81.25 0.72
17        s -3 -7.95 81.25 0.72
18       py -8.252
19        s 3 -7.4 81.25 1.21
20        s -3 -7.4 81.25 1.21
21        s -3 -7.9539 81.25 0.775
22        s 3 -7.9539 81.25 0.775
23        s 3 -7.4 81.25 1.435
24        s -3 -7.4 81.25 1.435
25        s 3 -7.9539 81.25 1
26        s -3 -7.9539 81.25 1
27        p 3 -8.546 80.75 3 -10.69051 79.75 2 -8.546 80.75
28        p 3 -8.546 81.75 3 -9.92234 82.75 2 -8.546 81.75
c  surfaces of the head
29        s 0 1.95 84.5 7.2
30        s 0 -1.95 84.5 7.2
31      c/y 0 84.5 7.2
32       pz 84.5
33       py -1.95
34       py 1.95
35      c/z 3.036 0 10.79
36      c/z -3.036 0 10.79
37       cz 9.7
38       pz 71.6
39      c/z 0 -0.79 7.79
40       pz 68
44      k/y -3 -5.4 81.25 0.33333 -1
45      k/y 3 -5.4 81.25 0.33333 -1
46       py -7.4
c surfaces of the graveyard
47      c/z 3 -8.25 50.1
48       pz 91.7
49       pz 45.8
c surfaces of the shield
50      c/z 0 -1.75 8.1
51       py -5.5
```

```
  52      c/z 0 -1.75 8.15
  53       pz 83.75
  54       pz 78.75
  55       pz 81.25
  56      c/y 5 81.25 4.465
  57      c/y -5 81.25 4.465
c surface for the bottom of the head
  58       pz 67.99

c DATA BLOCK
mode  p e
c MATERIALS
c eyelid skin
m1    1000.          -0.1
      6000.         -0.204 7000.         -0.042 8000.         -0.645
      11000.         -0.002 15000.         -0.001 16000.         -0.002
      17000.         -0.003 19000.         -0.001
c eye lens
m2    1000.          -0.096
      6000.         -0.195 7000.         -0.057 8000.         -0.646
      11000.         -0.001 15000.         -0.001 16000.         -0.003
      17000.         -0.001
c aqueous humour
m3    1000.          -0.112
      8000.         -0.888
c vitreous humour
m4    1000.          -0.112
      8000.         -0.888
c cornea
m5    1000.         -0.1016
      6000.         -0.1262 7000.         -0.0369 8000.         -0.7314
      11000.        -0.00065 15000.        -0.00065 16000.        -0.00195
      17000.        -0.00065
c ICRU 4-element tissue
m6    1000.          -0.101
      6000.         -0.111 7000.         -0.026 8000.         -0.762
c elemental lead
m7    82000.             1
imp:p   1 12r       0         1         0         1         $ 1, 99
imp:e   1 12r       0         1         0         1         $ 1, 99
c SOURCE
sdef pos=33.36 -8.25 45.89 par=2 erg=d1 vec=-1 0 1 dir=d2
si1 L  .018  .020  .022  .024  .026  .028  .030  .032  .034  .036  .038
```

```
     .040  .042  .044  .046  .048  .050  .052  .054  .056  .058  .060
     .062  .064  .066  .068  .070  .072  .074  .076  .078  .080
sp1    .0004 .0011 .0035 .0084 .0151 .0239 .0338 .0429 .0499 .0552 .0598
     .0622 .0633 .0622 .0594 .0563 .0538 .0503 .0482 .0506 .0401 .0334
     .0306 .0278 .0193 .0144 .0120 .0095 .0070 .0039 .0014 .0004
sb2 -31 3.5
c TALLIES
prdmp 2j 1
*f18:p,e 1
fc18 ENERGY DEPOSITED IN THE LEFT LENS (MeV)
*f28:p,e 2
fc28 ENERGY DEPOSITED IN THE RIGHT LENS (MeV)
fmesh4:p origin -7.75 -10 71.6 imesh 7.75  iints 232
                    jmesh 2     jints 180
                    kmesh 91.7  kints 301
nps 500000000
```

B.5 Shield #2 90-0

```
MCNP Input 90-0 Shield 2
c
c CELL BLOCK
c  cells of the eye
   1    2   -1.06 -4 -6 -8 -10 -12  $left lens
   2    2   -1.06 -5 -7 -9 -11 -13  $right lens
   3    4 -1.0089 -14 18 #1  $left vitreous humour
   4    4 -1.0089 -15 18 #2  $right vitreous humour
   5    3  -1.003 (-16 :-14 )-18 #1  $left aquous humour
   6    3  -1.003 (-15 :-17 )-18 #2  $right aqueous humour
   7    5  -1.076 (-22 :-19 )16 14  $left cornea
   8    5  -1.076 (-21 :-20 )17 15  $right cornea
   9    1   -1.09 (-23 :-25 )(-27 :28 )19 22  $left eyelid
  10    1   -1.09 (-24 :-26 )(-27 :28 )20 21  $right eyelid
c  cells of head
  20    6   -1.11 (32 -30 -33 ):(-29 32 34 ):(32 33 -34 -31 ) $upper head
  21    6   -1.11 (-32 -35 -36 -37 38 )(44 :46 )(45 :46 )23 24  $face
  22    6   -1.11 (-38 -39 -3 40 ):(-35 -36 -37 -38 3 40 ) $lower head
  23    0        (-40 -39 -3 58 ):(-35 -36 -37 -40 3 58 ) $bottom of head
c  cells of the world
  30    0        #1 #2 #3 #4 #5 #6 #7 #8 #9 #10 #20 #21 #22 $inside world
           #23 #40 #99
```

```
  40    0        47 :-49 :48  $outside world
c   cells of the shield
  99    7  -11.35 -53 54 -52 50 -51 (-56 :-57 :55 59 ) $x-ray eye shield

c SURFACES BLOCK
c  surfaces of the eye
   3       py 0
   4        s 3 -8.774 81.25 0.8
   5        s -3 -8.774 81.25 0.8
   6        s 3 -8.524 81.25 0.6
   7        s -3 -8.524 81.25 0.6
   8        s 3 -8.2419 81.25 0.5
   9        s -3 -8.2419 81.25 0.5
  10        s 3 -7.9289 81.25 0.595
  11        s -3 -7.9289 81.25 0.595
  12        s 3 -7.1439 81.25 1.25
  13        s -3 -7.1439 81.25 1.25
  14        s 3 -7.4 81.25 1.155
  15        s -3 -7.4 81.25 1.155
  16        s 3 -7.95 81.25 0.72
  17        s -3 -7.95 81.25 0.72
  18       py -8.252
  19        s 3 -7.4 81.25 1.21
  20        s -3 -7.4 81.25 1.21
  21        s -3 -7.9539 81.25 0.775
  22        s 3 -7.9539 81.25 0.775
  23        s 3 -7.4 81.25 1.435
  24        s -3 -7.4 81.25 1.435
  25        s 3 -7.9539 81.25 1
  26        s -3 -7.9539 81.25 1
  27        p 3 -8.546 80.75 3 -10.69051 79.75 2 -8.546 80.75
  28        p 3 -8.546 81.75 3 -9.92234 82.75 2 -8.546 81.75
c  surfaces of the head
  29        s 0 1.95 84.5 7.2
  30        s 0 -1.95 84.5 7.2
  31      c/y 0 84.5 7.2
  32        pz 84.5
  33        py -1.95
  34        py 1.95
  35      c/z 3.036 0 10.79
  36      c/z -3.036 0 10.79
  37        cz 9.7
  38        pz 71.6
```

```
  39      c/z 0 -0.79 7.79
  40       pz 68
  44      k/y -3 -5.4 81.25 0.33333 -1
  45      k/y 3 -5.4 81.25 0.33333 -1
  46       py -7.4
c surfaces of the graveyard
  47      c/z 3 -8.25 50.1
  48       pz 91.7
  49       pz 45.8
c surfaces of the shield
  50      c/z 0 -2.75 7.1
  51       py -6.5
  52      c/z 0 -2.75 7.15
  53       pz 82.75
  54        p -7 -7.1 79.5 0 -9.85 77 7 -7.1 79.5
  55       pz 79.25
  56      c/y 11 81.25 10.465
  57      c/y -11 81.25 10.465
  59      c/y 0 79.25 0.75
c surface for the bottom of the head
  58       pz 67.99

c DATA BLOCK
mode  p e
c MATERIALS
c eyelid skin
m1    1000.          -0.1
      6000.         -0.204 7000.         -0.042 8000.         -0.645
      11000.         -0.002 15000.         -0.001 16000.         -0.002
      17000.         -0.003 19000.         -0.001
c eye lens
m2    1000.          -0.096
      6000.         -0.195 7000.         -0.057 8000.         -0.646
      11000.         -0.001 15000.         -0.001 16000.         -0.003
      17000.         -0.001
c aqueous humour
m3    1000.          -0.112
      8000.         -0.888
c vitreous humour
m4    1000.          -0.112
      8000.         -0.888
c cornea
m5    1000.         -0.1016
```

```
     6000.         -0.1262 7000.         -0.0369 8000.         -0.7314
     11000.        -0.00065 15000.       -0.00065 16000.       -0.00195
     17000.        -0.00065
c ICRU 4-element tissue
m6    1000.          -0.101
     6000.          -0.111 7000.          -0.026 8000.          -0.762
c elemental lead
m7    82000.              1
c
imp:p   1 12r       0          1          0          1          $ 1, 99
imp:e   1 12r       0          1          0          1          $ 1, 99
c SOURCE
sdef pos=3 -58.25 81.25 par=2 erg=d1 vec=0 1 0 dir=d2
si1 L  .018  .020  .022  .024  .026  .028  .030  .032  .034  .036  .038
      .040  .042  .044  .046  .048  .050  .052  .054  .056  .058  .060
      .062  .064  .066  .068  .070  .072  .074  .076
sp1    .0004 .0011 .0035 .0084 .0151 .0238 .0336 .0427 .0515 .0581 .0627
      .0658 .0665 .0658 .0644 .0613 .0585 .0585 .0532 .0434 .0382 .0336
      .0259 .0193 .0158 .0123 .0088 .0056 .0025 .0004
sb2 -31 3.5
c TALLIES
prdmp 2j 1
*f18:p,e 1
fc18 ENERGY DEPOSITED IN THE LEFT LENS (MeV)
*f28:p,e 2
fc28 ENERGY DEPOSITED IN THE RIGHT LENS (MeV)
fmesh4:p origin -7.75 -10 71.6 imesh 7.75  iints 155
                    jmesh 2 jints 120
                    kmesh 91.7 kints 201
nps 500000000
```

B.6 Shield #3 90-30

```
MCNP Input 90-30 Shield 3
c
c CELL BLOCK
c  cells of the eye
   1    2   -1.06 -4 -6 -8 -10 -12  $left lens
   2    2   -1.06 -5 -7 -9 -11 -13  $right lens
   3    4 -1.0089 -14 18 #1  $left vitreous humour
   4    4 -1.0089 -15 18 #2  $right vitreous humour
   5    3  -1.003 (-16 :-14 )-18 #1  $left aquous humour
```

```
   6    3  -1.003 (-15 :-17 )-18 #2  $right aqueous humour
   7    5  -1.076 (-22 :-19 )16 14  $left cornea
   8    5  -1.076 (-21 :-20 )17 15  $right cornea
   9    1   -1.09 (-23 :-25 )(-27 :28 )19 22  $left eyelid
  10    1   -1.09 (-24 :-26 )(-27 :28 )20 21  $right eyelid
c  cells of head
  20    6   -1.11 (32 -30 -33 ):(-29 32 34 ):(32 33 -34 -31 ) $upper head
  21    6   -1.11 (-32 -35 -36 -37 38 )(44 :46 )(45 :46 )23 24  $face
  22    6   -1.11 (-38 -39 -3 40 ):(-35 -36 -37 -38 3 40 ) $lower head
  23    0        (-40 -39 -3 58 ):(-35 -36 -37 -40 3 58 ) $bottom of head
c  cells of the world
  30    0        #1 #2 #3 #4 #5 #6 #7 #8 #9 #10 #20 #21 #22 $inside world
        #23 #40 #99
  40    0        47 :-49 :48  $outside world
c   cells of the shield
  99    7  -11.35 -53 54 -52 50 -51 (-56 :-57 :55 59 ) $x-ray eye shield

c SURFACES BLOCK
c  surfaces of the eye
   3       py 0
   4        s 3 -8.774 81.25 0.8
   5        s -3 -8.774 81.25 0.8
   6        s 3 -8.524 81.25 0.6
   7        s -3 -8.524 81.25 0.6
   8        s 3 -8.2419 81.25 0.5
   9        s -3 -8.2419 81.25 0.5
  10        s 3 -7.9289 81.25 0.595
  11        s -3 -7.9289 81.25 0.595
  12        s 3 -7.1439 81.25 1.25
  13        s -3 -7.1439 81.25 1.25
  14        s 3 -7.4 81.25 1.155
  15        s -3 -7.4 81.25 1.155
  16        s 3 -7.95 81.25 0.72
  17        s -3 -7.95 81.25 0.72
  18       py -8.252
  19        s 3 -7.4 81.25 1.21
  20        s -3 -7.4 81.25 1.21
  21        s -3 -7.9539 81.25 0.775
  22        s 3 -7.9539 81.25 0.775
  23        s 3 -7.4 81.25 1.435
  24        s -3 -7.4 81.25 1.435
  25        s 3 -7.9539 81.25 1
  26        s -3 -7.9539 81.25 1
```

```
  27       p 3 -8.546 80.75 3 -10.69051 79.75 2 -8.546 80.75
  28       p 3 -8.546 81.75 3 -9.92234 82.75 2 -8.546 81.75
c  surfaces of the head
  29       s 0 1.95 84.5 7.2
  30       s 0 -1.95 84.5 7.2
  31      c/y 0 84.5 7.2
  32       pz 84.5
  33       py -1.95
  34       py 1.95
  35      c/z 3.036 0 10.79
  36      c/z -3.036 0 10.79
  37       cz 9.7
  38       pz 71.6
  39      c/z 0 -0.79 7.79
  40       pz 68
  44      k/y -3 -5.4 81.25 0.33333 -1
  45      k/y 3 -5.4 81.25 0.33333 -1
  46       py -7.4
c surfaces of the graveyard
  47      c/z 3 -8.25 50.1
  48       pz 91.7
  49       pz 45.8
c surfaces of the shield
  50      c/z 0 -2.75 7.1
  51       py -6.5
  52      c/z 0 -2.75 7.11
  53       pz 82.75
  54       p -7 -7.1 79.5 0 -9.85 77 7 -7.1 79.5
  55       pz 79.25
  56      c/y 11 81.25 10.465
  57      c/y -11 81.25 10.465
  59      c/y 0 79.25 0.75
c surface for the bottom of the head
  58       pz 67.99

c DATA BLOCK
mode  p e
c MATERIALS
c eyelid skin
m1    1000.           -0.1
      6000.          -0.204 7000.          -0.042 8000.          -0.645
      11000.          -0.002 15000.          -0.001 16000.          -0.002
      17000.          -0.003 19000.          -0.001
```

```
c eye lens
m2    1000.          -0.096
      6000.          -0.195 7000.          -0.057 8000.          -0.646
      11000.         -0.001 15000.         -0.001 16000.         -0.003
      17000.         -0.001
c aqueous humour
m3    1000.          -0.112
      8000.          -0.888
c vitreous humour
m4    1000.          -0.112
      8000.          -0.888
c cornea
m5    1000.          -0.1016
      6000.          -0.1262 7000.          -0.0369 8000.          -0.7314
      11000.         -0.00065 15000.        -0.00065 16000.        -0.00195
      17000.         -0.00065
c ICRU 4-element tissue
m6    1000.          -0.101
      6000.          -0.111 7000.          -0.026 8000.          -0.762
c elemental lead
m7    82000.              1
c
imp:p   1 12r       0          1          0          1          $ 1, 99
imp:e   1 12r       0          1          0          1          $ 1, 99
c SOURCE
sdef pos=28 -51.55 81.25 par=2 erg=d1 vec=-1 1.732 0 dir=d2
si1 L  .018  .020  .022  .024  .026  .028  .030  .032  .034  .036  .038
       .040  .042  .044  .046  .048  .050  .052  .054  .056  .058  .060
       .062  .064  .066  .068  .070  .072  .074  .076
sp1    .0004 .0011 .0035 .0084 .0151 .0238 .0336 .0427 .0515 .0581 .0627
       .0658 .0665 .0658 .0644 .0613 .0585 .0585 .0532 .0434 .0382 .0336
       .0259 .0193 .0158 .0123 .0088 .0056 .0025 .0004
sb2 -31 3.5
c TALLIES
prdmp 2j 1
*f18:p,e 1
fc18 ENERGY DEPOSITED IN THE LEFT LENS (MeV)
*f28:p,e 2
fc28 ENERGY DEPOSITED IN THE RIGHT LENS (MeV)
fmesh4:p origin -7.75 -10 71.6 imesh 7.75  iints 155
                  jmesh 2 jints 120
                  kmesh 91.7 kints 201
nps 500000000
```

B.7 Shield #4 90-60

```
MCNP Input 90-60 Shield 4
c
c CELL BLOCK
c  cells of the eye
   1    2   -1.06 -4 -6 -8 -10 -12  $left lens
   2    2   -1.06 -5 -7 -9 -11 -13  $right lens
   3    4 -1.0089 -14 18 #1  $left vitreous humour
   4    4 -1.0089 -15 18 #2  $right vitreous humour
   5    3  -1.003 (-16 :-14 )-18 #1  $left aquous humour
   6    3  -1.003 (-15 :-17 )-18 #2  $right aqueous humour
   7    5  -1.076 (-22 :-19 )16 14  $left cornea
   8    5  -1.076 (-21 :-20 )17 15  $right cornea
   9    1   -1.09 (-23 :-25 )(-27 :28 )19 22  $left eyelid
  10    1   -1.09 (-24 :-26 )(-27 :28 )20 21  $right eyelid
c  cells of head
  20    6   -1.11 (32 -30 -33 ):(-29 32 34 ):(32 33 -34 -31 ) $upper head
  21    6   -1.11 (-32 -35 -36 -37 38 )(44 :46 )(45 :46 )23 24  $face
  22    6   -1.11 (-38 -39 -3 40 ):(-35 -36 -37 -38 3 40 ) $lower head
  23    0        (-40 -39 -3 58 ):(-35 -36 -37 -40 3 58 ) $bottom of head
c  cells of the world
  30    0        #1 #2 #3 #4 #5 #6 #7 #8 #9 #10 #20 #21 #22 $inside world
        #23 #40 #99
  40    0        47 :-49 :48  $outside world
c   cells of the shield
  99    7  -11.35 -53 -52 50 -51 61 (-54 :-60 ) $x-ray eye shiel
        (-56 :-57 :55 59 )

c SURFACES BLOCK
c  surfaces of the eye
   3       py 0
   4        s 3 -8.774 81.25 0.8
   5        s -3 -8.774 81.25 0.8
   6        s 3 -8.524 81.25 0.6
   7        s -3 -8.524 81.25 0.6
   8        s 3 -8.2419 81.25 0.5
   9        s -3 -8.2419 81.25 0.5
  10         s 3 -7.9289 81.25 0.595
  11         s -3 -7.9289 81.25 0.595
```

```
  12       s 3 -7.1439 81.25 1.25
  13       s -3 -7.1439 81.25 1.25
  14       s 3 -7.4 81.25 1.155
  15       s -3 -7.4 81.25 1.155
  16       s 3 -7.95 81.25 0.72
  17       s -3 -7.95 81.25 0.72
  18      py -8.252
  19       s 3 -7.4 81.25 1.21
  20       s -3 -7.4 81.25 1.21
  21       s -3 -7.9539 81.25 0.775
  22       s 3 -7.9539 81.25 0.775
  23       s 3 -7.4 81.25 1.435
  24       s -3 -7.4 81.25 1.435
  25       s 3 -7.9539 81.25 1
  26       s -3 -7.9539 81.25 1
  27       p 3 -8.546 80.75 3 -10.69051 79.75 2 -8.546 80.75
  28       p 3 -8.546 81.75 3 -9.92234 82.75 2 -8.546 81.75
c  surfaces of the head
  29       s 0 1.95 84.5 7.2
  30       s 0 -1.95 84.5 7.2
  31      c/y 0 84.5 7.2
  32       pz 84.5
  33       py -1.95
  34       py 1.95
  35      c/z 3.036 0 10.79
  36      c/z -3.036 0 10.79
  37       cz 9.7
  38       pz 71.6
  39      c/z 0 -0.79 7.79
  40       pz 68
  44      k/y -3 -5.4 81.25 0.33333 -1
  45      k/y 3 -5.4 81.25 0.33333 -1
  46       py -7.4
c surfaces of the graveyard
  47      c/z 3 -8.25 50.1
  48       pz 91.7
  49       pz 45.8
c surfaces of the shield
  50      c/z 0 -2.75 7.1
  51       py -6.25
  52      c/z 0 -2.75 7.11
  53       pz 82.75
  54      c/y 1.25 82 5
```

```
  60      c/y -1.25 82 5
  55       pz 79.25
  56      c/y 11 81.25 10.465
  57      c/y -11 81.25 10.465
  59      c/y 0 79.25 0.75
  61       pz 77.25
c surface for the bottom of the head
  58       pz 67.99

c DATA BLOCK
mode  p e
c MATERIALS
c eyelid skin
m1    1000.          -0.1
      6000.         -0.204 7000.         -0.042 8000.         -0.645
      11000.         -0.002 15000.         -0.001 16000.         -0.002
      17000.         -0.003 19000.         -0.001
c eye lens
m2    1000.          -0.096
      6000.         -0.195 7000.         -0.057 8000.         -0.646
      11000.         -0.001 15000.         -0.001 16000.         -0.003
      17000.         -0.001
c aqueous humour
m3    1000.          -0.112
      8000.         -0.888
c vitreous humour
m4    1000.          -0.112
      8000.         -0.888
c cornea
m5    1000.         -0.1016
      6000.         -0.1262 7000.         -0.0369 8000.         -0.7314
      11000.        -0.00065 15000.        -0.00065 16000.        -0.00195
      17000.        -0.00065
c ICRU 4-element tissue
m6    1000.          -0.101
      6000.         -0.111 7000.         -0.026 8000.         -0.762
c elemental lead
m7    82000.             1
c
imp:p   1 12r       0          1          0          1          $ 1, 99
imp:e   1 12r       0          1          0          1          $ 1, 99
c SOURCE
sdef pos=46.3 -33.25 81.25 par=2 erg=d1 vec=-1.732 1 0 dir=d2
```

```
si1 L  .018  .020  .022  .024  .026  .028  .030  .032  .034  .036  .038
     .040  .042  .044  .046  .048  .050  .052  .054  .056  .058  .060
     .062  .064  .066  .068  .070  .072  .074  .076
sp1    .0004 .0011 .0035 .0084 .0151 .0238 .0336 .0427 .0515 .0581 .0627
     .0658 .0665 .0658 .0644 .0613 .0585 .0585 .0532 .0434 .0382 .0336
     .0259 .0193 .0158 .0123 .0088 .0056 .0025 .0004
sb2 -31 3.5
c TALLIES
prdmp 2j 1
*f18:p,e 1
fc18 ENERGY DEPOSITED IN THE LEFT LENS (MeV)
*f28:p,e 2
fc28 ENERGY DEPOSITED IN THE RIGHT LENS (MeV)
fmesh4:p origin -7.75 -10 71.6 imesh 7.75  iints 155
                    jmesh 2 jints 120
                    kmesh 91.7 kints 201
nps 500000000
```

B.8 Shield #5 90-90

```
MCNP Input 90-90 Shield 5
c
c CELL BLOCK
c  cells of the eye
   1    2   -1.06 -4 -6 -8 -10 -12  $left lens
   2    2   -1.06 -5 -7 -9 -11 -13  $right lens
   3    4 -1.0089 -14 18 #1  $left vitreous humour
   4    4 -1.0089 -15 18 #2  $right vitreous humour
   5    3  -1.003 (-16 :-14 )-18 #1  $left aquous humour
   6    3  -1.003 (-15 :-17 )-18 #2  $right aqueous humour
   7    5  -1.076 (-22 :-19 )16 14  $left cornea
   8    5  -1.076 (-21 :-20 )17 15  $right cornea
   9    1   -1.09 (-23 :-25 )(-27 :28 )19 22  $left eyelid
  10    1   -1.09 (-24 :-26 )(-27 :28 )20 21  $right eyelid
c  cells of head
  20    6   -1.11 (32 -30 -33 ):(-29 32 34 ):(32 33 -34 -31 ) $upper head
  21    6   -1.11 (-32 -35 -36 -37 38 )(44 :46 )(45 :46 )23 24  $face
  22    6   -1.11 (-38 -39 -3 40 ):(-35 -36 -37 -38 3 40 ) $lower head
  23    0        (-40 -39 -3 58 ):(-35 -36 -37 -40 3 58 ) $bottom of head
c  cells of the world
  30    0        #1 #2 #3 #4 #5 #6 #7 #8 #9 #10 #20 #21 #22 $inside world
```

```
        #23 #40 #99
  40    0        47 :-49 :48  $outside world
c   cells of the shield
  99    7  -11.35 -53 -52 50 -51 60 (-56 :-57 :55 59 ) $x-ray eye shield

c SURFACES BLOCK
c  surfaces of the eye
   3       py 0
   4       s 3 -8.774 81.25 0.8
   5       s -3 -8.774 81.25 0.8
   6       s 3 -8.524 81.25 0.6
   7       s -3 -8.524 81.25 0.6
   8       s 3 -8.2419 81.25 0.5
   9       s -3 -8.2419 81.25 0.5
  10       s 3 -7.9289 81.25 0.595
  11       s -3 -7.9289 81.25 0.595
  12       s 3 -7.1439 81.25 1.25
  13       s -3 -7.1439 81.25 1.25
  14       s 3 -7.4 81.25 1.155
  15       s -3 -7.4 81.25 1.155
  16       s 3 -7.95 81.25 0.72
  17       s -3 -7.95 81.25 0.72
  18       py -8.252
  19       s 3 -7.4 81.25 1.21
  20       s -3 -7.4 81.25 1.21
  21       s -3 -7.9539 81.25 0.775
  22       s 3 -7.9539 81.25 0.775
  23       s 3 -7.4 81.25 1.435
  24       s -3 -7.4 81.25 1.435
  25       s 3 -7.9539 81.25 1
  26       s -3 -7.9539 81.25 1
  27       p 3 -8.546 80.75 3 -10.69051 79.75 2 -8.546 80.75
  28       p 3 -8.546 81.75 3 -9.92234 82.75 2 -8.546 81.75
c  surfaces of the head
  29       s 0 1.95 84.5 7.2
  30       s 0 -1.95 84.5 7.2
  31      c/y 0 84.5 7.2
  32       pz 84.5
  33       py -1.95
  34       py 1.95
  35      c/z 3.036 0 10.79
  36      c/z -3.036 0 10.79
  37       cz 9.7
```

```
  38      pz 71.6
  39      c/z 0 -0.79 7.79
  40      pz 68
  44      k/y -3 -5.4 81.25 0.33333 -1
  45      k/y 3 -5.4 81.25 0.33333 -1
  46      py -7.4
c surfaces of the graveyard
  47      c/z 3 -8.25 50.1
  48      pz 91.7
  49      pz 45.8
c surfaces of the shield
  50       s 0 -4.125 81.25 7.1
  51      py -6
  52       s 0 -4.125 81.25 7.11
  53      pz 83
  55      pz 79.25
  56      c/y 11 81.25 10.465
  57      c/y -11 81.25 10.465
  59      c/y 0 79.25 0.75
  60      c/z 0 -2.75 7.1
c surface for the bottom of the head
  58      pz 67.99

c DATA BLOCK
mode  p e
c MATERIALS
c eyelid skin
m1    1000.          -0.1
      6000.          -0.204 7000.          -0.042 8000.          -0.645
      11000.         -0.002 15000.         -0.001 16000.         -0.002
      17000.         -0.003 19000.         -0.001
c eye lens
m2    1000.          -0.096
      6000.          -0.195 7000.          -0.057 8000.          -0.646
      11000.         -0.001 15000.         -0.001 16000.         -0.003
      17000.         -0.001
c aqueous humour
m3    1000.          -0.112
      8000.          -0.888
c vitreous humour
m4    1000.          -0.112
      8000.          -0.888
c cornea
```

```
m5    1000.          -0.1016
      6000.          -0.1262 7000.          -0.0369 8000.          -0.7314
      11000.         -0.00065 15000.        -0.00065 16000.        -0.00195
      17000.         -0.00065
c ICRU 4-element tissue
m6    1000.          -0.101
      6000.          -0.111 7000.           -0.026 8000.           -0.762
c elemental lead
m7    82000.               1
c
imp:p   1 12r       0          1          0          1          $ 1, 99
imp:e   1 12r       0          1          0          1          $ 1, 99
c SOURCE
sdef pos=53 -8.25 81.25 par=2 erg=d1 vec=-1 0 0 dir=d2
si1 L  .018  .020  .022  .024  .026  .028  .030  .032  .034  .036  .038
       .040  .042  .044  .046  .048  .050  .052  .054  .056  .058  .060
       .062  .064  .066  .068  .070  .072  .074  .076
sp1    .0004 .0011 .0035 .0084 .0151 .0238 .0336 .0427 .0515 .0581 .0627
       .0658 .0665 .0658 .0644 .0613 .0585 .0585 .0532 .0434 .0382 .0336
       .0259 .0193 .0158 .0123 .0088 .0056 .0025 .0004
sb2 -31 3.5
c TALLIES
prdmp 2j 1
*f18:p,e 1
fc18 ENERGY DEPOSITED IN THE LEFT LENS (MeV)
*f28:p,e 2
fc28 ENERGY DEPOSITED IN THE RIGHT LENS (MeV)
fmesh4:p origin -7.75 -10 71.6 imesh 7.75  iints 155
                  jmesh 2 jints 120
                  kmesh 91.7 kints 201
nps 500000000
```

B.9 Shield #6 45-0

```
MCNP Input 45-0 Shield 6
c
c CELL BLOCK
c  cells of the eye
   1    2   -1.06 -4 -6 -8 -10 -12  $left lens
   2    2   -1.06 -5 -7 -9 -11 -13  $right lens
   3    4 -1.0089 -14 18 #1  $left vitreous humour
```

```
   4    4 -1.0089 -15 18 #2  $right vitreous humour
   5    3  -1.003 (-16 :-14 )-18 #1  $left aquous humour
   6    3  -1.003 (-15 :-17 )-18 #2  $right aqueous humour
   7    5  -1.076 (-22 :-19 )16 14  $left cornea
   8    5  -1.076 (-21 :-20 )17 15  $right cornea
   9    1   -1.09 (-23 :-25 )(-27 :28 )19 22  $left eyelid
  10    1   -1.09 (-24 :-26 )(-27 :28 )20 21  $right eyelid
c  cells of head
  20    6   -1.11 (32 -30 -33 ):(-29 32 34 ):(32 33 -34 -31 ) $upper head
  21    6   -1.11 (-32 -35 -36 -37 38 )(44 :46 )(45 :46 )23 24  $face
  22    6   -1.11 (-38 -39 -3 40 ):(-35 -36 -37 -38 3 40 ) $lower head
  23    0        (-40 -39 -3 58 ):(-35 -36 -37 -40 3 58 ) $bottom of head
c  cells of the world
  30    0        #1 #2 #3 #4 #5 #6 #7 #8 #9 #10 #20 #21 #22 $inside world
        #23 #40 #99 #100
  40    0        47 :-49 :48  $outside world
c   cells of the shield
  99    7  -11.35 -53 -52 50 -51 60 (-56 :-57 :55 59 ) $x-ray eye shield
 100    7  -11.35 (-52 60 -55 ((57 -62 ):(56 -61 ))):(-52 60 -59 63 55 )
       $nose piece

c SURFACES BLOCK
c  surfaces of the eye
   3       py 0
   4        s 3 -8.774 81.25 0.8
   5        s -3 -8.774 81.25 0.8
   6        s 3 -8.524 81.25 0.6
   7        s -3 -8.524 81.25 0.6
   8        s 3 -8.2419 81.25 0.5
   9        s -3 -8.2419 81.25 0.5
  10         s 3 -7.9289 81.25 0.595
  11         s -3 -7.9289 81.25 0.595
  12         s 3 -7.1439 81.25 1.25
  13         s -3 -7.1439 81.25 1.25
  14         s 3 -7.4 81.25 1.155
  15         s -3 -7.4 81.25 1.155
  16         s 3 -7.95 81.25 0.72
  17         s -3 -7.95 81.25 0.72
  18        py -8.252
  19         s 3 -7.4 81.25 1.21
  20         s -3 -7.4 81.25 1.21
  21         s -3 -7.9539 81.25 0.775
  22         s 3 -7.9539 81.25 0.775
```

```
  23       s 3 -7.4 81.25 1.435
  24       s -3 -7.4 81.25 1.435
  25       s 3 -7.9539 81.25 1
  26       s -3 -7.9539 81.25 1
  27       p 3 -8.546 80.75 3 -10.69051 79.75 2 -8.546 80.75
  28       p 3 -8.546 81.75 3 -9.92234 82.75 2 -8.546 81.75
c  surfaces of the head
  29       s 0 1.95 84.5 7.2
  30       s 0 -1.95 84.5 7.2
  31      c/y 0 84.5 7.2
  32       pz 84.5
  33       py -1.95
  34       py 1.95
  35      c/z 3.036 0 10.79
  36      c/z -3.036 0 10.79
  37       cz 9.7
  38       pz 71.6
  39      c/z 0 -0.79 7.79
  40       pz 68
  44      k/y -3 -5.4 81.25 0.33333 -1
  45      k/y 3 -5.4 81.25 0.33333 -1
  46       py -7.4
c surfaces of the graveyard
  47      c/z 3 -8.25 50.1
  48       pz 91.7
  49       pz 45.8
c surfaces of the shield
  50       s 0 -4.125 81.25 7.1
  51       py -6
  52       s 0 -4.125 81.25 7.11
  53       pz 83
  55       pz 79.592
  56      c/y 11 81.25 10.465
  57      c/y -11 81.25 10.465
  59      c/y 0 79.25 0.75
  60      c/z 0 -2.75 7.1
  61      c/y 11 81.25 10.475
  62      c/y -11 81.25 10.475
  63      c/y 0 79.25 0.74
c surface for the bottom of the head
  58       pz 67.99

c DATA BLOCK
```

```
mode  p e
c MATERIALS
c eyelid skin
m1    1000.          -0.1
      6000.         -0.204 7000.         -0.042 8000.         -0.645
      11000.         -0.002 15000.         -0.001 16000.         -0.002
      17000.         -0.003 19000.         -0.001
c eye lens
m2    1000.          -0.096
      6000.         -0.195 7000.         -0.057 8000.         -0.646
      11000.         -0.001 15000.         -0.001 16000.         -0.003
      17000.         -0.001
c aqueous humour
m3    1000.          -0.112
      8000.         -0.888
c vitreous humour
m4    1000.          -0.112
      8000.         -0.888
c cornea
m5    1000.          -0.1016
      6000.         -0.1262 7000.         -0.0369 8000.         -0.7314
      11000.        -0.00065 15000.        -0.00065 16000.        -0.00195
      17000.        -0.00065
c ICRU 4-element tissue
m6    1000.          -0.101
      6000.         -0.111 7000.         -0.026 8000.         -0.762
c elemental lead
m7    82000.              1
imp:p   1 12r       0          1          0          1 1r        $ 1, 100
imp:e   1 12r       0          1          0          1 1r        $ 1, 100
c SOURCE
sdef pos=3 -43.61 45.89 par=2 erg=d1 vec=0 1 1 dir=d2
si1 L  .018  .020  .022  .024  .026  .028  .030  .032  .034  .036  .038
       .040  .042  .044  .046  .048  .050  .052  .054  .056  .058  .060
       .062  .064  .066  .068  .070  .072  .074  .076  .078  .080
sp1    .0004 .0011 .0035 .0084 .0151 .0239 .0338 .0429 .0499 .0552 .0598
       .0622 .0633 .0622 .0594 .0563 .0538 .0503 .0482 .0506 .0401 .0334
       .0306 .0278 .0193 .0144 .0120 .0095 .0070 .0039 .0014 .0004
sb2 -31 3.5
c TALLIES
prdmp 2j 1
*f18:p,e 1
fc18 ENERGY DEPOSITED IN THE LEFT LENS (MeV)
```

```
*f28:p,e 2
fc28 ENERGY DEPOSITED IN THE RIGHT LENS (MeV)
fmesh4:p origin -7.75 -10 71.6 imesh 7.75  iints 155
                jmesh 2 jints 120
                kmesh 91.7 kints 201
nps 500000000
```